


4-2014

## Evaluation of the Tensile, Water Diffusion, and Water Hydrolysis Properties of Graphene Oxide/Polyamide-11 Composites and Their Synthesis

Christopher Houston Komatsu  
*College of William and Mary*

Follow this and additional works at: <https://scholarworks.wm.edu/honorsthesis>

 Part of the [Materials Chemistry Commons](#), [Organic Chemistry Commons](#), and the [Polymer Chemistry Commons](#)

---

### Recommended Citation

Komatsu, Christopher Houston, "Evaluation of the Tensile, Water Diffusion, and Water Hydrolysis Properties of Graphene Oxide/Polyamide-11 Composites and Their Synthesis" (2014). *Undergraduate Honors Theses*. Paper 11.

<https://scholarworks.wm.edu/honorsthesis/11>

This Honors Thesis is brought to you for free and open access by the Theses, Dissertations, & Master Projects at W&M ScholarWorks. It has been accepted for inclusion in Undergraduate Honors Theses by an authorized administrator of W&M ScholarWorks. For more information, please contact [scholarworks@wm.edu](mailto:scholarworks@wm.edu).

Evaluation of the Tensile, Water Diffusion, and Water Hydrolysis Properties of Graphene  
Oxide/Polyamide-11 Composites and Their Synthesis

Christopher Houston Komatsu

Bachelor of Science, the College of William and Mary 2014

A Senior Honors Thesis Presented for a Bachelor of Science Degree in Chemistry from the  
College of William and Mary

Department of Chemistry

The College of William and Mary,  
April, 2014

APPROVAL PAGE

This Thesis is submitted in fulfillment of the requirements for Honors in Chemistry; Bachelor of  
Science Degree

---

Christopher Houston Komatsu

Approved by the Committee, April, 2014

---

Committee Chair  
David Kranbuehl, Chemistry  
The College of William and Mary

---

Christopher J. Abelt, Chemistry

---

David W. Thompson, Chemistry

---

Daniel J. Doherty, Government

## Abstract

Graphene oxide (GO) is a nanoparticle derived from pristine graphene and shows increasing promise for applications as a reinforcement material for polymer composites. Pristine graphene forms the basal plane of graphite and is one of the strongest materials known to man and exhibits excellent gas barrier properties. Polyamide-11 (PA-11) is a specialty polymer of the Nylon class and is commonly used in offshore oil pipes due to its excellent mechanical properties and superior resistance to hydrolysis compared to other polyamides. However, degradation by hydrolysis of PA-11 in the aqueous environments of these pipes still poses significant safety and budget concerns. This paper explores the advantages in tensile, water diffusion, and water hydrolysis properties of GO/PA-11 composites. Two separate batches of composites were made by polymerizing GO/11-Aminoundecanoic Acid dispersions in-situ. The batch with a faster heating rate during polymerization showed superior tensile properties at low GO concentrations and a lower diffusion coefficient at higher GO concentrations. The batch with the slower heating rate showed an improved equilibrium molecular weight at low GO concentrations but the tensile properties showed no improvement compared to the neat system.

## **Acknowledgements**

Professor David Kranbuehl

John-Andrew Samuel Hocker

Ryan Shintani

Professor Christopher Abelt

Professor David Thompson

Professor Daniel Doherty

Chemistry Department at the College of William and Mary

Roy Charles Center

Friends, Family, and Colleagues in Lab

# Table of Contents

Chapter	Page Number
1	Introduction.....1
1.1	Polyamide-11.....1
1.2	Graphene Oxide.....4
2	Instrumentation.....10
2.1	Material Testing System.....10
2.1.1	Theory.....10
2.1.2	Sample Preparation.....16
2.2	Size Exclusion Chromatography-Multi-Angle Laser Light Scattering.....17
2.2.1	Size Exclusion Chromatography Theory.....17
2.2.2	Multi-Angle Laser Light Scattering Theory.....23
2.2.3	Sample Preparation.....29
2.3	Differential Scanning Calorimetry.....30
2.3.1	Theory.....30
2.3.2	Sample Preparation.....34
3	Experimentation.....35
3.1	Synthesis of GO/PA-11 Samples.....35
3.1.1	Theory.....35
3.1.2	Sample Preparation.....36
3.2	Water Diffusion/Absorption Study.....47

3.2.1	Theory.....	47
3.2.2	Sample Preparaion.....	50
3.3	Aging Study.....	52
3.3.1	Theory.....	52
3.3.2	Sample Preparation.....	53
4	Results.....	55
4.1	GO/PA-11 Tensile Data.....	55
4.2	GO/PA-11 DI Water Diffusion Data.....	59
4.3	GO/PA-11 Aging Study Data.....	72
4.4	GO/PA-11 Differential Scanning Calorimetry Data.....	76
5	Discussion.....	80
5.1	Differential Scanning Calorimetry.....	80
5.2	Tensile Properties.....	83
5.3	GO/PA-11 Water Diffusion/Absorption.....	96
5.4	Aging Study.....	101
6	Conclusion.....	105
	References.....	107

# Chapter 1: Introduction

## 1.1 Polyamide-11

Polyamide-11 (PA-11) is a specialty polymer of the Nylon class with mechanical and chemical properties that make it very suitable for various engineering applications.<sup>1</sup> Like all polyamides, PA-11 has a very good combination of high strength, flexibility, toughness, abrasion resistance, low coefficient of friction, low creep, and resistance to solvents, bases, fungi, and body fluids.<sup>1</sup> However, all polyamides are susceptible to moisture uptake resulting in changes in dimensional and mechanical properties.<sup>1</sup> Thus, they are also susceptible to neutral and acid hydrolysis.<sup>1</sup> Unlike other polyamides with less methylene groups such as PA-6, PA-11 has better moisture resistance and dimensional stability due to the lower solubility of the additional methylene groups in its monomer chain.<sup>1</sup> The added methylene groups also act to slightly decrease the crystallinity,  $T_m$ , and other mechanical properties compared to other polyamides like PA-6.<sup>1</sup> Table 1.1.1 lists some mechanical properties for commercial grade PA-11.<sup>2</sup>

**Table 1.1.1: Tensile Properties of Commercial PA-11\***

Elongation at Break (%)	Young's Modulus (Mpa)	Tensile Stress (Mpa)	$T_g$ (C°)	$T_m$ (C°)	Crystallinity (%)
251±3	70±6	119±14	44.5	180.5±0.1	24.4±1

\* All values listed are averages from a previous study except for  $T_g$

The mechanical and chemical properties make PA-11 ideal for use as deep-water oil pipes, or “risers.”<sup>2</sup> These risers transport crude oil from a well on the ocean floor to the surface and must withstand the enormous pressures of the deep sea while encasing crude oil and production water.<sup>2</sup> Figure 1.1.2 shows the various layers that compose these risers.<sup>3</sup> Layer (1) is a flexible “z-locked” steel that protects against abrasion during maintenance and also protects against collapse when pumping is ceased.<sup>3</sup> Layer (2) is a polymer that contains the crude oil and



production water during extraction.<sup>3</sup> Layers (3) and (4) are typically steel tape wound around the flexible polymer layer.<sup>3</sup> These layers are designed to contain the internal pressure as well as reinforce the polymer layer against radial and axial stress.<sup>3</sup> The outermost layer is made of rubber and protects the riser against abrasion from objects and particles in the open sea.<sup>3</sup> The most common material used in the polymer layer is PA-11.<sup>3</sup>

**Figure 1.1.2: Cross Section of Riser Pipe**



The PA-11 layer of the riser comes into contact with all chemicals in the crude oil and production water extract.<sup>3</sup> During the course of oil extraction, seawater fills the underground oil reservoir.<sup>3</sup> As a result, the concentration of seawater in the crude oil extract increases as it is pumped from the reservoir.<sup>3</sup> The seawater that gets into the riser during extraction is referred to as production water.<sup>3</sup> Water hydrolysis of PA-11 is a phenomenon that has been studied extensively over the past decade.<sup>3</sup> First, Meyer et al.<sup>4</sup> created a kinetic model for neutral (pH=7) water hydrolysis of in-house synthesized PA-11. In the same year, Jacques, et al.<sup>5</sup> derived a kinetic model for the hydrolysis of commercial PA-11 in pure water. Then Glover et al.<sup>2</sup> conducted a kinetic study on the temperature dependent effects of organic alcohols and acids present in the production water on the hydrolysis of PA-11. More recently, Hocker et al.<sup>3</sup> published a thesis where it was determined that small carboxylic acids significantly increase the rate of hydrolysis of PA-11 and reduce its molecular weight even more so than water hydrolysis because the hydrocarbon chains are more soluble in the PA-11 matrix. Most recently, Romão, et al.<sup>6</sup> conducted another study on the aging of commercial PA-11 at variable temperature in neutral water (pH=7) and in production water from an oilfield (pH=5.5). The fact that the hydrolysis effects are dependent upon the diffusion of these chemicals into the PA-11 matrix suggests that the combination of certain nanocomposite materials can inhibit the hydrolysis effect by decreasing the permeability into the PA-11 matrix.

Decreasing the hydrolysis of PA-11 would have a significant impact on its use as an engineering material. A higher molecular weight results in a higher relative entanglement in the solid phase because molecular weight is directly related to the average chain length.<sup>3</sup> This increased entanglement leads to a higher toughness.<sup>3</sup> If the molecular weight is below a certain value, then the polymer shows significantly lower toughness.<sup>3</sup> The toughness mostly correlates to

the percent elongation.<sup>3</sup> However, significant changes in the percent elongation will drastically change all of the mechanical properties.<sup>3</sup> The percent elongation decays drastically below a sharply defined molecular weight ( $\bar{M}_w$ ) that is known as the ductile-brittle transition.<sup>4</sup> It is important to note that this transition occurs rapidly and the mechanical properties are relatively constant with molecular weight until the ductile-brittle transition is reached.<sup>4</sup> If the strain of the polymer in the riser pipes is below 50%, then it is considered too brittle for use.<sup>3</sup> This occurs at approximately  $25,000 \frac{g}{mol}$ .<sup>3</sup> Therefore, molecular weight is the primary variable that determines a polymer's mechanical properties.<sup>3</sup> Synthesizing a PA-11 composite that ages slower or increases the equilibrium molecular weight in a hydrolytic environment to above the ductile-brittle transition would make the risers much safer and cost effective.

## 1.2 Graphene Oxide

The nanoparticle filler studied in this paper is graphene oxide (GO)—a functionalized form of pristine graphene (PG).<sup>7</sup> Pristine graphene is a nearly perfect, two-dimensional, crystalline sheet of  $SP^2$  bonded carbon that shows excellent electrical, thermal, optical, and mechanical properties.<sup>8,9</sup> PG is reported to have a Young's modulus of 0.5 – 1 TPa, a tensile strength of 130 GPa, and to be completely impermeable to most gases.<sup>10,11</sup> These properties make PG an excellent reinforcement material for use in polymer composites. However, obtaining individual PG sheets for industrial use has proven to be a very difficult if not an impossible task.

Pristine graphene forms the basal plane of graphite; in essence, graphite is multiple PG sheets stacked on top of each other via Van der Waals forces as shown in Figure 1.2.1.<sup>9,12</sup> The first attempt at isolating PG sheets from graphite was conducted by mechanical cleavage with scotch tape.<sup>8</sup> However, this method is tedious and not suitable for large-scale industrial use.<sup>8</sup> A typical PG sheet isolated from this method is illustrated in Figure 1.2.2.<sup>12</sup>

**Figure 1.2.1: Graphite**

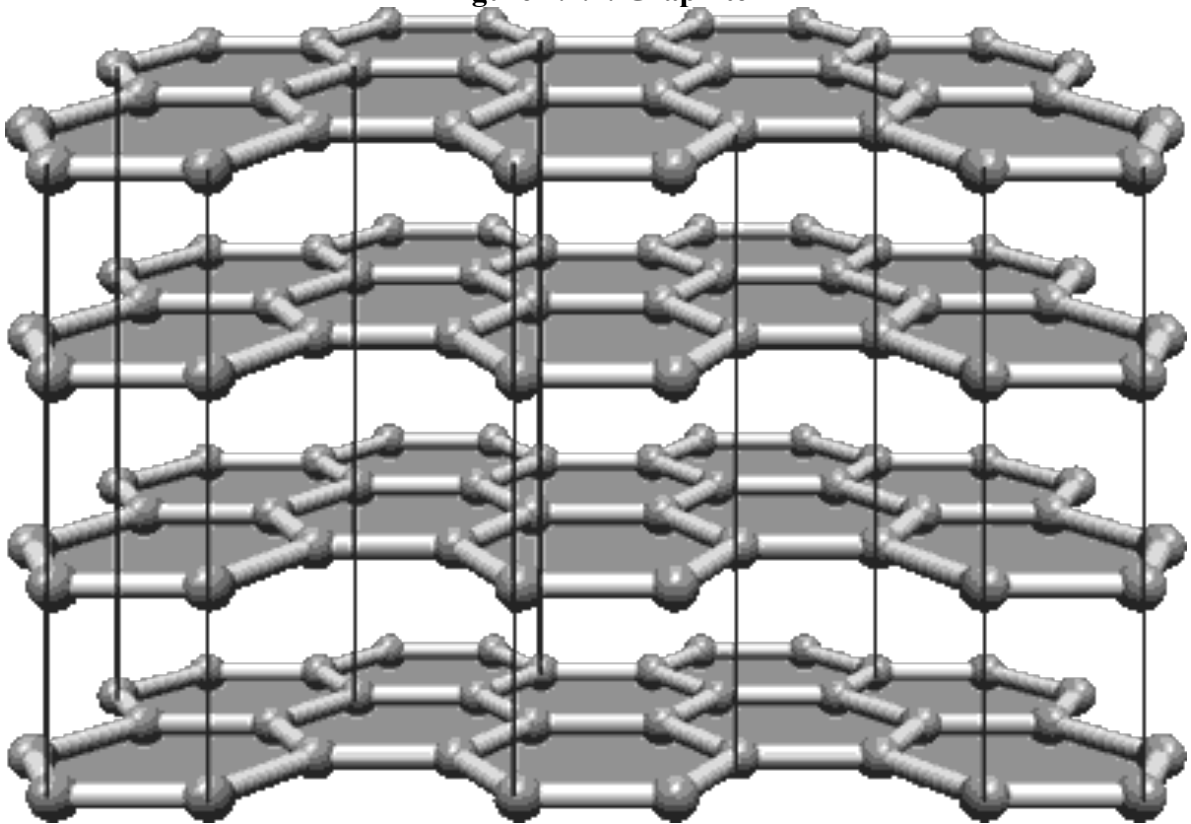
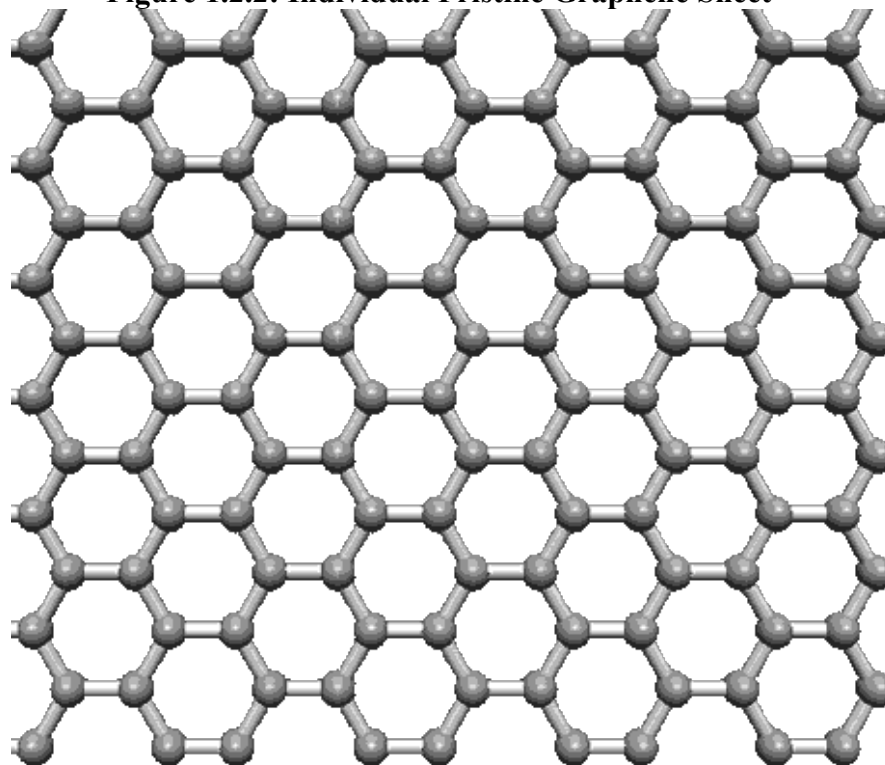
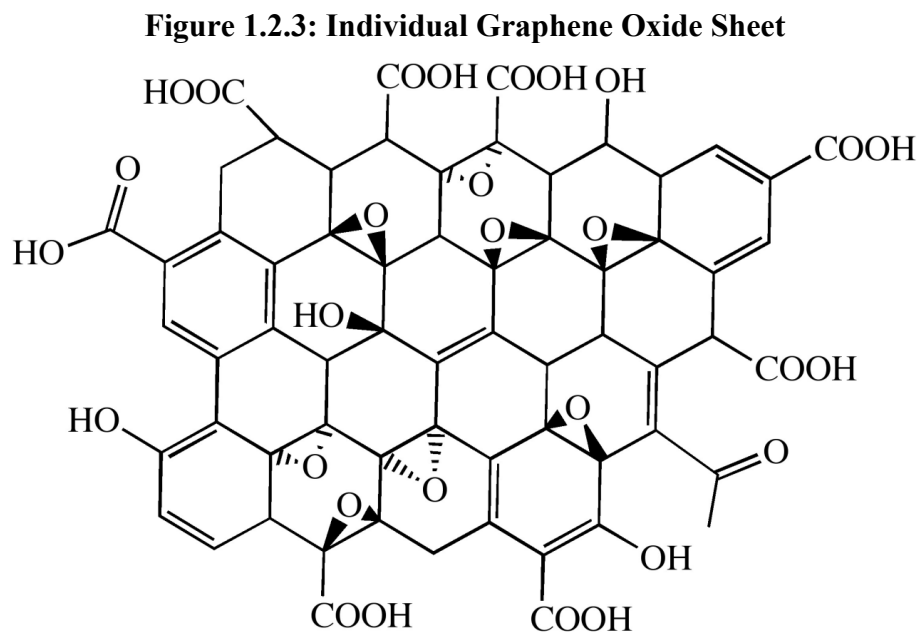


**Figure 1.2.2: Individual Pristine Graphene Sheet**



Isolating individual sheets of functionalized graphene such as graphene oxide has proven much more successful. The techniques for isolating GO sheets involve the conversion of graphite into graphite oxide and then exfoliation—separation—of the graphite oxide into individual Graphene Oxide sheets.<sup>8</sup> The most commonly used method for converting graphite into graphite oxide is called the Hummers' method.<sup>8</sup> This method oxidizes graphite in concentrated  $\text{H}_2\text{SO}_4$  and uses  $\text{KMnO}_4$  and  $\text{NaNO}_3$  as oxidants.<sup>8</sup> Graphite oxide is then exfoliated into Graphene Oxide sheets by ultrasonication in a polar solvent such as water.<sup>8</sup> The resulting GO sheets have an amorphous, mostly  $\text{SP}^3$  structure with tertiary alcohols and epoxides in the middle of the GO sheets while carboxylic acid groups line the edges.<sup>13</sup> The dimensions of these GO sheets are  $\sim 1$  nm thick,  $\sim 500$  nm in length and a surface area of  $\sim 1 \mu\text{m}^2$ .<sup>11,14</sup> Exfoliation via ultrasonication is possible because the electronegative hydroxyl and epoxide groups form a repulsive force

between the GO sheets that drastically weakens the Van Der Waals attraction between them. In addition to the oxygen functionalities, some  $SP^2$  carbon bonds remain and there is some evidence suggesting that these groups are aromatic.<sup>13</sup> A typical GO sheet is depicted in Figure 1.2.3.<sup>15</sup> Thus, GO has very different features than PG sheets and the two materials should not be confused.



Because of the different structural features, GO sheets also exhibit slightly different properties than PG sheets. Unlike pristine graphene, graphene oxide sheets are hydrophilic due to their polar oxygen functionalities and readily disperse in water and some other polar solvents.<sup>13,16</sup> Additionally, the GO sheets are electronically insulating unlike PG due to the broken  $SP^2$  network.<sup>16</sup> For the purposes of this paper, the tensile properties of GO are assumed to be less but roughly the same as that of PG. A  $\pi$ -bond in and of itself is very weak compared to a  $\sigma$ -bond. Thus, the main difference in an  $SP^2$  system versus an  $SP^3$  system would be a hindrance to rotation indicating that PG would be less flexible than GO. Indeed, there is evidence to show that

the modulus of GO approaches that of PG.<sup>14</sup> However, it is possible to partially reverse the degradation of these properties.

Reducing GO can reverse the degradation of these properties to an extent.<sup>13,16</sup> Chemical, thermal, and electrochemical reduction techniques have shown an increase in the carbon-to-oxygen (C:O) ratio from ~2:1, initially after oxidation, to as high as 10.3:1 and 23.9:1 for chemical and electrochemical reductions respectively.<sup>13</sup> However, as indicated by the C:O ratios, it is not possible to eliminate all oxygen functionalities. Moreover, all of these reduction techniques have negative drawbacks. Chemical reduction leaves structural defects in the form of introducing heteroatom impurities that interrupt the SP<sup>2</sup> network.<sup>13</sup> Thermal reduction leaves structural defects in the form of holes and topological defects that also disrupt the SP<sup>2</sup> network.<sup>13</sup> Electrochemical reduction appears to be the most mild in terms of disrupting the SP<sup>2</sup> network but the reduced GO sheets deposit onto the electrodes making bulk production difficult.<sup>13</sup> Although current reduction techniques can approach the structure of PG from GO, it is not possible to produce truly pristine graphene from graphene oxide using current techniques; it is only possible to approach the structure of PG.

However, the polarity of unreduced GO might make it ideal for homogenous dispersions in more polar polymers such as PA-11. Lahiri et al.<sup>10</sup> claim to have dispersed unoxidized graphene sheets into ultrahigh molecular weight polyethylene (UHMWPE) achieving very homogenous composite systems. Unoxidized graphene sheets are compatible in UHMWPE because of the highly non-polar polymer matrix. In addition to homogeneity, this group achieved very impressive tensile improvements especially at concentrations of GO as low as 0.1% by weight.<sup>10</sup> At higher concentrations, the GO sheets became aggregated resulting in less homogenous dispersions and degradation of tensile properties.<sup>10</sup> However, it is doubtful that the

Lahiri group achieved complete exfoliation of graphite particles via sonication as will be elaborated later. Compton, et al.<sup>11</sup> published another interesting paper where GO particles were functionalized with phenyl isocyanate, thermally reduced, and successfully dispersed in polystyrene films. Since the oxygen groups were functionalized with phenyl isocyanates, the GO sheets are non-polar and are compatible with a non-polar polystyrene matrix. This group studied the effects on the solubility and permeability of oxygen through the GO/polystyrene composites.<sup>11</sup> The results consisted of an unprecedented reduction in oxygen solubility and permeability at just 0.02% by volume.<sup>11</sup> These results deviate drastically from all existing mathematical models for permeability and show that these functionalized GO particles were as effective at reducing oxygen permeability as clay-based nanoparticles at ~25-30 times higher concentrations.<sup>11</sup> Both papers have important implications for GO/polyamide-11 composites.

Our work here in Kranbuehl lab has studied the mechanical properties and hydrolysis of PA-11 for some time now in an effort to improve the safety and efficiency of risers in offshore oil production. Given the results from these previous papers by Lahiri et al. and Compton et al., I concluded that graphene oxide had enormous potential for use in a GO/PA-11 composite. I hypothesized that unreduced GO particles dispersed in PA-11 should increase the tensile properties, decrease the diffusion of water into the polymer matrix, and in turn slow down or possibly even inhibit the aging process.



## Chapter 2: Instrumentation

### 2.1 Material Testing System (MTS)

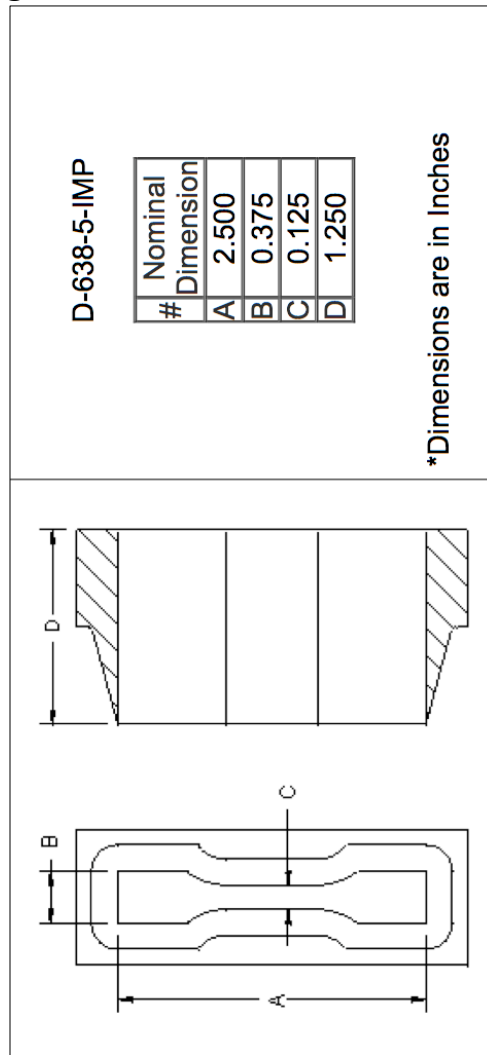
The tensile properties of the GO/PA-11 samples were examined using a Material Testing Systems MTS 810.<sup>2</sup> A strain rate of 0.25 inches/minute (6.35 mm/minute) was used for all tensile tests in this paper. The average strain rate was measured to be 6.34 mm/minute with a standard deviation of 0.06 mm/minute. Values such as the strain (percent elongation), Young's modulus, and tensile stress were calculated from the MTS data using a MATLAB program created by John Andrew Hocker. The instrument records time, strain, and force in a “.txt” file that is then entered into the MATLAB program along with the measurements taken during the sample preparation.<sup>2</sup>

#### 2.1.1 Theory

The act of stretching a material is known as “tensioning.”<sup>n</sup> The stress ( $\sigma$ ) on a sample refers to the amount of perpendicular force applied per cross sectional area of sample in order to stretch it; this quantity has the units of pressure.<sup>17</sup> The amount that a sample stretches is known as the strain ( $\epsilon$ ) and is often represented as percent elongation.<sup>17</sup> These two quantities are related by the equation  $\sigma = E \cdot \epsilon$ .<sup>17</sup> The quantity “E” is known as the Young's modulus and is defined as the ratio of the stress over strain ( $E = \sigma/\epsilon$ ).<sup>17</sup> The modulus is a constant and is specific to a particular material.<sup>17</sup> Moreover, the modulus measures stiffness or a resistance to deformation in general.<sup>17</sup> This deformation (or stretching) is not to be confused with breaking.<sup>17</sup> Tensile properties such as the strain, Young's modulus, and stress are very useful in determining the engineering applications of a material. The average molecular weight ( $\bar{M}_w$ ), percent crystallinity, and temperature can vary these properties.<sup>2</sup>

Another factor that can cause variations in the tensile measurements is the geometry of the sample used.<sup>2</sup> There are a variety of geometries to choose from; each is suited to a particular material for a particular application. Because the GO/PA-11 samples are not brittle, the dog bone shape of the ASTM D-638 localizes the strain and applied force to an identifiable region of the dog bones.<sup>2</sup> Thus, this region should have a consistent cross section while stretching. All samples discussed in this paper were cut using the ASTM D-638-5-IMP test die.<sup>6</sup> Figure 2.1.1.1 below illustrates the die's dimensions.<sup>2</sup>

**Figure 2.1.1.1: ASTM D-638-5-IMP Dimensions**



The strain rate is yet another factor that greatly affects the measured tensile properties. If a sample is stretched too quickly, there will not be enough time for the polymer chains to stress-relax.<sup>2</sup> Thus, the polymer will likely break prematurely.<sup>17</sup> If the sample is stretched too slowly, the measurements will not represent the sample's mechanical properties in a typical use environment and result in an abnormally high resistance to breakage.<sup>2,17</sup> Therefore, the MTS 810 was preset to the 6.35 mm/minute strain rate mentioned earlier.

There are two methods to calculate the stress on a sample from the force readings given by the MTS 810.<sup>2</sup> The first consists of dividing the force by the initial cross-sectional area of the dog bone's tensile region to give the stress on a sample at that time.<sup>2</sup> The operator can use a caliper to measure the average thickness and width of the dog bone in the tensile region. The length of the dog bone would only be necessary to calculate the strain if the instrument did not already record that in the output file. The problem with this calculation is that it does not account for the reduction in cross sectional area as the dog bone stretches.<sup>2</sup> Calculating the stress on a sample by using the original cross sectional area is known as the "engineering stress."<sup>2</sup> This calculation results in an underestimation of the actual stress applied to a material since its cross sectional area continuously decreases.<sup>2</sup> To calculate the "true stress," the researcher can assume that the volume of the tensile region in the dog bone remains constant beginning with equation 2.1.1.1.<sup>2</sup>

$$V_{initial} = L_{initial} \cdot A_{initial} \quad (2.1.1.1)$$

Given that the volume remains constant, equation 2.1.1.1 becomes equation 2.1.1.2.<sup>17</sup>

$$V_{initial} = V_{time} \quad (2.1.1.2)$$

Here,  $V_{time}$  is the volume at any time during the experiment.<sup>2</sup> Combining equations 2.1.1.1 and 2.1.1.2 results in equation 2.1.1.3.<sup>2</sup>

$$L_{initial} \cdot A_{initial} = L_{time} \cdot A_{time} \quad (2.1.1.3)$$

Solving for  $A_{time}$  gives equation 2.1.1.4.<sup>2</sup>

$$A_{time} = \frac{L_{initial} \cdot A_{initial}}{L_{time}} \quad (2.1.1.4)$$

This equation allows the researcher to calculate the stress at any time during the experiment because the MTS 810 records strain along with the time and applied force.<sup>2</sup>

Another correction that must be made is referred to as the Morten's modulus correction. This correction accounts for stretching of the dog bone between where the hydraulic clamps grip the sample and where the tensile region begins. The dog bone is divided into three sections on either side of the tensile region. The tensile region ( $l_1$ ) is 12 mm in length and 4 mm wide. Thus, cross sectional area of the tensile region is  $A_1 = 4 \cdot t$  where  $t$  is the thickness. The next section is the neck region between the tensile region and the head of the dog bone where the width increases gradually. Both neck regions are approximately 6.5 mm in length giving a total length of 13 mm ( $l_2$ ) and an average width of 7 mm. The cross sectional area of the neck region is approximately given by  $A_2 = 7 \cdot t$ . The third region is the region between the "cut" where the neck begins to the edge of where the hydraulic clamps gripped the dog bone. Measuring the lengths of this region on both sides of the dog bone gives ( $l_3$ ). The width in this head region is approximately 10 mm giving a cross sectional area of  $A_3 = 10 \cdot t$ . As mentioned before, the stress is given by the applied force divided by the cross sectional area as shown in equation 2.1.1.5.<sup>17</sup>

$$\sigma = \frac{F}{A} \quad (2.1.1.5)$$

From the preceding information, the total strain would be the sum of the strain in each section of the dog bone shown in equation 2.1.1.6.

$$\varepsilon_{tot} = \sum \varepsilon_i = \varepsilon_1 \cdot l_1 + \varepsilon_2 \cdot l_2 + \varepsilon_3 \cdot l_3 \quad (2.1.1.6)$$

Substituting the strain terms in equation 6 for the modulus and stress gives equation 2.1.1.7.

$$\varepsilon_{tot} = \left( \frac{1}{E_{correct}} \right) \cdot (\sigma_1 \cdot l_1 + \sigma_2 \cdot l_2 + \sigma_3 \cdot l_3) \quad (2.1.1.7)$$

Rearranging equation 2.1.1.7 and substituting the stress terms for the quantity in equation 2.1.1.5 gives equation 2.1.1.8.

$$E_{correct} = \frac{Force}{\varepsilon_{tot}} \left( \frac{l_1}{A_1} + \frac{l_2}{A_2} + \frac{l_3}{A_3} \right) \quad (2.1.1.8)$$

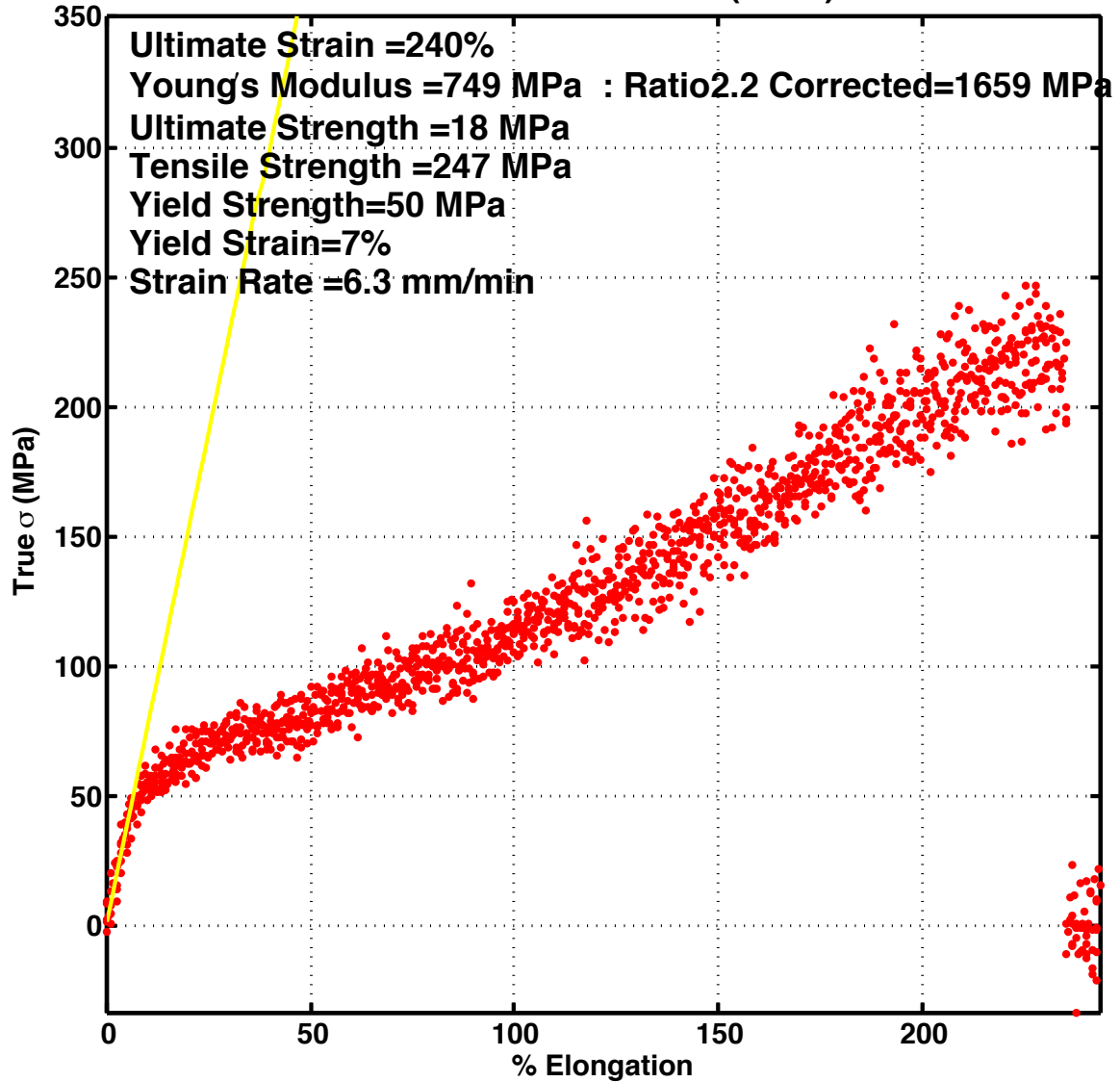
A conversion factor is given by the ratio of the corrected modulus over the original modulus in equation 2.1.1.9.

$$Correction\ Factor = \frac{E_{correct}}{E_{original}} \quad (2.1.1.9)$$

The correction factor typically seen throughout this paper on all samples is ~2 indicating that there is significant stretching outside of the tensile region that equation 2.1.1.8 takes into account. Most of this stretching appears to be localized in the neck region and not the head region where the MTS clamps the dog bones.

Once the stress and strain are calculated at each measurement time, the stress can be plotted versus the strain to get a stress-strain curve.<sup>2</sup> The global maximum of stress on this curve is referred to as the tensile stress or tensile strength.<sup>17</sup> This quantity refers to the ultimate load that a material can handle before breaking.<sup>17</sup> Again, breaking is not to be confused with stretching. The modulus is calculated by taking the slope of the initial linear region of a true stress-strain curve.<sup>2</sup> A typical stress-strain curve is shown in Figure 2.1.1.2 below.

Figure 2.1.1.2: Stress-Strain Curve of a Neat PA-11 System  
DB 0715 PA-11 Crosscut aged in DI Water  
@ Concentration Neat  
Aerobic Ambient C (DB A)



### **2.1.2 Sample Preparation**

After the GO/PA-11 samples were polymerized, they were cut into dog bones using the ASTM D-638-5-IMP test die and a Carver Laboratory Press Model C.<sup>2</sup> Great care was taken examining the films for surface defects such as creases, bubbles, and cracks. If the samples did have any creases, cracks, or bubbles, that region of the film was avoided for cutting. If the defect in the film could not be avoided, the dye was placed so that the defect would be in one of the two head regions rather than the critical tensile region of the dog bone.

Then the cut dog bones were carefully measured with a mechanical caliper. Three width measurements were taken at equidistant points inside the tensile region of the dog bone. These widths were then averaged together. Then a total of four thickness measurements were taken on either side of two equidistant points in the tensile region of the dog bone. These thickness measurements were also averaged together. Multiplying the average width times the average thickness gives the rectangular cross sectional area to calculate the stress.

## 2.2 Size Exclusion Chromatography – Multi-Angle Laser Light Scattering

The apparatus used to determine molecular weights ( $\bar{M}_w$ ) of GO/PA-11 samples in this paper was a High Performance Liquid Chromatography (HPLC) system using in-line Size Exclusion Chromatography (SEC) columns that are coupled with a Multi-Angle Laser Light Scattering (MALLS) system.<sup>2</sup> Both systems provide two separate  $\bar{M}_w$  readings to ensure an accurate measurement of each sample. The solvent used to dissolve the polymer samples and to serve as the mobile phase is 1,1,1,3,3,3-hexafluoroisopropanol (HFIP).<sup>2</sup> The SEC system uses HFIP-LG, and HFIP-805, and HFIP-803 columns made by Shodex in Japan.<sup>2</sup> The HPLC/SEC system is fed by a Waters 515 model pump with a flow rate of 0.6 mL/minute.<sup>2</sup> The pump reservoir is constantly sparged with Helium under atmospheric pressure.<sup>2</sup> A Wyatt Optilab 803 dynamic Refractive Index (RI) detector is in-line with the SEC columns to measure the eluent.<sup>2</sup> The light scattering detector used for the MALLS instrument is the Wyatt miniDAWN with a wavelength ( $\lambda$ ) of 690 nm with scattering angles ( $\theta$ ) of 45°, 90°, and 135°.<sup>2</sup>

### 2.2.1 Size Exclusion Chromatography Theory

The SEC method is essentially a process for separating macromolecules according to their size.<sup>17</sup> The solute particles in a good solvent are not closed clusters of bare polymer chains but rather random, open coils of single polymer chains that are fully solvated by solvent molecules.<sup>17</sup> Because each random coil of a polymer chain has a size (chain length) that is proportional to its molecular weight ( $\bar{M}_w$ ), separating each polymer chain according to its size will also separate—or “fractionate”—each polymer chain according to its molecular weight.<sup>2,17</sup> The concentrations of each of these fractions can then be weighted and averaged to obtain  $\bar{M}_w$ .

A system commonly used to separate these random coil particles by their size—and the one used in this paper—consists of solid, cross-linked, polystyrene-divinyl benzene copolymer



beads where the cross-links serve as porous openings.<sup>17</sup> Although these cross-linked polymer beads do not dissolve in the solvent, the solvent (HFIP) is compatible with the polymer segments and causes these beads to swell.<sup>2,17</sup> When the beads swell, the pores open to a definite diameter.<sup>17</sup> As the dissolved solute particles flow past these beads, particles larger than the pore sizes of the beads are uninhibited and elute first.<sup>17</sup> Dissolved particles that are on the scale of the pore diameters or smaller permeate the pores to varying degrees.<sup>17</sup> It is important to note that particles smaller than the pore diameters are still separated by their molecular weights because the smallest particles will be able to travel the furthest into the porous tunnels of the beads.<sup>17</sup> Dissolved polymer particles with sizes on the order of the pore diameters will merely “sample” the pores before continuing through the columns.<sup>17</sup> Thus, even a column with beads of a single pore size would be able to fractionate a relatively polydispersed sample.

However, fractionating of a polymer sample is made more effective by using multiple columns in series with beads of different pore sizes.<sup>17</sup> In Kranbuehl lab for example, three columns are used; each with a different stationary phase to serve a different purpose. The HFIP-LG column serves to capture destructive impurities before they reach the more expensive analytical columns but does negligible fractionation.<sup>3</sup> Following this column is the HFIP-805 column that contains beads that fractionate at  $4 \times 10^6$  g/mol polystyrene exclusion limit.<sup>3</sup> Then the eluent passes through the HFIP-803 column with the smallest pore sizes that fractionate at  $7 \times 10^4$  g/mol polystyrene exclusion limit.<sup>3</sup> Thus, the resolution of the fractionating process is greatly improved with multiple columns in series.

After passage through the column system, the detection method used in this paper is an RI measurement.<sup>2</sup> The RI detector mentioned previously measures the difference in the refractive index between the eluted solution and the pure solvent.<sup>17</sup> Assuming that the RI difference

between polymer and solvent only depends on concentration and not molecular weight, plotting the RI as a function of time shows the molecular weight fractions as a series of peaks.<sup>17</sup>

Because SEC fractionation is a secondary method of molecular weight determination, it requires calibration with a monodispersed, polymer standard with a known molecular weight.<sup>17</sup> Usually, this polymer standard can even be a different polymer than the one being analyzed because most polymers have a universal calibration parameter that relates different polymers based upon their size.<sup>17</sup> This parameter is the product of the intrinsic viscosity and the monodispersed molecular weight:  $[\eta] \cdot M$ .<sup>17</sup> This parameter is proportional to the root-mean square end-to-end distance of a random coil particle.<sup>17</sup> Therefore, plotting  $\text{Log}([\eta] \cdot M)$  versus elution volume provides a calibration curve. The assumption that the universal calibration parameter is the same for all polymers at the same elution volume yields equation 2.2.1.1.<sup>17</sup>

$$\log([\eta]_x \cdot M_x) = \log([\eta]_s \cdot M_s) \quad (2.2.1.1)$$

The subscripts x and s indicate the unknown and the standard respectively.<sup>17</sup> Substituting for the intrinsic viscosity via the Mark-Houwink relationship shown in equation 2.2.1.2 gives equation 2.2.1.3.<sup>17</sup>

$$[\eta]_j = K_j M_j^{a_j} \quad (2.2.1.2)$$

$$\text{Log}(M_x) = \left(\frac{1}{1+a_x}\right) \text{Log}\left(\frac{K_s}{K_x}\right) + \frac{1+a_s}{1+a_x} \text{Log}(M_s) \quad (2.2.1.3)$$

In equation 2.2.1.2, K and a are both constants unique to a specific polymer and must be either pre-determined or listed in the literature.<sup>17</sup> Given that these constants are known, equation 2.2.1.3 would ideally provide an excellent way to relate the molecular weights of two different polymers with the same elution volumes.<sup>17</sup>

However, this universal calibration method does not work with PA-11 and non-polar SEC columns such as the ones we use in Kranbuehl lab.<sup>18</sup> Laun, et al.<sup>19</sup> showed that hydrophobic

interactions with the relatively less polar carbon backbone of PA-11 and the non-polar polystyrene based beads leads to greater elution volumes per calibration parameter value. Instead, we create a calibration curve by plotting the monodisperse  $M_w$  of each fraction—measured by light scattering—to the elution volumes from the SEC system.<sup>18</sup> There was one complication with this technique. Eluted chains with the same molecular weight had higher elution volumes with higher *average*  $\bar{M}_w$  samples.<sup>18</sup> Although the slopes of the curves remained constant, the intercepts of the curves shifted.<sup>18</sup> Thus John Andrew Hocker derived a function to account for this shift in the intercept shown in equation 2.2.1.4.<sup>18</sup>

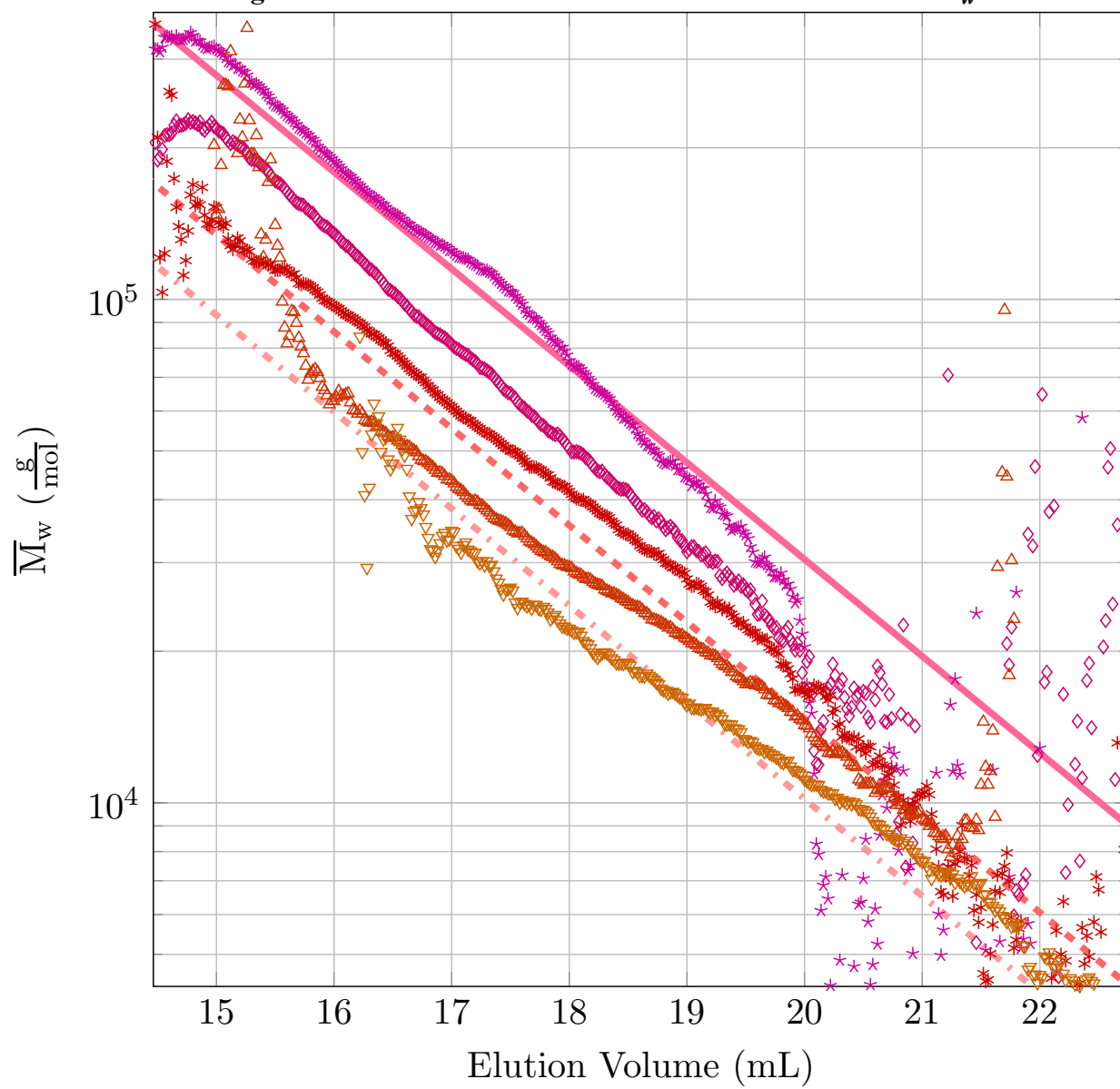
$$\ln(M_w) = m_{EF} \cdot X_v + (m_{\bar{M}_w} \cdot \ln(X_{\bar{M}_w}) + b_{\bar{M}_w}) \quad (2.2.1.4)$$

The symbols in this equation are as follows:  $M_w$  is the molecular weight at each fraction;  $m_{EF}$  is the average slope determined from the calibration curves;  $X_v$  is the elution volume;  $m_{\bar{M}_w}$  is the ratio of the intercept over the average molecular weight ( $\bar{M}_w$ ) and is thus the slope of the function that calculates the intercept in parentheses;  $X_{\bar{M}_w}$  is the average  $\bar{M}_w$ ;  $b_{\bar{M}_w}$  is the intercept of the function calculating the intercept for equation 2.2.1.4.<sup>18</sup> The average slope of the curves along with the function calculating the intercepts were derived from a total of 39 samples of lab polymerized and commercial PA-11.<sup>18</sup> Thus, equation 2.2.1.4 provides a relationship between the measured elution volumes of any PA-11 sample and all 39 calibration curves.<sup>18</sup>

To ensure accurate results and that the SEC system is calibrated, a polymer standard with a known molecular weight was run bi-weekly. The two standards used were BESNO P-40TLOS PA-11 granules and a polymethyl methacrylate (PMMA) standard produced by Polymer Laboratories.<sup>3</sup> The PA-11 standard has an independently tested  $\bar{M}_w$  of  $39,000 \pm 2,000 \frac{g}{mol}$  while the PMMA standard has an independently verified  $\bar{M}_w$  of  $28,900 \pm 1,000 \frac{g}{mol}$ .<sup>3</sup> The accuracy of

the SEC system was determined by performing six runs on a solution of commercial PA-11—mentioned above—and a solution of neat PA-11 that we polymerized.<sup>18</sup> The commercial PA-11 samples resulted in a  $\bar{M}_w$  with a standard deviation of  $\pm 3 \frac{Kg}{mol}$  ( $\pm 2\%$ ) while the polymerized samples resulted in a standard deviation of  $\pm 4 \frac{Kg}{mol}$  ( $\pm 6\%$ ).<sup>18</sup> This method yielded the most precise  $\bar{M}_w$  for both commercial and polymerized samples.<sup>18</sup> Figure 2.2.1.1 shows a plot of five of the 39 calibration samples having molecular weights ( $\bar{M}_w$ ) of  $147,470 \frac{g}{mol}$ ,  $96,780 \frac{g}{mol}$ ,  $52,140 \frac{g}{mol}$ ,  $24,340 \frac{g}{mol}$ , and  $12,180 \frac{g}{mol}$  respectively.<sup>18</sup>

Figure 2.2.1.1: SEC Calibration Curves With 5 Different  $\bar{M}_w$ s



Several potential issues can arise in SEC that were avoided in our particular apparatus. First, the polystyrene-divinyl benzene copolymer beads are hydrophobic so as to prevent the hydrophilic polyamide particles from chemically adsorbing onto the surface of the beads.<sup>17</sup> Adsorption onto the beads would cause clogging of the columns or a severely distorted elution pattern.<sup>17</sup> Secondly, the Waters 515 pump has dual plungers that can lead to fluctuations of 5-10 psi.<sup>2</sup> These fluctuations could cause signal noise in the elution patterns.<sup>2</sup> To mitigate this effect, 0.005" (interior diameter) Stainless Steel tubing was added post-detector to increase the pressure of the system to ~500 psi.<sup>3</sup> At this high pressure, the small fluctuations become negligible and the flow rate through the columns remains roughly constant. Lastly, to prevent any large and damaging contaminants such as dust particles from getting into the SEC system, the injected sample first passes through a 2  $\mu\text{m}$  filter—also known as a “frit”—with a 1/8" outside diameter.<sup>3</sup> Whenever this frit became clogged, the pressure would spike and the frit was replaced.<sup>3</sup>

### **2.2.2 Multi-Angle Laser Light Scattering Theory**

After the polymer solution elutes from the SEC system, it then passes through the MALLS system where a light scattering measurement of each fraction is recorded.<sup>2</sup> Unlike the SEC technique, Light Scattering is a primary method of determining the  $\bar{M}_w$  of a polymer.<sup>17</sup>

Lord Rayleigh was the first to describe the light scattering properties of a dilute gas by showing that the intensity of scattered light is directly proportional to the angle of scattered light—relative to the incident beam—and the molecular weight of the gas.<sup>17</sup> Later, Albert Einstein modified Rayleigh's equation for use on liquids.<sup>17</sup> The problem with liquids is that there are strong intermolecular forces—such as London dispersion forces, dipole forces, and hydrogen bonding—that are not present in gases.<sup>17</sup> Einstein compensated for these effects by showing that light scattering in liquids arose from local fluctuations in the density due to random, thermal

motions of molecules; these local density fluctuations result in fluctuations in refractive index and thus scatter light more so than in gases.<sup>17</sup> When investigating solutions, an additional problem arises in that there are local fluctuations in the concentration of solute.<sup>17</sup> Peter Debye further modified Rayleigh's original equation to account for the local fluctuations in refractive index due to local fluctuations in concentration of solute.<sup>17</sup> However, Debye also found that these fluctuations in concentration correspond to changes in the osmotic pressure.<sup>20</sup> Debye's relationship describing the excess scattering caused by only the solute is illustrated in equation 2.2.2.1.<sup>17,20</sup>

$$R'(\theta) = \frac{2\pi^2 n_0^2 (n - n_0)^2 [1 + \cos^2(\theta)] RT}{\lambda^4 N_A C \left(\frac{\delta P}{\delta C}\right)_T} = \frac{i'(\theta) r^2}{I_0} \quad (2.2.2.1)$$

The variables in the equation are as follows:  $n_0$  is the refractive index of the pure solvent;  $n$  is the refractive index of solution;  $\theta$  is the angle between the incident ray of light and the scattered ray of light;  $R$  is the universal gas constant;  $T$  is the temperature;  $i'(\theta)$  is the intensity of scattered light per unit volume of the system that is detected at angle  $\theta$  to the incident beam;  $r$  is the path length of the system;  $\lambda$  is the wavelength of the incident light;  $N_A$  is Avogadro's number;  $C$  is the concentration of solution;  $P$  is the osmotic pressure of the solution; and  $I_0$  is the intensity of incident light.<sup>17</sup>

In order to find the molecular weight with equation 2.2.2.1, a few modifications must be made. The "turbidity" of a solution is defined as the decrease in the intensity of a beam of light because of only scattering.<sup>17</sup> This quantity is represented in equation 2.2.2.2.<sup>17</sup>

$$\tau = \frac{I'_s}{I_0} \quad (2.2.2.2)$$

In this equation,  $I'_s$  is the total intensity of light that is scattered per unit path length through the system.  $I_0$  is the intensity of the incident light. Notice that the quantity in equation 2.2.2.1 is the

ratio of the intensity of scattered light at angle  $\theta$  per unit path length  $r$  over the intensity of incident light.<sup>17</sup> Therefore, integrating equation 2.2.2.1 over all angles of polar coordinates gives equation 2.2.2.3.<sup>17</sup>

$$\tau = \frac{I'_s}{I_0} = \frac{32\pi^3 n_0^2 (n-n_0)^2 RT}{3\lambda^4 N_A c \left(\frac{\delta P}{\delta c}\right)_T} \quad (2.2.2.3)$$

Rearranging this equation gives equation 2.2.2.4.<sup>17</sup>

$$\frac{Hc}{\tau} = \frac{1}{RT} \left(\frac{\delta P}{\delta c}\right)_T \quad (2.2.2.4)$$

The value of H is given by equation 2.2.2.5.<sup>17</sup>

$$H = \frac{32\pi^3 n_0^2}{3\lambda^4 N_A} \left(\frac{n-n_0}{c}\right)^2 \quad (2.2.2.5)$$

Finally, substitution of  $\left(\frac{\delta P}{\delta c}\right)_T$  with the virial expansion for osmotic pressure gives equation 2.2.2.6.<sup>17,20</sup>

$$\frac{Hc}{\tau} = \frac{1}{\bar{M}_w} (1 + 2\Gamma c + 3g\Gamma^2 c^2 + \dots) \quad (2.2.2.6)$$

In this equation,  $\Gamma$  is the 2nd virial coefficient and  $g\Gamma^2$  is the 3<sup>rd</sup> virial coefficient.<sup>17</sup> Thus, extrapolating equation 2.2.2.6 in the limit of infinite dilution under this model ideally gives the reciprocal of  $\bar{M}_w$ .<sup>17</sup>

However, equation 2.2.2.6 does not account for macromolecular size of the polymer chains.<sup>17</sup> If the average size of the largest dimension of the polymer chains is longer than  $\lambda/20$ , then a dissymmetry of scattered light about  $90^\circ$  will be observed.<sup>17</sup> This dissymmetry is due to destructive interference of light scattered off of the same polymer chain.<sup>17</sup> Two rays of light that are initially in phase from the source travel different path lengths as they are scattered off of different parts of the same polymer chain and arrive at the detector out of phase to some degree.<sup>17</sup> The path length difference between two rays approaches zero as  $\theta$  between the incident



and scattered rays approaches zero resulting in no intra-particle, destructive interference.<sup>17</sup>

However as  $\theta$  increases, the path length difference between the two rays increases meaning that the destructive interference is greater at  $180^\circ - \theta$  (the backward direction) than it is at  $\theta$  (forward direction).<sup>17</sup> This effect results in a disproportionate lack of intensity in the rear direction.<sup>17</sup> Thus, equation 2.2.2.7 includes a scattering function— $P(\theta)$ —that approaches 1 as  $\theta$  approaches  $0^\circ$ .<sup>17</sup>

$$\frac{Kc}{R(\theta)} = \frac{1}{\bar{M}_w P(\theta)} + \frac{2\Gamma c}{\bar{M}_w} + \frac{3g\Gamma^2 c^2}{\bar{M}_w} + \dots \quad (2.2.2.7)$$

It is important to note that the Debye form of the Rayleigh ratio is used and not the integrated form since the scattering function must be taken into account at each angle.<sup>17</sup> The quantity K is given by equation 2.2.2.8.<sup>17</sup>

$$K = \frac{2\pi^2 n_0^2}{\lambda^4 N_A} \left( \frac{n - n_0}{c} \right)^2 \quad (2.2.2.8)$$

One can solve for  $\bar{M}_w$  by extrapolating equation 2.2.2.7 in the limit that  $c$  and  $\theta$  approach zero.<sup>17</sup>

A plot of the left side of equation 2.2.2.7 versus  $c$  and  $\theta$  is known as a Zimm plot; the intercept that results from both limits extrapolated to zero gives the reciprocal of  $\bar{M}_w$ .<sup>17</sup> It is important to reiterate the fact that the molecular weight calculated is the weight averaged molecular weight ( $\bar{M}_w$ ) since heavier matter scatters light more than lighter matter when controlling for concentration as indicated by the original Rayleigh ratio for gases.<sup>17</sup>

In our lab however, the solutions entering the MALLS system can already be assumed to be very dilute since they are fractionated in the SEC system.<sup>3</sup> This very dilute solution provides a very good approximation of zero concentration that can be used to simplify equation 2.2.2.7. Therefore, we only need to extrapolate  $\theta$  to zero in what is known as a Debye plot.<sup>3</sup> Expanding the  $P(\theta)$  used for GO/PA-11 samples in our lab from equation 2.2.2.7 gives equation 2.2.2.9.<sup>2</sup>

$$\frac{Kc}{R'(\theta)} = \frac{1}{\bar{M}_w} \left( 1 + \frac{16\pi^2}{3\lambda^2} \langle r_g^2 \rangle \sin^2 \left( \frac{\theta}{2} \right) \right) \quad (2.2.2.9)$$

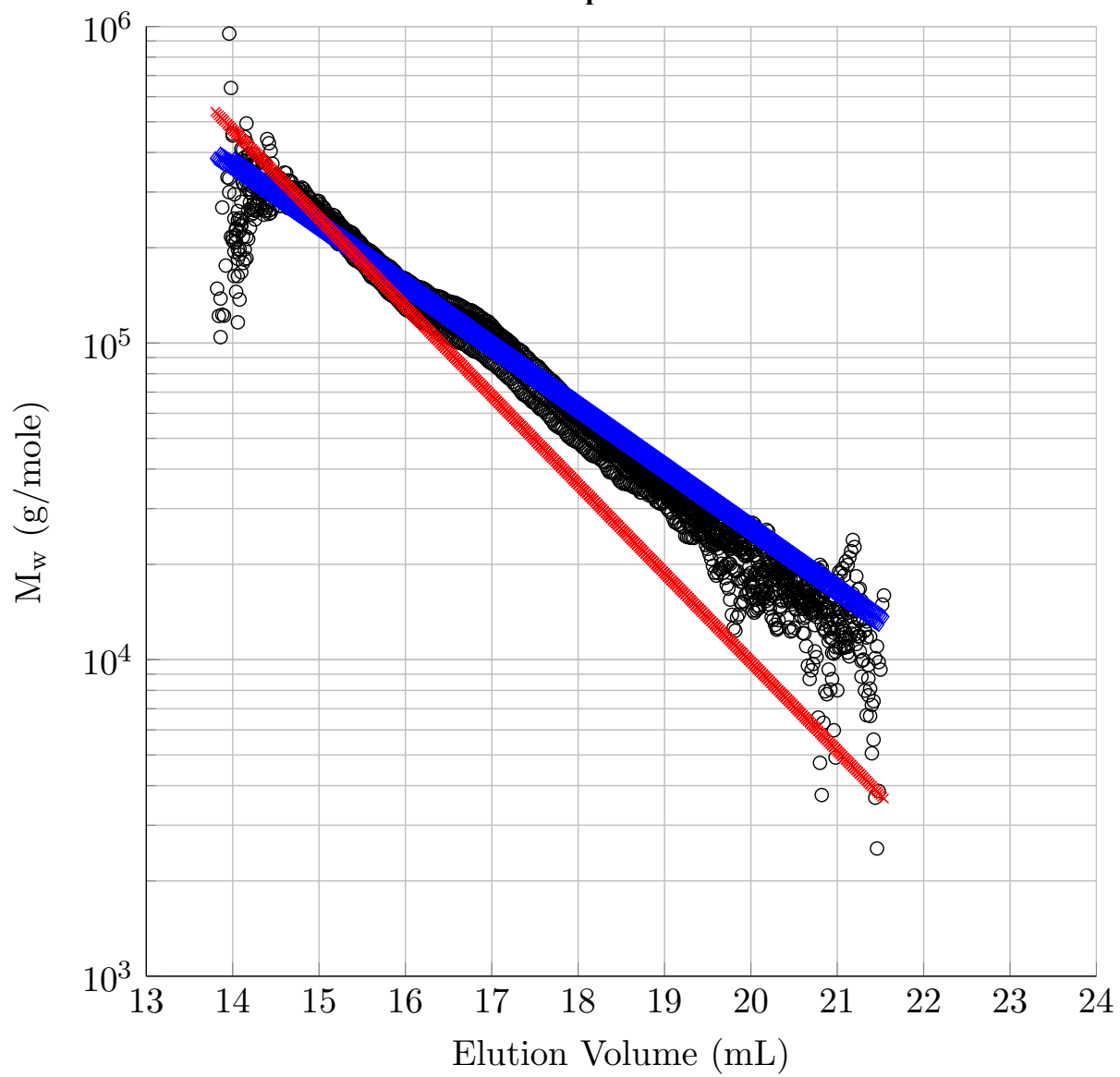
In this equation,  $\langle r_g^2 \rangle$  is the mean square radius of gyration.<sup>2</sup> For the purposes in our lab, K is represented as equation 2.2.2.10.<sup>2</sup>

$$K = \frac{4\pi^2 n_0^2}{\lambda^4 N_A} \left( \frac{dn}{dc} \right)^2 \quad (2.2.2.10)$$

In this case, the quantity  $\left( \frac{n-n_0}{c} \right)$  is replaced by  $\left( \frac{dn}{dc} \right)$  as the refractive index increment of polymer in a solvent.<sup>2</sup> The  $\left( \frac{dn}{dc} \right)$  value for PA-11 in HFIP is 0.253.<sup>2</sup>

The accuracy of the MALLs instrument was determined by the same methods as for the SEC instrument described earlier. The standard deviation for the Commercial PA-11 was found to be  $\pm 6 \frac{Kg}{mol}$  ( $\pm 6\%$ ) while the standard deviation for the samples that we polymerized was found to be  $\pm 8 \frac{Kg}{mol}$  ( $\pm 13\%$ ).<sup>18</sup> Figure 2.2.2.1 below shows the calculated  $\bar{M}_w$ s verses elution volume for the SEC (in blue), light scattering (black dots), and SEC without the intercept shift correction (in red).<sup>18</sup>

**Figure 2.2.2.1: SEC-Corrected, MALLS, and SEC-Uncorrected Curves For a Commercial PA-11 Sample**



### 2.2.3 Sample Preparation

The procedure for preparing an SEC-MALLS injection began with drying all GO/PA-11 samples in a 100 C<sup>o</sup> oven for 1 hour. After drying, the samples were weighed and dissolved in HFIP at a concentration of 2 mg/mL<sup>2</sup>. Without filtering, the large GO particles would have the potential to clog the frit, clog the SEC columns, and distort the light scattering measurements. Thus, we first filtered the GO/PA-11 solutions by extracting the solution into a syringe and then pushing the solution back out through a syringe filter into the solution vial. The syringe filters used were Phenomenex 0.45 μm Polytetrafluoroethylene (PTFE) hydrophobic syringe filters with a 25 mm diameter polypropylene casing. Then a solution sample of 100 μL was injected.<sup>3</sup>

## 2.3 Differential Scanning Calorimetry (DSC)

The Differential Scanning Calorimeter used to test all GO/PA-11 samples in this paper was a Thermal Advantage DSC Q20. We used aluminum DSC Consumables Incorporated pans. The analysis for all samples was done in Thermal Advantage Universal Analysis with integration limits set at 140 C° to 200 C°.

### 2.3.1 Theory

Because PA-11 is a semi-crystalline polymer, it is important to characterize the crystallinity of all GO/PA-11 samples to eliminate crystallinity as a variable when examining its mechanical properties.<sup>17</sup> Semi-crystalline polymers are generally tougher than totally amorphous ones.<sup>17</sup> Moreover, they can be bent more without breaking, they resist impact better, they are more dense, and they are less affected by temperature changes or solvent penetration than completely amorphous polymers.<sup>17,20</sup> Thus, we must control for crystallinity in order to isolate a relationship between the GO concentration and the mechanical and chemical properties.

Semi-crystalline polymers are characterized as containing small domains where the polymer chains have formed ordered, three-dimensional lattice structures due to intermolecular attractions.<sup>17</sup> These intermolecular attractions include London dispersion forces, dipole-dipole interactions, and hydrogen bonding.<sup>17</sup> In this context, these crystalline domains can be viewed as pseudo cross-links holding the polymer chains together especially since they have a similar toughening and stiffening effect as actual cross links below the crystalline melting temperature ( $T_m$ ).<sup>17</sup> However, it is important to note that the surrounding amorphous matrix consists of randomly entangled polymer chains.<sup>17</sup>

In order for crystallization to occur, the process must be thermodynamically and kinetically favorable. To be thermodynamically favorable, the free energy change ( $\Delta G_{T,P}$ ) at

constant temperature indicated in equation 2.3.1.1 must be negative for the process to be spontaneous.<sup>17</sup>

$$\Delta G_{T,P} = \Delta H - T\Delta S \quad (2.3.1.1)$$

Because crystallization consists of the ordering of polymer chains, the entropy term ( $\Delta S$ ) is obviously negative.<sup>20</sup> This means that not only does the change in enthalpy ( $\Delta H$ ) have to be negative, but the temperature must also be low enough so that the free energy change remains negative.<sup>20</sup> At the polymer melting temperature ( $T_m$ ),  $T = \frac{\Delta H}{\Delta S}$  and the free energy change is zero indicating a system at equilibrium.<sup>17</sup> The obvious conclusion from this is that decreasing the temperature makes the free energy change of crystallization more negative and more spontaneous.<sup>17</sup> However, as the temperature approaches the glass transition temperature ( $T_g$ ), the chains become much less mobile and are not able to attain the ideal conformations to form the ordered domains.<sup>17</sup> Once the temperature reaches  $T_g$ , crystallization is almost entirely quenched.<sup>17</sup> Therefore, there is a temperature between the  $T_m$  and the  $T_g$  at which the rate of crystallization goes through a maximum.<sup>17</sup> This temperature of maximum crystallization is given by equation 2.3.1.2.<sup>17</sup>

$$T_{\max\text{cryst.}} = T_g + \left(\frac{2}{3}\right)(T_m - T_g) \quad (2.3.1.2)$$

As hinted above, two properties of a polymer are required for crystalline domains to form: symmetry about the polymer chain and strong intermolecular attractions.<sup>20</sup> The negative enthalpy term in equation 2.3.1.1 represents the intermolecular forces required for crystallization.<sup>20</sup> In order for the polymer chains to obtain an ordered conformation where intermolecular forces are optimized, the chains themselves must have a symmetry that allows for close stacking of the chains.<sup>20</sup> It is important to note that a polymer need only have one of these

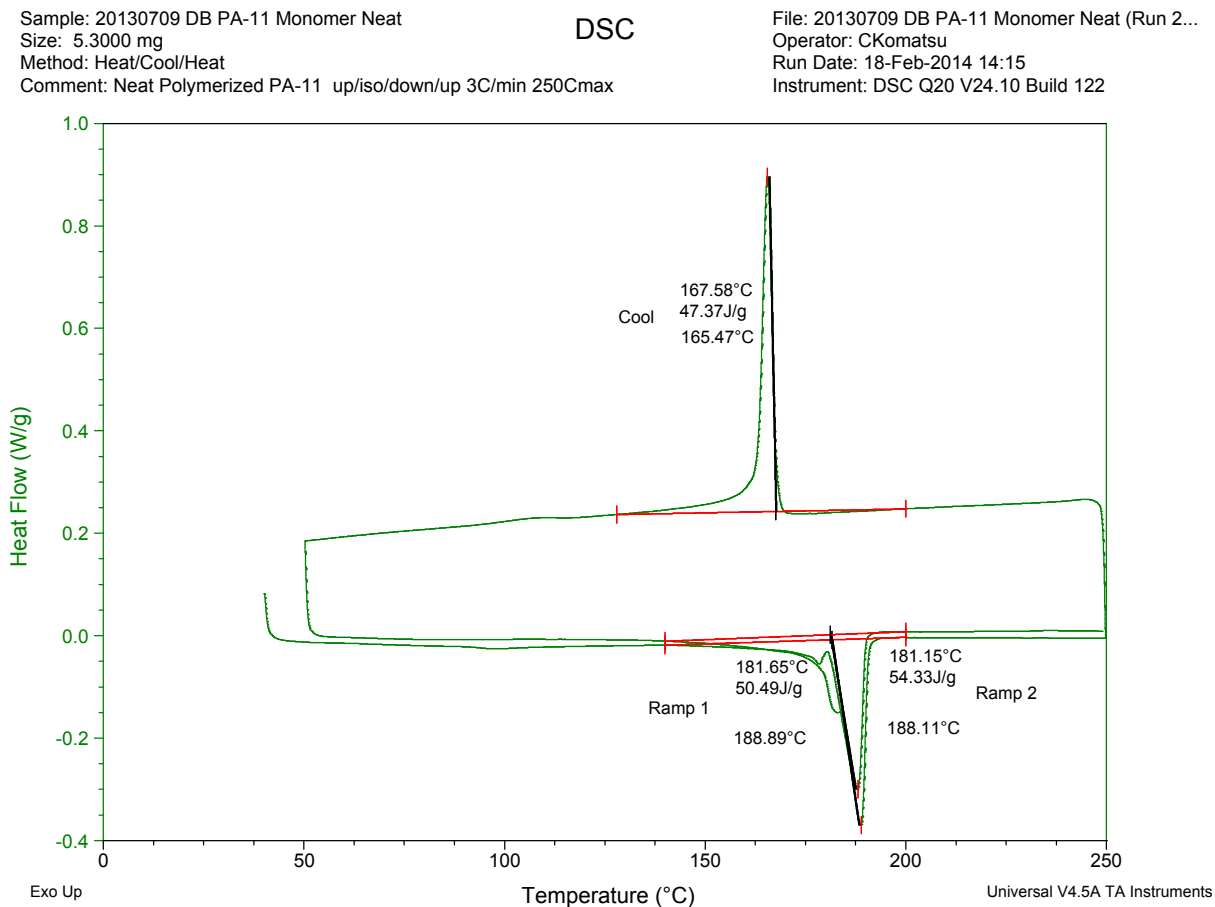
properties for crystallization—also known as “annealing”—to occur. Polyethylene for example has no functional groups for dipole or hydrogen bonding interactions but is linear and rod-like and tends to crystallize very well given little branching.<sup>20</sup> Polyamides on the other hand, while still relatively symmetric, rely more on strong intermolecular hydrogen bonding interactions for the crystalline domains to form.<sup>20</sup>

A differential scanning calorimeter (DSC) is the most common instrument to measure the amount of crystallinity in a polymer.<sup>17</sup> This instrument measures the change in enthalpy of a polymer sample inside of an aluminum pan compared to a reference aluminum pan with just air.<sup>17</sup> Since air is present inside both aluminum pans, any difference in the enthalpy changes between the two samples will be exclusively due to the polymer.<sup>17</sup> Any peak that the instrument plots indicates a “thermal event” where there is a difference in the change in enthalpy between the two pans.<sup>17</sup> The typical procedure is a heat ramp to above the  $T_m$  of a given polymer. Once the  $T_m$  is approached, the instrument plots a positive change in enthalpy in the pan with the polymer sample indicating the crystalline regions are melting.<sup>17</sup> For most polymers, a sharp, defined peak is observed for  $T_m$  unlike the  $T_g$ .<sup>17</sup> Weakly formed crystals melt at the lower temperature end of the peak while more well formed crystals melt at the higher temperature portion of the peak. Once the plot returns to the baseline, the peak can be integrated using software to get the total enthalpy in J/g of the melted crystalline domains.<sup>17</sup> This enthalpy is then divided by the change in enthalpy value for a 100% crystalline polymer standard—190 J/g for PA-11—and multiplied by 100 to yield the percent crystallinity of the polymer sample.<sup>2</sup>

In this paper, we not only wanted to know the crystallinity of each GO/PA-11 sample after it was polymerized but we also wanted to know how the GO concentration would affect the percent crystallinity. Thus, we used a procedure of one ramp at a rate of 3 C°/minute to 250 C°—

well above the  $T_m$  of PA-11—to ensure that all crystalline domains were melted. Then each GO/PA-11 sample was cooled at a rate of 3 C°/minute to 50 C° followed by another ramp to 250 C°. The first ramp gives the raw crystallinity of the polymerized and pressed GO/PA-11 sample but it also ensures that each sample has the same thermal history before the second ramp is conducted. Thus, the second ramp should indicate the effect of only the GO concentration on the annealing properties of the GO/PA-11 samples. Constant integration limits for all samples allows for a valid comparison of the enthalpy values. A typical DSC plot is shown in figure 2.3.1.1 below.

**Figure 2.3.1.1: DSC Plot of Neat PA-11 Sample**





### 2.3.2 Sample Preparation

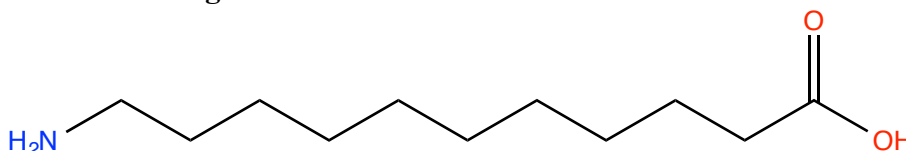
The GO/PA-11 sample masses were measured to 1/10000 of a gram using a Sartorius BP 221S scale. Because the DSC runs from the samples polymerized in the summer were taken out of the dog bones after they were stretched, care was taken not to cut the samples used in the DSC out of the tensile regions of the dog bones where the crystallinity would be different after stretching.<sup>17</sup> Thus, samples were taken from the head region near where the MTS 810 clamped the dog bone bone; there is theoretically negligible stretching in this region. The DSC runs from the samples polymerized in November were taken from other parts of the films that were not cut into dog bones. The procedure that was pre-programmed into the instrument was a ramp at 3 C°/minute to 250 C° followed by a cooling cycle at 3 C°/minute to 50 C° and then a second ramp to 250 C°.

## Chapter 3: Experimental

### 3.1 Synthesis of GO/PA-11 Samples

There were two different batches of GO/PA-11 composites that were polymerized and pressed under slightly different conditions. From now on in this paper, the GO/PA-11 composites that were polymerized from June 2013 – September 2013 will be known as the “summer samples.” The samples that were polymerized in November 2013 will be known as the “November samples.” The 11-Aminoundecanoic Acid monomer was supplied by Sigma-Aldrich and is depicted in Figure 3.1.0.1 below. The oven that was used to carry out both polymerizations was a Model 19 Precision Vacuum Oven. A Carver Laboratory Press Model C was used to heat press the polymerized samples into films.

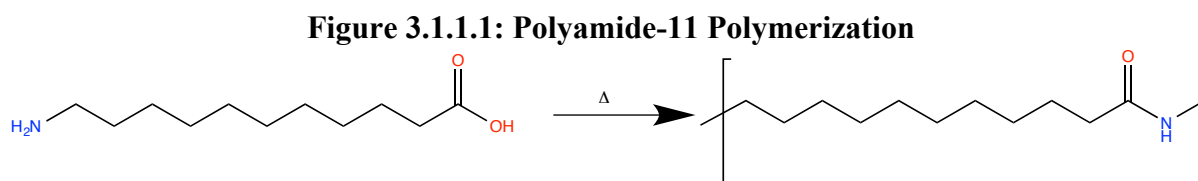
**Figure 3.1.0.1: 11-Aminoundecanoic Acid**



#### 3.1.1 Theory

The polymerization of 11-Aminoundecanoic Acid into Polyamide-11 is a Step Polymerization between the acid end of one monomer and the amine end of another monomer.<sup>1</sup> Essentially the monomer self-polymerizes given the proper heat input. Because a byproduct of the reaction is water, water must be constantly removed in order to drive the equilibrium of the polymerization reaction to the right.<sup>1</sup> Although cyclization is possible with bifunctional monomers such as 11-Aminoundecanoic Acid, it is not favorable when there is a high concentration of monomer.<sup>1</sup> In our case, the water that the monomer is dispersed in boils off before it reaches the polymerization temperature. We have observed that polymerization does not

happen to a significant extent until the reaction reaches at least  $\sim 220\text{ C}^\circ$ . Because the mechanism of polymerization is a Step Polymerization, high molecular weight is only obtained at high percent conversion.<sup>1</sup> This percent conversion is related to the time that the system polymerizes.<sup>1</sup> For our purposes, “polymerization time” refers to the time between when the oven is reaches  $190\text{ C}^\circ$  upon heating and the time when the oven reaches  $190\text{ C}^\circ$  upon cooling. We have also observed that oxidation of the PA-11 chains occurs when in the melt phase so the reaction is done in an inert atmosphere. The polymerization reaction of 11-Aminoundecanoic Acid into PA-11 is shown in Figure 3.1.1.1.



### Sample Preparation

We used a modified version of the Hummers’ method described in the introduction to synthesize the Graphene Oxide material. First, a 15 L battery jar was cooled to  $0\text{ C}^\circ$  in an ice bath and filled with 0.35 L of  $66\text{ C}^\circ$  concentrated sulfuric acid. Then 15 g of flake graphite was added in addition to 7.5 g of  $\text{NaNO}_3$ . While stirring vigorously, 45 g of  $\text{KMnO}_4$  was added slowly so as to not raise the temperature of the suspension above  $20\text{ C}^\circ$ . Then the battery jar was removed from the bath and maintained at  $\sim 35\text{ C}^\circ$  for 30 minutes. Afterwards, the mixture turned brownish gray and evolved some gas. Then 0.7 L of water was slowly stirred in which caused a violent evolution of gas and reached a temperature of  $98\text{ C}^\circ$ . This temperature was maintained for 15 minutes. The mixture was then diluted to approximately 14 L with warm water and treated with 3%  $\text{H}_2\text{O}_2$ . The color changed to bright yellow indicating proper treatment. Then the suspension was placed into an ultracentrifuge and allowed to air dry.

Each summer sample was made with one neat (no GO) dispersion and one loaded (with GO) dispersion of ~2 g of 11-Aminoundecanoic Acid in deionized (DI) water. The loaded sample was dispersed in ~40 mL of DI water filtered through a Millipore water purification unit to eliminate any dust particles in the dispersion. The neat sample was dispersed in ~40 mL of ordinary DI water. Both dispersions were then ultrasonicated for ~1 hour. Afterwards, they were poured into a beaker lined with Teflon sheets to make removal of the polymer simple. These beakers were then put into the oven under a constant flow of Argon through the inlet valve while the outlet valve was left open to allow water vapor from the dispersions and from the condensation reaction escape. Ideally, this would drive the equilibrium of the Step Polymerization reaction to the right.<sup>1</sup> All of the summer samples had polymerization times of ~3-4 hours with an average peak temperature of ~235 C°. This temperature was measured with the thermocouple in the air above the samples. Since the dispersions are partially suspended in air by Teflon sheets inside the beaker, this placement of the thermocouple was found to give the more accurate reading. There was some random variation in the oven temperature at the same setting of  $\pm 10$  C°. After the 3-4 hour polymerization time was achieved, the oven was turned off while allowing the Argon to flow and cool the samples until the temperature reached ~150 C° where there is negligible oxidation. Once at room temperature, the samples were removed. Figure 3.1.1.2 below shows the lump polymer of a neat system as it was just removed from the oven.

**Figure 3.1.1.2: Lump of Neat Polymerized PA-11 Before Pressing**



Once the lump polymer samples are removed from the oven, they are ready for heat pressing. First, two aluminum plates were used as interfaces between the polymer sample and the heated plates on the press since the aluminum plates are smoother. Scientific Commodities Inc. Teflon sheets with a listed thickness of 0.003 inches were used to contain the polymer lump while in the heat press so that the polymer will not stick to the plates. One sheet was placed on the top plate and the other sheet was placed on the bottom plate before carefully placing the polymer lump between the two plates with Teflon sheets in a sandwich configuration. The plates were secured in place using Kapton tape that will not melt at the 250 C° temperature of the press plates. The heat press was turned on and both plates were allowed to heat up to 250 C° prior to pressing. Once the plates were at temperature, the stacked, aluminum plates containing polymer were carefully placed onto the bottom plate of the heat press. A hose from an Argon cylinder was fitted with a glass pipette tube and held in place by a wring stand holder attached to the arm that holds the bottom plate of the heat press. The pipette was aimed in between the Teflon sheets just enough to get Argon flow over the polymer but not enough so as to impede the pressing of the plates. Immediately, we pumped the press until the two plates came together. The pressing time usually took ~2-5 minutes.

This pressing technique led to inconsistent film thicknesses and surface defects on the films as shown in Figures 3.1.1.3 and 3.1.1.4. It is also important to note that there was a noticeable cracking noise as the sample was being pressed indicating that it had not completely melted and was not at temperature. Sometimes the Teflon sheets were torn or cut where it was pressed against solid polymer. The polymerization dates, dog bone cut dates, and concentrations of GO are listed in Table 3.1.1.1 below; note the date scheme that will be used throughout this paper: (year)(month)(day).

**Table 3.1.1.1: Summer Samples**

GO Concentration (% by weight)	Polymerization Date	Cut Date
0.0	20130708	20130709
0.1	20130708	20130709
0.0	20130709	20130710
1.0	20130709	20130710
0.0	20130712	20130715
0.1	20130712	20130715
0.0	20130722	20130724
0.5	20130722	20130724
0.0	20130918	20130919
1.5	20130918	20130919

**Figure 3.1.1.3: 20130919 Neat PA-11 Film After Pressing**





**Figure 3.1.1.4: 20130919 1.5% GO/PA-11 Film After Pressing**



The November samples were much more controlled than the summer samples. Instead of polymerizing one neat and one loaded sample at a time, a neat dispersion and four loaded dispersions of 0.1%, 0.5%, 1.0%, and 1.5% GO by weight were polymerized together in the same oven. This would eliminate the variation in heating time and peak temperature between samples. Except for the pressing technique, most of the other procedures were the same as for the summer samples. However, ~3 g of 11-Aminoundecanoic Acid was used in each dispersion instead of ~2 g as for the summer samples. This increase in quantity of monomer was necessary since the aging study for which these samples were intended for requires more material. Each loaded dispersion was dispersed in ~40 mL Millipore DI water and ultrasonicated for ~1 hour along with a neat dispersion that was dispersed in ~40 mL regular DI water. A total of five beakers lined with Teflon sheets were used for the five dispersions and placed into the oven under Argon flow. These samples had a peak temperature of ~238 C° and had a polymerization time of ~5 hours. After the desired time was reached, the oven was turned off and allowed to cool under Argon flow to ~150 C° at which point the Argon was cut off. Once at room temperature, the polymer lumps were removed.

The pressing technique for these November samples differed significantly from that of the summer samples. The original intent of these samples was to use them in a different gas diffusion experiment but we used these for the Aging Study instead. The gas diffusion experiment that we intended to use these samples for required that there be no bubbles in the films and that there be uniform thickness. To allow for a more uniform thickness and less wrinkling and tearing of the Teflon sheets, we switched to using thicker (0.060 inch) ePlastics Teflon boards that were cut out into squares to fit the aluminum plates. Although less prone to wrinkling and tearing, these Teflon Boards are still prone to indentations and punctures by hard

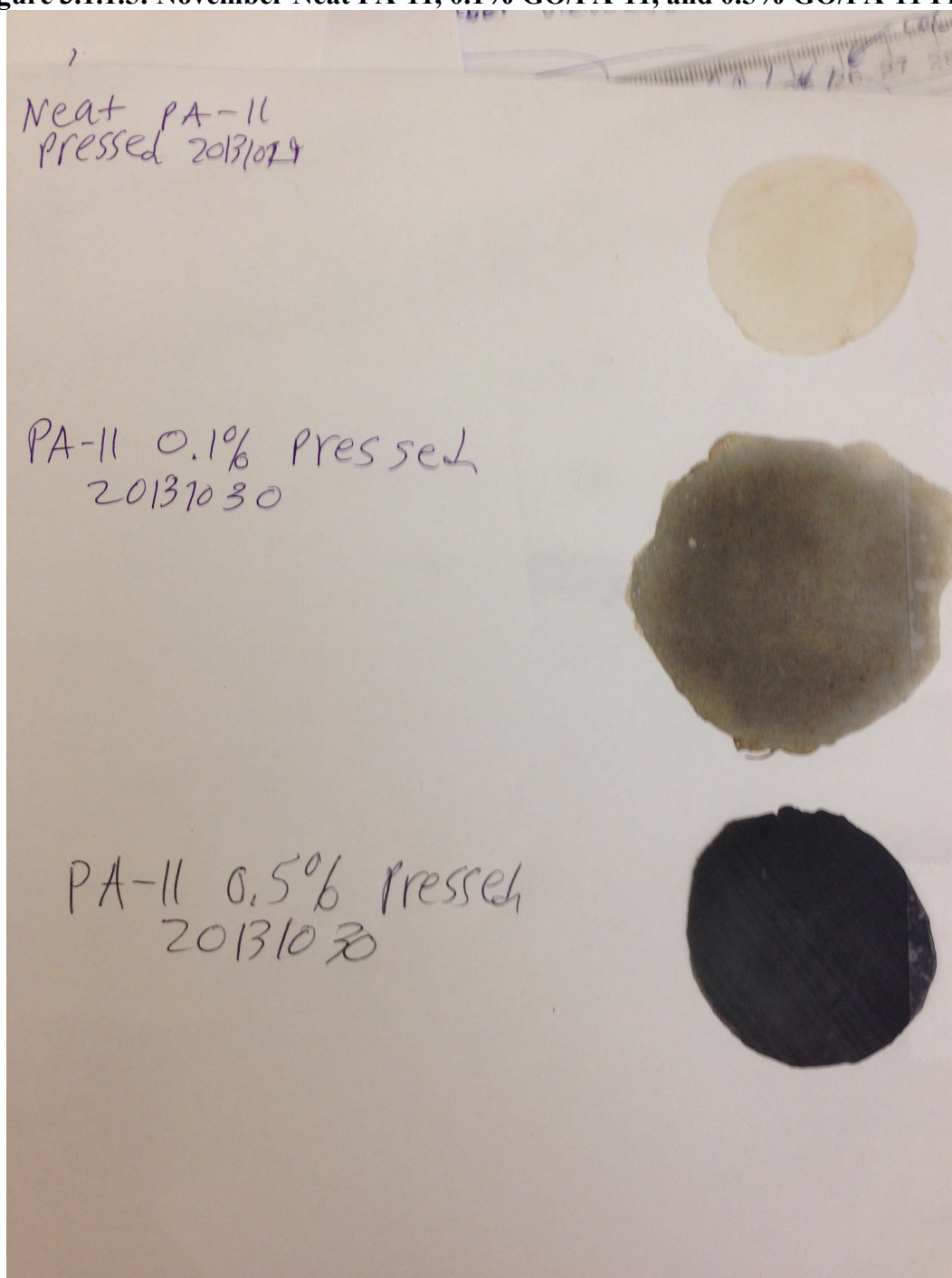
objects at high temperature. Additionally, the polymer lump was cut with a knife so that one piece with two parallel, flat faces would come into contact with the Teflon boards to minimize poking or indentations. The Teflon boards were secured against the aluminum plates by taping the edges of the Teflon to the plates using Kapton tape. This would ensure that the Teflon boards would not warp at temperature before pressing leading to uneven film thickness. The next issue that we resolved was uniform melting of the polymer before pressing. We inserted a thermocouple attached to a handheld thermometer in between the plates to monitor the temperature of the Teflon. Before, we had noticed that the Teflon was not necessarily at the same temperature as the heat press plates since the temperature gauges were attached to the plates and not the Teflon or sample. However, waiting for the polymer to completely melt before pumping the press led to significant oxidation due to the longer time that the sample was in the press and at temperature. To solve this, we wrapped all sides of the sandwiched plates containing the polymer sample with the thinner Teflon sheets. This would contain the argon and channel it around all sides of the polymer and indeed this led to almost no oxidation when done properly. The sheets were taped in place using Kapton tape. The glass pipette and thermocouple were fed through holes poked into the Teflon sheets.

Once the sample was prepared with the sandwiched aluminum plates, it was ready for pressing. Once the press was at temperature ( $\sim 240\text{ C}^\circ$ ), the sandwiched plates containing the sample were placed on the bottom heat press plate. The thermocouple and Argon pipette were then inserted through the Teflon sheets. The press was pumped just enough to allow the top aluminum plate to contact the to top plate of the heat press without applying any pressure. The temperature of the Teflon was monitored with the thermometer until it reached  $200\text{ C}^\circ$ . At and above this temperature, it was noticed that the aluminum plates slowly came together under their

own weight as the polymer melted. The heat press was pumped only to keep the top aluminum plate flush with the top heat plate without applying any pressure. Once the two aluminum plates came together, the operator waited five minutes before pumping the hydraulic lever of the press ~150 times rapidly. Then the sandwiched aluminum plates were removed from the press and placed on top of a steel plate on a desk to dissipate the heat. A heavy lead brick was placed on top of the sandwiched aluminum plates to keep pressure on the film in order to press out any bubbles that may have formed. A cardboard box was placed over the brick and plates with the Argon pipette poking through the top of it to provide a relatively inert environment while cooling. Once the plates were at a temperature that allowed for handling without thermal gloves, the plates were removed and opened.

This process led to much smoother and consistent films. There were no surface defects or bubbles when done properly. There were thickness variations across the film but there was not a defined thickness gradient like the summer samples. We also noticed that there were no cracking noises even when pumping the press very rapidly indicating that the polymer sample was uniformly melted. The entire process from allowing the Teflon to reach ~240 C° to the plates cooling the in the cardboard box took anywhere from ~45 minutes to 1 hour. These November samples were polymerized on 20131022 together but were pressed on different dates. Neat PA-11, 0.1% by weight GO/PA-11, and 0.5% by weight GO/PA-11 films pressed from the November polymerization are shown in Figure 3.1.1.5. However, these samples shown were not used in the Aging Study but are virtually identical since they came from the same polymerized lump.

**Figure 3.1.1.5: November Neat PA-11, 0.1% GO/PA-11, and 0.5% GO/PA-11 Films**



## 3.2 Water Diffusion/Absorption Study

The water diffusion/absorption study was conducted with halves of the dog bones from the tensile tests in 20 mL scintillation vials. A Sartorius BP 221S scale was used to measure the mass of the GO/PA-11 samples to the nearest 1/10000 of a gram. It is important to note that this study was only done on the summer samples.

### 3.2.1 Theory

This water diffusion/absorption test was intended to be a preliminary indicator of whether or not adding GO in PA-11 could inhibit the diffusion of water into the PA-11 matrix. If the results indicate that there was in fact a reduction in the diffusion coefficient, then the aging process of PA-11 via the water hydrolysis mechanism might also be slowed down or suppressed entirely.

Polyamides readily absorb small molecules such as water and alcohols.<sup>21</sup> Therefore, measurement of the diffusion coefficient can provide great insight into the transport mechanism for a certain small molecule such as water into the polymer matrix.<sup>21</sup> It is important to note that the crystalline regions of the polymer are considered impenetrable to small molecules; therefore all diffusion occurs in the amorphous region of the PA-11 matrix.<sup>22</sup> Classical diffusion is known as Fickian Diffusion and is given by Fick's Second Law shown in equation 3.2.1.1.<sup>21</sup>

$$\frac{\partial c}{\partial t} = D \frac{\partial^2 c}{\partial x^2} \quad (3.2.1.1)$$

In this equation,  $c$  is the concentration of the difusant,  $D$  is the diffusion coefficient,  $t$  is the time, and  $x$  is the distance along the diffusion direction.<sup>21</sup> Solving for this partial differential equation gives equation 3.2.1.2.<sup>21</sup>

$$d = kt^{1/2} \quad (3.2.1.2)$$

In this equation,  $d$  is the position of the wave front of the diffusant verses time,  $t$  is the time, and  $k$  is the proportionality constant related to the square root of the diffusion coefficient  $D$ .<sup>21</sup>

Wessel, et al.<sup>21</sup> note that the average diffusion coefficient can be calculated from the initial gradient of the absorption curve of a gravimetrically determined mass uptake. Thus, they derived equation 3.2.1.3.<sup>21</sup>

$$\frac{M_t}{M_{max}} = \frac{4}{\sqrt{\pi}} \cdot \sqrt{\frac{Dt}{l^2}} \quad (3.2.1.3)$$

In this equation,  $M_t$  is the mass uptake at time  $t$  ([mass at time =  $t$ ] – [mass at time = 0]),  $M_{max}$  is the mass uptake at saturation, and  $l$  is the thickness of the film.<sup>21</sup> Rearranging equation 3 gives equation 3.2.1.4.<sup>21</sup>

$$\left(\frac{M_t}{M_{max}}\right)^2 \cdot \left(\frac{\pi}{16}\right) \cdot l^2 = Dt \quad (3.2.1.4)$$

This equation should give a linear relationship during the initial part of the absorption curve with the slope equal to  $D$ .<sup>21</sup> Thus, we now have an equation to relate the mass uptake of a GO/PA-11 film piece in water over time to the diffusion coefficient just by measuring the change in mass verses time.

The apparatus that we decided to use consists of a 20 mL scintillation vial filled with DI water and two film samples—one neat and one loaded—for each vial. Since all of the summer samples had already been tensile tested at this point, we decided to use the halves of the dog bones as the film samples for this test assuming that most of the stretching had occurred in the neck and tensile regions and not in the head region where we expected most of the absorption to occur. However, there is an inherent problem with this kind of test. Fickian diffusion describes a single wave front diffusing along a single axis.<sup>21</sup> The Fickian model alone does not account for two wave fronts diffusing in opposite directions to each other through both faces of the dog bone

as is the case in our system. Theoretically, there is diffusion through all faces of the dog bone including that of the edges. However, calculating the percent area of the edge of one of the thicker dog bones gave only ~5% edge area to the total surface area of the dog bone. Given that this was a relatively thicker dog bone than the rest, the percent edge areas would be less in the rest of the dog bones since the other dimensions were about the same given the die used to cut them. Therefore we assumed that the diffusion through the edges would be negligible.

However, the bifacial diffusion aspect is not negligible. I modified equation 4 by dividing the thickness of the sample,  $l$ , by 2 since the sample would reach saturation when one wave front meets the other wave front in the center of the sample. This value would correspond to the wave front propagating through half of the thickness of the film assuming that both wave fronts propagate at equal velocities. Thus, this modification gives equation 3.2.1.5.

$$\left(\frac{M_t}{M_{max}}\right)^2 \cdot \left(\frac{\pi}{16}\right) \cdot \left(\frac{l}{2}\right)^2 = Dt \quad (3.2.1.5)$$

The mass and time data was worked up first on an excel file calculating the left side of the equation from the mass changes at each time. Then the output was placed into columns on a .txt file and worked up in the MATLAB program using the curve fitting function. A plot of the left side of this equation versus the time was fitted with an inverse exponential fit given by equation 3.2.1.6.

$$f(t) = \left(\frac{M_t}{M_{max}}\right)^2 \cdot \left(\frac{\pi}{16}\right) \cdot \left(\frac{l}{2}\right)^2 = Dt = Ae^{-bt} + C \quad (3.2.1.6)$$

An output for the values of  $A$ ,  $b$ , and  $C$  was selected by the lowest sum of squares error (SSE) by changing the “Robust” and “Algorithm” settings. Given the output for the various values, taking the derivative of equation 3.2.1.6 when  $t$  is equal to zero (which is “ $-b \cdot A$ ”) gives the initial slope of the curve at time equal to zero. The value for this slope is taken as equal to  $D$ .



It is important to differentiate between diffusivity and permeability. Gas permeability is given by equation 3.2.1.7 below.<sup>11</sup>

$$P = S \times D \quad (3.2.1.7)$$

In this equation, P is the permeability coefficient, S is the solubility coefficient, and D is the diffusion coefficient.<sup>11</sup> The permeability coefficient is the volume of gas passing through a barrier per thickness, time, and applied pressure.<sup>23</sup> The diffusion coefficient represents the rate at which the front of a gas passes through a material due to a concentration gradient.<sup>21</sup> This concentration gradient corresponds to a chemical potential.<sup>24</sup> The solubility coefficient refers to favorable interactions between a gas and the molecules of the barrier.<sup>11</sup> The diffusion of a gas through a material with a nanofiller is dependent on the concentration and the aspect ratio (length/thickness) of a nanofiller.<sup>11</sup> The solubility is typically only dependent on the concentration.

### 3.2.2 Sample Preparation

One half of a neat dog bone and its corresponding loaded half dogbone were placed into a desiccator for at least one week—using NaOH pellets as a desiccant. The listed relative humidity in a desiccator for NaOH at 25 C° is 8.24±2%.<sup>25</sup> Just before the Water Diffusion/Absorption test began, each polymer film sample was placed into a 100 C° oven for 1 hour. Then the sample was taken out of the oven and placed into the desiccator while it was transported to the scale to measure its “0” time mass. Then the sample was placed into 20 mL scintillation vial that was then filled to brim with DI water. Whenever a researcher subsequently massed a sample, it was first buffed dry with a kimwipe. Then it was placed on the scale for measurement. After measurement, it was immediately returned to the scintillation vial and refilled with DI water.

Measurements were taken at the following intervals: 0, 30 minutes, 2 hours, 5 hours, 12 hours, 24 hours, 2 days, 4 days, 6 days, 14 days.

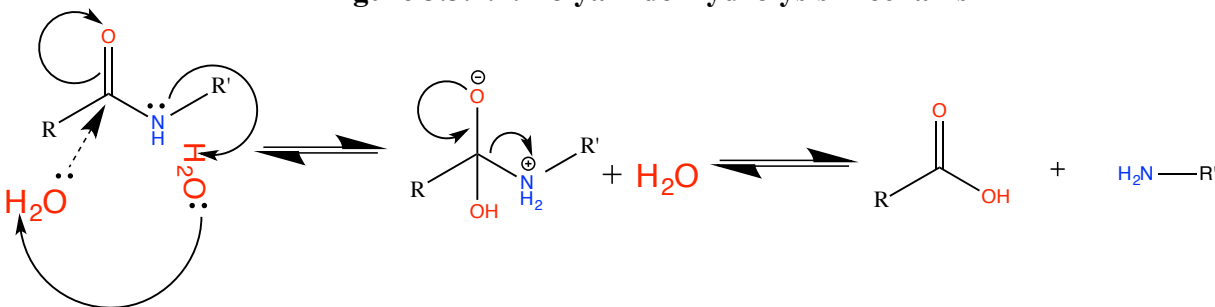
### 3.3 Aging Study

The aging study was conducted over the course of 83 days in a 100 C° oven. The vessels used to contain the polymer samples and DI water were glass Ace No. 40 heavy walled pressure tubes.<sup>2</sup> The instrument used to measure the dissolved oxygen content was an Oakton Dissolved Oxygen Meter.

#### 3.3.1 Theory

The mechanism for neutral (pH = 7) amide hydrolysis was determined by Zahn's<sup>26</sup> work on N-methylacetamide. Unlike the acid catalyzed pathway, the carbonyl oxygen is not protonated before nucleophilic attack by the water molecule on the carbonyl carbon.<sup>26</sup> Instead, the amide nitrogen is protonated and a hydroxide ion attacks the carbonyl carbon in a concerted process.<sup>26</sup> A proton dissociates from the water molecule involved nucleophilic attack and "hops" water molecules until it protonates the amide nitrogen.<sup>26</sup> The second step involves the dissociation of the amide bond to form a lone pair on the amide nitrogen.<sup>26</sup> The result is one amine and one carboxylic acid chain end. This reaction is illustrated in Figure 3.3.1.1.<sup>26</sup>

**Figure 3.3.1.1: Polyamide Hydrolysis Mechanism**



As shown by Figure 3.3.1.1, the hydrolysis reaction is part of an equilibrium reaction with polymerization.<sup>2</sup> Therefore, altering the temperature, concentrations of reactions and products, and the pH will shift the equilibrium one way or the other. The concentration of amide bonds is proportional to the molecular weight of the sample.<sup>2</sup> Indeed, Meyer, et al.<sup>4</sup> showed that

at pH = 5 and pH = 3 with HCl does lower the equilibrium molecular weight since the concentration of acidic hydrogen is increased. However, Hocker, et al.<sup>3</sup> showed that lengthening the carbon chain—regardless of pH—in organic acids leads to faster diffusion into the sample and also lowers the molecular weight. Jacques, et al.<sup>5</sup> showed that increasing the temperature of commercial PA-11 in neutral water also decrease the equilibrium molecular weight. In our experiment, all of these variables were controlled for given that the GO/PA-11 samples were immersed in the same DI water in the same oven at a constant temperature of 100 C°.

Kinetic fits for neutral water hydrolysis of PA-11 have been well established in the past. Meyer, et al.<sup>4</sup> derived a kinetic model for the neutral water hydrolysis of in-house polymerized PA-11 in 2001. That same year, Jacques, et al.<sup>5</sup> derived a kinetic fit for neutral water hydrolysis of commercial PA-11. Meyer, et al.<sup>4</sup> showed that a large excess of water allows its concentration to be assumed constant. Jacques, et al.<sup>5</sup> showed that for his 3 mm thick samples, the diffusion process is relatively fast compared to the rate of hydrolysis. Deriving a kinetic fit for the neutral water hydrolysis of these GO/PA-11 composite samples is beyond the scope of this thesis. We only seek to compare the relative rates of hydrolysis and the equilibrium molecular weights of these GO/PA-11 samples. Thus, the kinetic aspects of GO/PA-11 hydrolysis will not be discussed further.

### 3.3.2 Sample Preparation

After being pressed into films, the November GO/PA-11 samples were then cut into 1 cm x 1 cm squares. These squares were then put into pressure tubes that were subsequently filled with DI water. Then the filled pressure tubes were bubbled with Argon gas for ~30 minutes to reduce if not remove any oxygen from the DI water. The dissolved oxygen content was measured to be no greater than  $0.90 \frac{mg}{L}$  for all samples. This step was done in order to isolate the

hydrolysis reaction on PA-11 from any possible oxidation that could exaggerate the data.<sup>2</sup> Then the pressure tubes were sealed with an O-ring and a Teflon cap before being placed in the 100 C° oven.

## Chapter 4: Results

### 4.1 GO/PA-11 Tensile Data

The results from the MTS 810 using the ASTM D-638-5-IMP test die are shown below.<sup>2</sup> The strain rate was pre-set into the MTS 810 instrument to the industry accepted value of 6.35 mm/min or 0.25 inch/minute.<sup>8</sup> The strain rate was measured to be an average of 6.34 mm/min with a standard deviation of 0.06 mm/min. Results from dog bones that broke early at defects were discarded. Table 4.1.1 lists the tensile values for each neat system that was polymerized simultaneously with each loaded system listed in Table 4.1.2. Samples with the same “cut date” indicate that they were polymerized simultaneously. Figure 4.1.1 shows the ultimate strain and Young’s modulus verses GO concentration for the summer samples—with the neat systems averaged together—and the November samples. Figure 4.1.2 shows the Tensile Strength verses GO concentration for both the summer—with the neat values averaged—and November samples.

**Table 4.1.1: Neat Summer GO/PA-11 Sample Tensile Values**

<b>Loading (% GO by weight)</b>	<b>Cut Date</b>	<b>Ultimate Strain (%)</b>	<b>Correction Factor</b>	<b>Corrected Young's Modulus (Mpa)</b>	<b>Tensile Stress (Mpa)</b>	<b>Sample Size (# bones)</b>
0.0	20130715	430±40	2.2±0	670±80	270±20	2
0.0	20130724	430±80	2.1±0	890±50	280±80	3
0.0	20130710	390±70	2.2±0	800±20	250±80	2
0.0	20130919	450±20	2.0±0	800±200	328±7	2
0.0*	-----	420±50	2.1±0	800±100	280±60	9

<sup>a</sup>The average strain rate was measured to be 6.34 mm/min with a standard deviation of 0.06 mm/min

\* Average values of neat samples

**Table 4.1.2: Summer GO/PA-11 Sample Tensile Data Table With Neat Systems Averaged<sup>a</sup>**

<b>Loading (% GO by Weight)</b>	<b>Ultimate Strain (%)</b>	<b>Correction Factor</b>	<b>Corrected Young's Modulus (Mpa)</b>	<b>Tensile Stress (Mpa)</b>	<b>Sample Size (# bones)</b>
0.0 <sup>*</sup>	420±50	2.1±0	800±100	280±60	9
0.1	480±40	2.2±0	1000±100	360±40	4
0.5	180±70	2.1±0	1100±300	140±50	5
1.0	130±20	2.2±0	1200±300	110±20	3
1.5	41±2	2.2±0	1200±200	70±20	2

<sup>\*</sup>Each loaded sample was polymerized together with a corresponding neat sample; all neat samples were averaged together

<sup>a</sup>The average strain rate was measured to be 6.34 mm/min with a standard deviation of 0.06 mm/min

**Table 4.1.3: November GO/PA-11 Sample Tensile Data Table<sup>a</sup>**

<b>Loading (% GO by weight)</b>	<b>Press Date</b>	<b>Ultimate Strain (%)</b>	<b>Correction Factor</b>	<b>Corrected Young's Modulus (Mpa)</b>	<b>Tensile Stress (Mpa)</b>	<b>Sample Size (# of Bones)</b>
0.0	20131108	350±70	2.1±0	1200±30	290±60	2
0.1	20131111	230±10	2.2±0	1210±30	180±20	2
0.5	20131112	26±6	2.1±0	1300±200	60±1	2
1.0	20131112	50±10	2.1±0	1190±20	76.0±0.7	2
1.5	20131112	28±3	2.1±0	1500±200	90±10	2

<sup>a</sup>The average strain rate was measured to be 6.34 mm/min with a standard deviation of 0.06 mm/min

Figure 4.1.1: GO/PA-11 Ultimate Strain and Young's Modulus

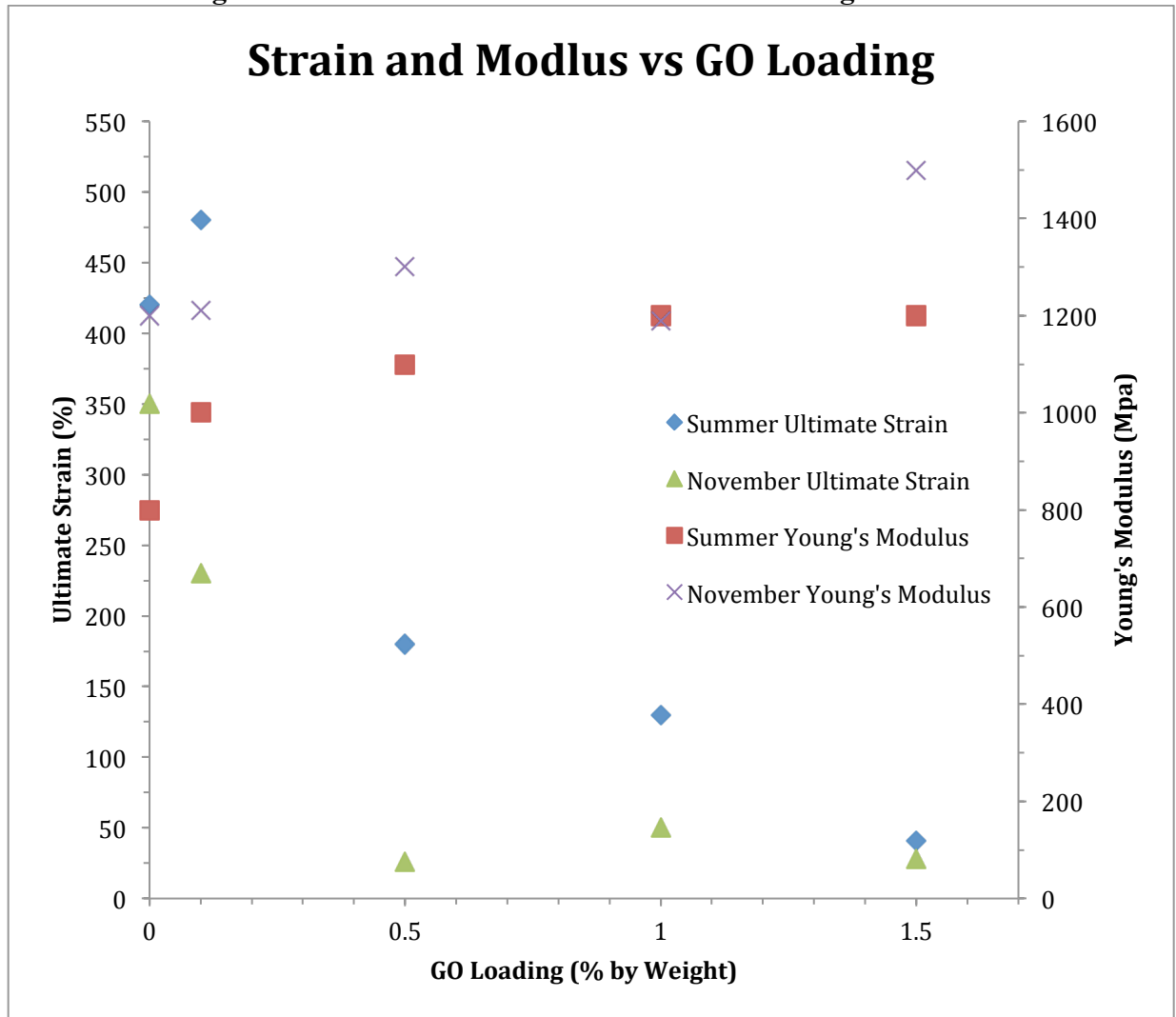
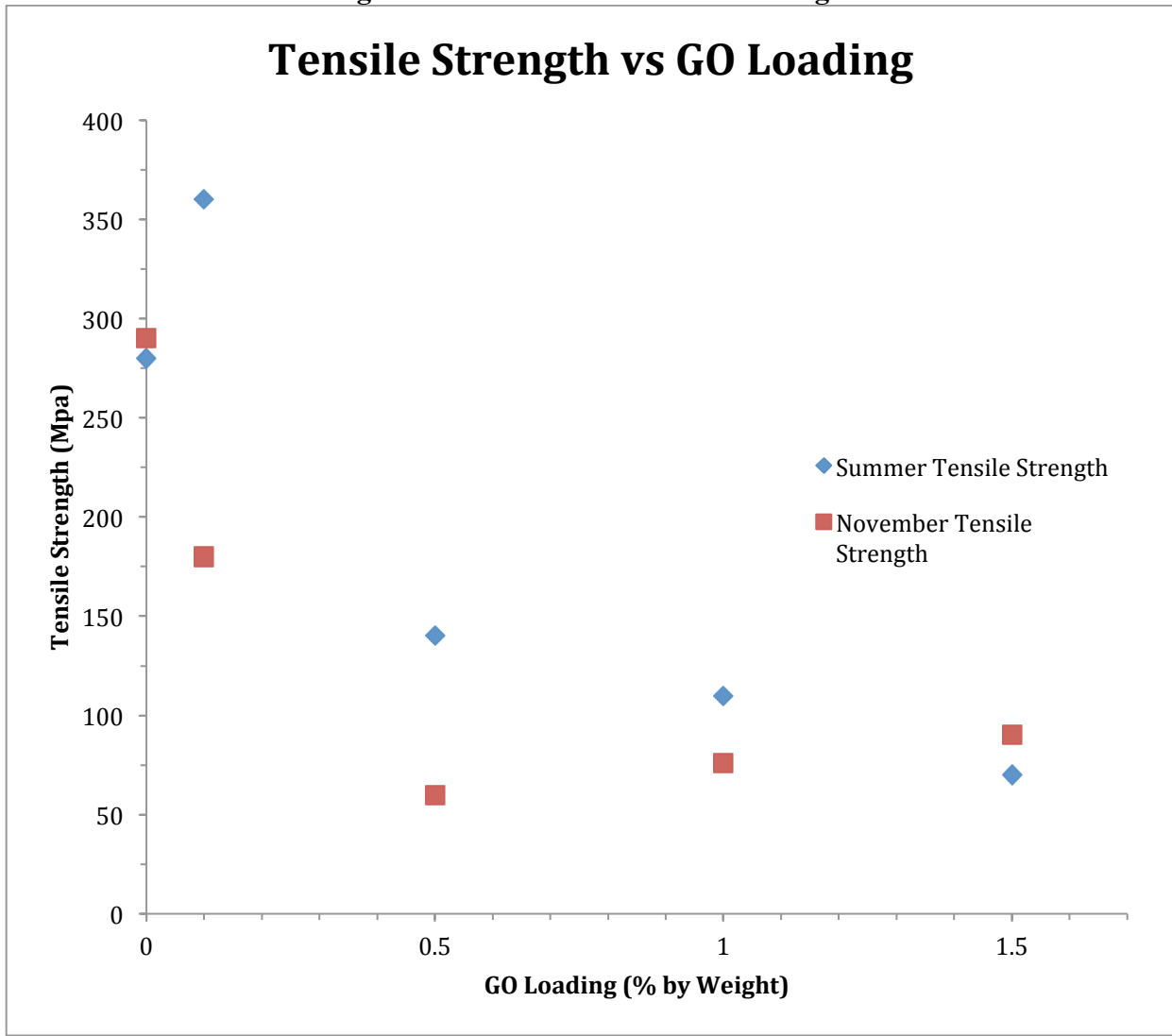




Figure 4.1.2: GO/PA-11 Tensile Strength



## 4.2 GO/PA-11 DI Water Diffusion Data

The DI water diffusion data displayed below was only done on the summer samples as mentioned earlier. Table 4.2.1 lists the measured DI water diffusion coefficients for each Neat and loaded sample. It is important to note that neat and GO composite samples with the same date indicate that they were polymerized simultaneously in the oven but in two different beakers. Figure 4.2.1 plots the diffusion coefficients of the neat samples listed by their “cut date.” Table 4.2.2 lists the diffusion coefficients and the fit parameters of the loaded samples and an average value for all of the neat samples. Figure 4.2.2 depicts the corresponding plot of the averaged neat diffusion coefficients with that of the loaded samples. Table 4.2.3 lists the percent change in mass at specified time intervals. The systems that were cut on 20130919 were not able to be measured at 5,760 minutes due to a scheduling conflict. Figure 4.2.3 illustrates the plot of percent change in mass verses time of the neat samples. Table 4.2.4 and Figure 4.2.4 show the same data with the neat values averaged together. Tables 4.2.5 - 4.2.12 and Figures 4.2.5 - 4.2.12 show the data for the water diffusion test according to equation 3.2.1.5 and the inverse exponential fit according to equation 3.2.1.6. The value of “d” is equal to the left side of equation 3.2.1.5 at time “t” and the values of “A” and “b” are the fit parameters.

**Table 4.2.1: Calculated GO/PA-11 Diffusion Coefficients**

Loading (% GO by weight)	Cut date *	D (mm <sup>2</sup> /min)
0.0	20130709	1.01E-09
0.1	20130709	3.55E-10
0.0	20130724	1.54E-09
0.5	20130724	6.98E-10
0.0	20130710	8.53E-10
1.0	20130710	4.66E-10
0.0	20130919	1.20E-09
1.5	20130919	9.62E-11

\*Samples with the same cut date indicate they were polymerized together

**Figure 4.2.1: GO/PA-11 Diffusion Coefficients For Neat Samples**

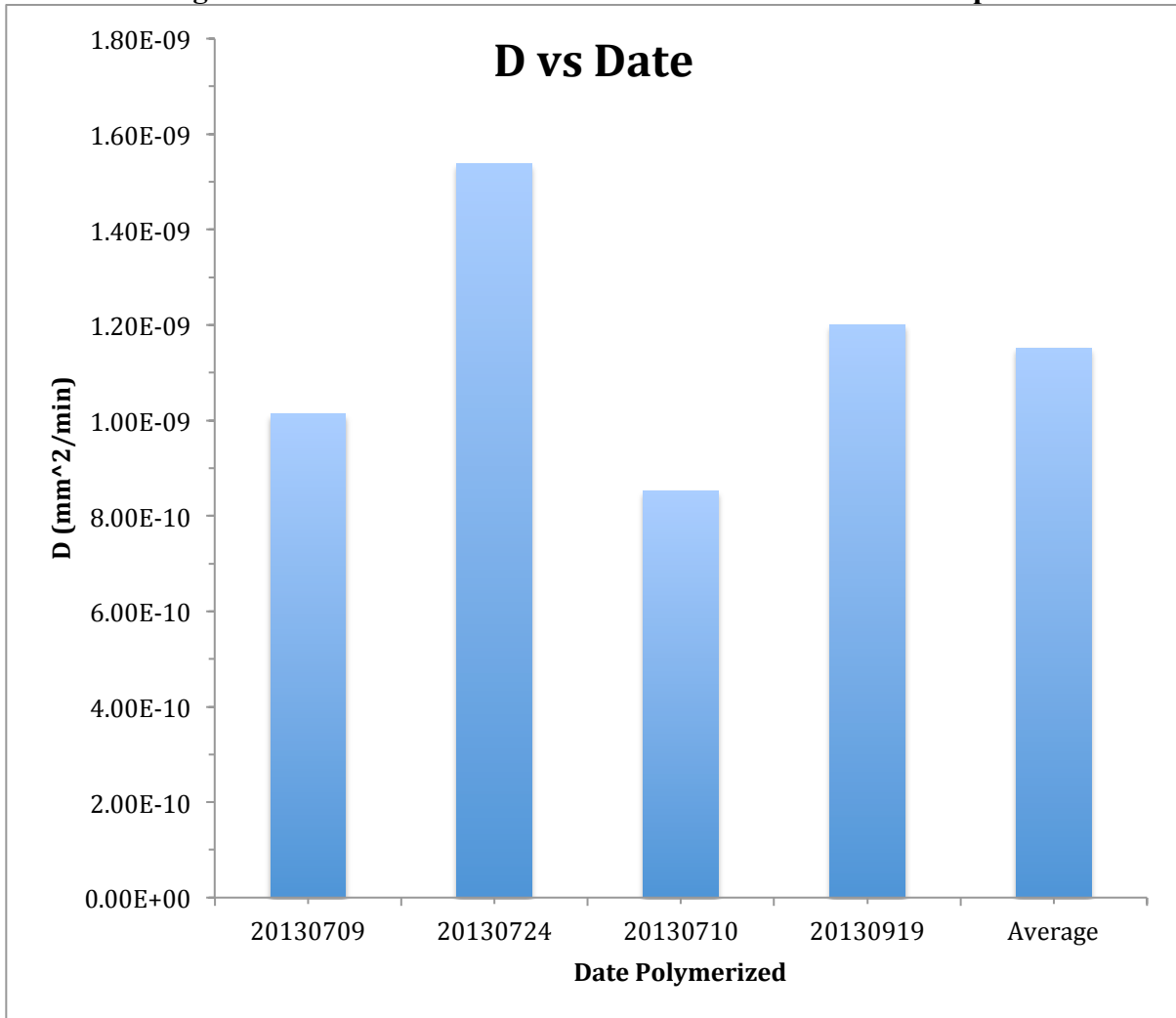


**Table 4.2.2: GO/PA-11 Diffusion Coefficients and Fit Parameters With Neat Values Averaged**

Loading (% GO by weight)	D (mm <sup>2</sup> /min)	A	b
0.0	1.2±0.3E-9	-1.57±0.9E-06	1.04±0.9E-03
0.1	3.55E-10	-5.17E-07	6.87E-04
0.5	6.98E-10	-1.88E-06	3.72E-04
1.0	4.66E-10	-6.13E-07	7.61E-04
1.5	9.62E-11	-1.78E-07	5.40E-04

**Figure 4.2.2: Calculated GO/PA-11 Diffusion Coefficients With Neat Values Averaged**

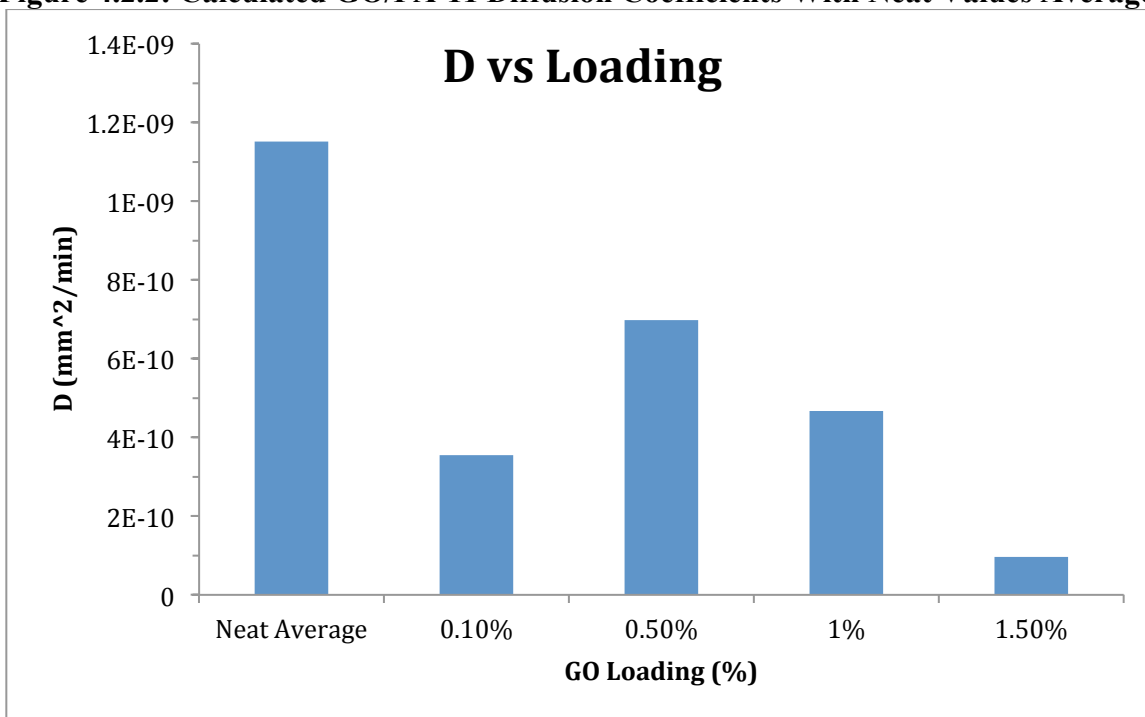


**Table 4.2.3: Percent Mass Change for Each Neat GO/PA-11 Sample**

Time (minutes)	Mass Change (%)			
	Cut 20130709	Cut 20130724	Cut 20130710	Cut 20130919
0	0.00	0.00	0.00	0.00
30	0.17	0.65	0.34	0.00
120	0.34	0.78	0.69	0.25
300	0.59	1.31	0.91	0.51
720	0.76	1.57	1.26	0.89
1,440	0.85	1.57	1.49	1.14
2,880	1.27	1.57	1.60	1.27
5,760	1.44	1.83	1.83	-----*
8,640	1.44	1.83	1.71	1.52
20,160	1.52	1.70	1.83	1.52

\*Data points not taken

**Figure 4.2.3: Percent Mass Change For Each Neat GO/PA-11 Sample**

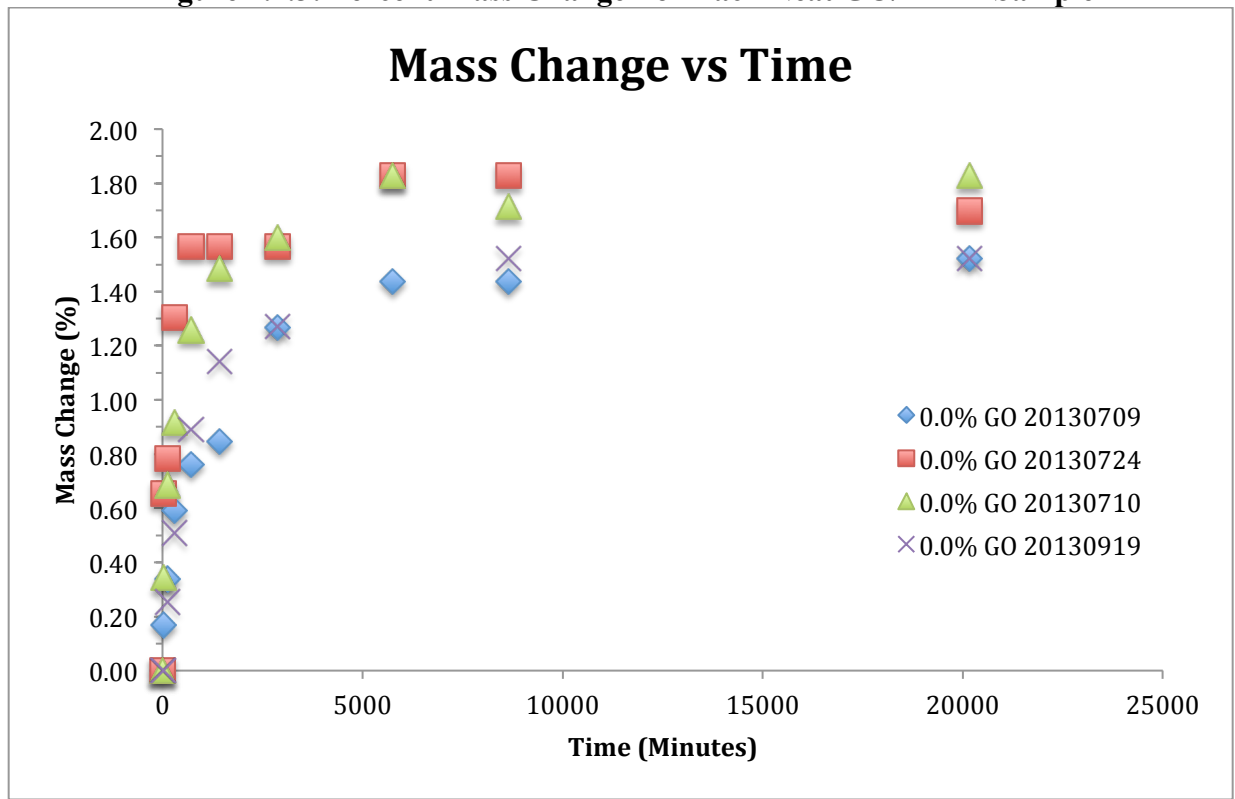


**Table 4.2.4: GO/PA-11 Percent Mass Change With Neat Values Averaged**

Time (minutes)	Weight Change (%)				
	-----	Cut 20130709	Cut 20130724	Cut 20130710	Cut 20130919
	0.0% GO by Weight	0.1% GO by weight	0.5% GO by weight	1% GO by weight	1.5% GO by weight
0	0.00±0	0.00	0.00	0.00	0.00
30	0.3±0.3	0.28	0.62	0.27	0.20
120	0.5±0.3	0.42	0.62	0.41	0.60
300	0.8±0.4	0.99	0.73	0.68	1.00
720	1.1±0.4	1.13	1.25	1.08	1.20
1,440	1.3±0.3	1.13	1.25	1.22	1.20
2,880	1.4±0.2	1.55	1.66	1.36	1.60
5,760	1.7±0.2	1.55	1.98	1.49	-----*
8,640	1.6±0.2	1.55	1.87	1.49	1.80
20,140	1.6±0.2	1.69	2.08	1.49	1.80

\* Data point not taken for the loaded or neat sample; the neat system average for this time interval does not include a value from this cut date

**Figure 4.2.4: GO/PA-11 Percent Mass Change With Neat Values Averaged**

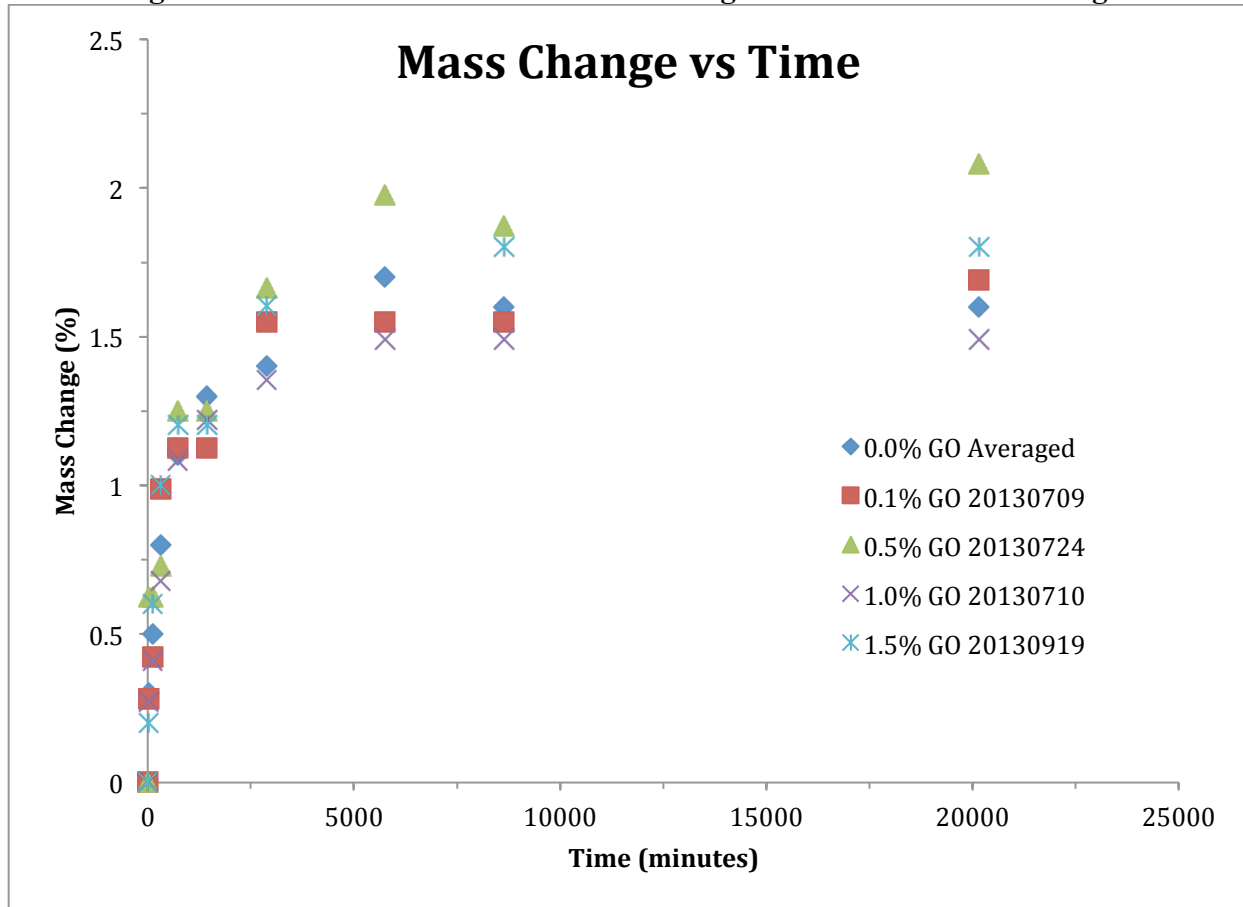


**Table 4.2.5: Water Diffusion Data and Fit for 20130709 Neat PA-11 Sample\***

Time (minutes)	d (mm <sup>2</sup> )	f(t)=Ae <sup>-bt</sup>	A	b
0	0.00E+00	2.00E-09	-2.51E-06	4.04E-04
30	3.14E-08	3.22E-08		
120	1.25E-07	1.21E-07		
300	3.84E-07	2.88E-07		
720	6.35E-07	6.35E-07		
1,440	7.84E-07	1.11E-06		
2,880	1.76E-06	1.73E-06		
5,760	2.27E-06	2.27E-06		
8,640	2.27E-06	2.43E-06		
20,160	2.54E-06	2.51E-06		

\*SSE is 5.49E-14 and R<sup>2</sup> is 0.9941

**Figure 4.2.5: Water Diffusion Plot of Data and Fit for 20130709 Neat Sample**

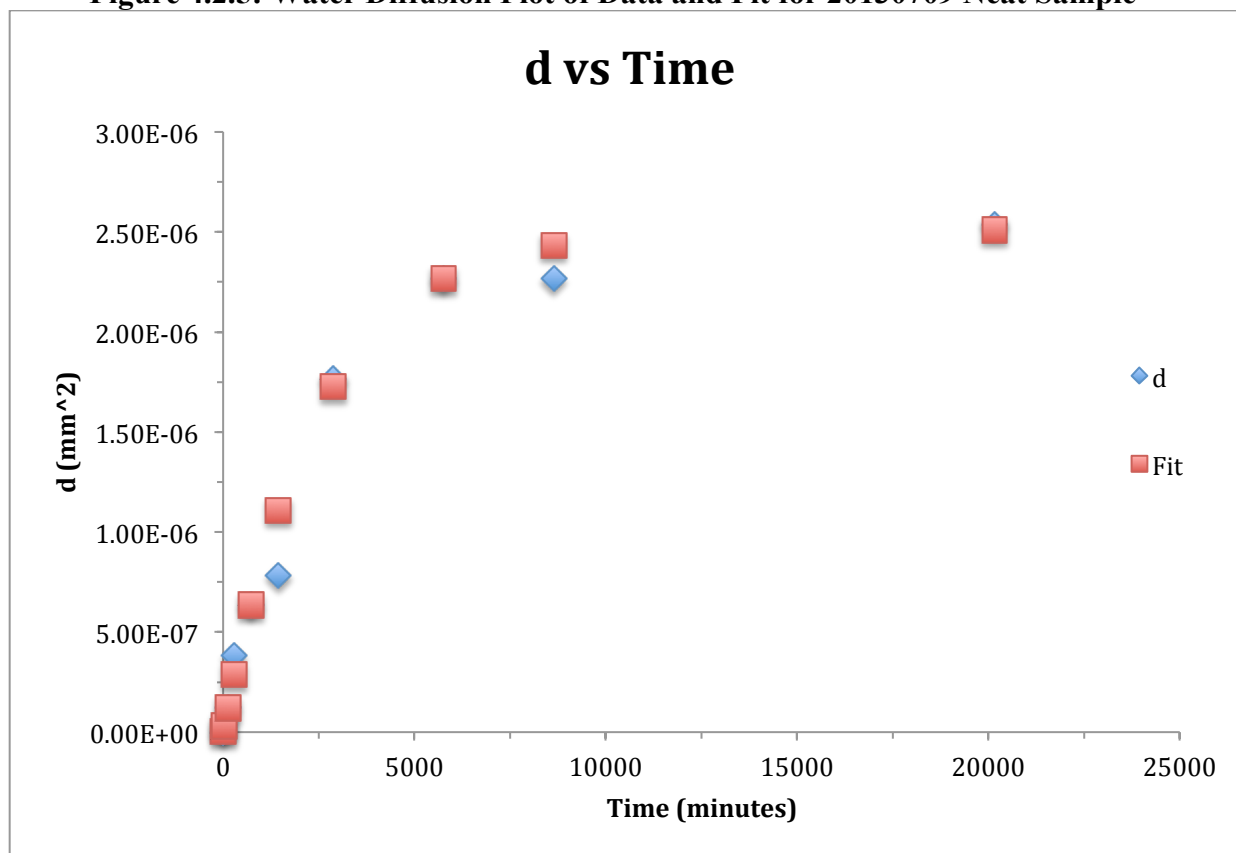


**Table 4.2.6: Water Diffusion Data and Fit for 20130709 0.1% GO/PA-11 Sample\***

Time (minutes)	d (mm <sup>2</sup> )	f(t)=Ae <sup>-bt</sup>	A	b
0	0.00E+00	2.37E-08	-5.17E-07	6.87E-04
30	1.66E-08	3.42E-08		
120	3.74E-08	6.46E-08		
300	2.03E-07	1.20E-07		
720	2.66E-07	2.25E-07		
1,440	2.66E-07	3.48E-07		
2,880	5.02E-07	4.69E-07		
5,760	5.02E-07	5.30E-07		
8,640	5.02E-07	5.39E-07		
20,160	5.98E-07	5.40E-07		

\*SSE is 2.36E-14 and R<sup>2</sup> is 0.9489

**Figure 4.2.6: Water Diffusion Plot of data and Fit for 20130709 0.1% GO/PA-11 Sample**

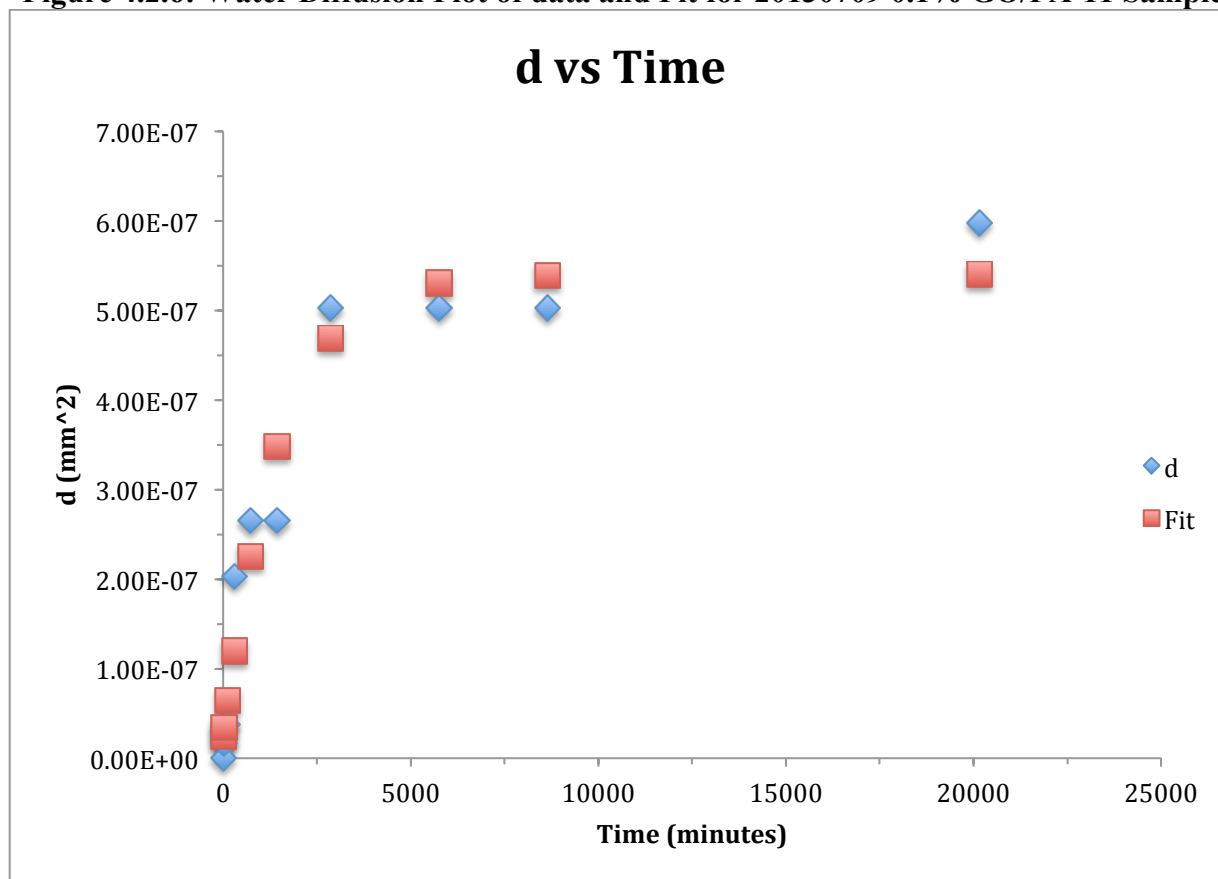




**Table 4.2.7: Water Diffusion Data and Fit for 20130724 Neat PA-11 Sample\***

Time (minutes)	d (mm <sup>2</sup> )	f(t)=Ae <sup>-bt</sup>	A	b
0	0.00E+00	1.99E-08	-6.54E-07	2.35E-03
30	9.79E-08	6.45E-08		
120	1.41E-07	1.81E-07		
300	3.92E-07	3.51E-07		
720	5.64E-07	5.54E-07		
1,440	5.64E-07	6.52E-07		
2,880	5.64E-07	6.73E-07		
5,760	7.67E-07	6.74E-07		
8,640	7.67E-07	6.74E-07		
20,160	6.62E-07	6.74E-07		

\*SSE is 4.22E-14 and R<sup>2</sup> is 0.9406

**Figure: 4.2.7: Water Diffusion Plot of Data and Fit for 20130724 Neat PA-11 Sample**

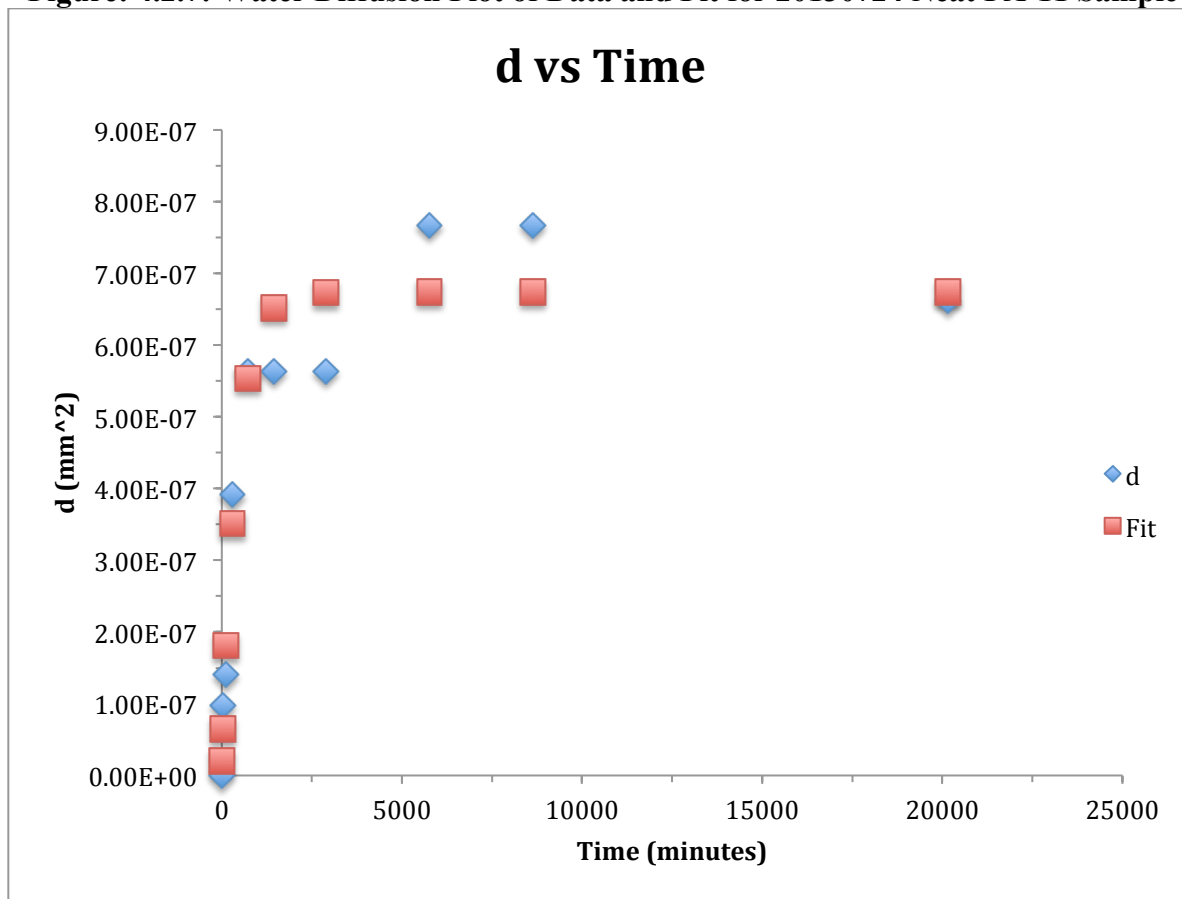


**Table 4.2.8: Water Diffusion Data and Fit for 20130724 0.5% GO/PA-11 Sample\***

Time (minutes)	d (mm <sup>2</sup> )	f(t)=Ae <sup>-bt</sup>	A	b
0	0.00E+00	1.05E-07	-1.88E-06	3.72E-04
30	1.88E-07	1.26E-07		
120	1.88E-07	1.87E-07		
300	2.56E-07	3.03E-07		
720	7.52E-07	5.46E-07		
1,440	7.52E-07	8.84E-07		
2,880	1.34E-06	1.34E-06		
5,760	1.89E-06	1.76E-06		
8,640	1.69E-06	1.91E-06		
20,160	2.09E-06	1.98E-06		

\*SSE is 1.50E-13 and R<sup>2</sup> is 0.9727

**Figure 4.2.8: Water Diffusion Plot of Data and Fit for 20130724 0.5% GO/PA-11 Sample**

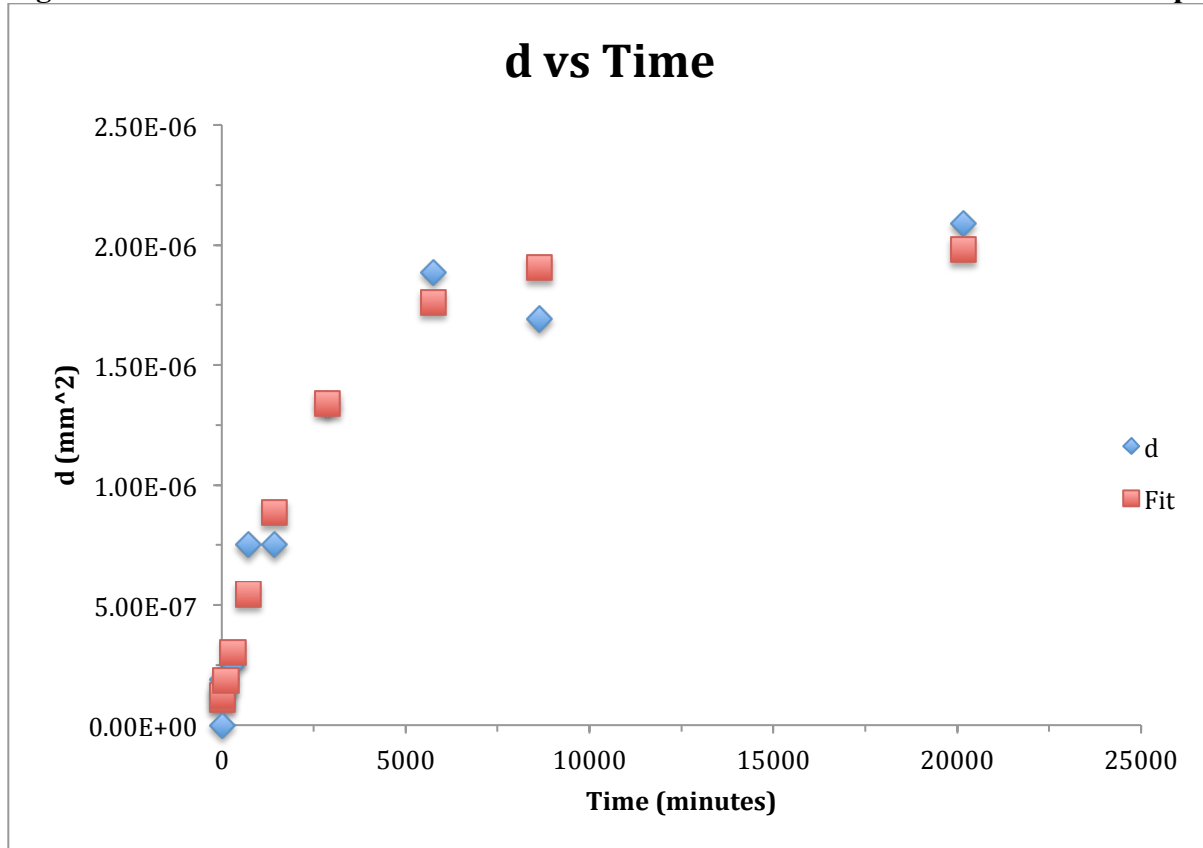


**Table 4.2.9: Water Diffusion Data and Fit for 20130710 Neat PA-11 Sample\***

Time (minutes)	d (mm <sup>2</sup> )	f(t)=Ae <sup>-bt</sup>	A	b
0	0.00E+00	3.70E-08	-1.05E-06	8.12E-04
30	4.06E-08	6.23E-08		
120	1.62E-07	1.35E-07		
300	2.88E-07	2.64E-07		
720	5.45E-07	5.02E-07		
1,440	7.62E-07	7.62E-07		
2,880	8.83E-07	9.87E-07		
5,760	1.15E-06	1.08E-06		
8,640	1.01E-06	1.09E-06		
20,160	1.15E-06	1.09E-06		

\*SSE is 3.11E-14 and R<sup>2</sup> is 0.9833

**Figure 4.2.9: Water Diffusion Plot of Data and Fit for 20130710 Neat PA-11 Sample**

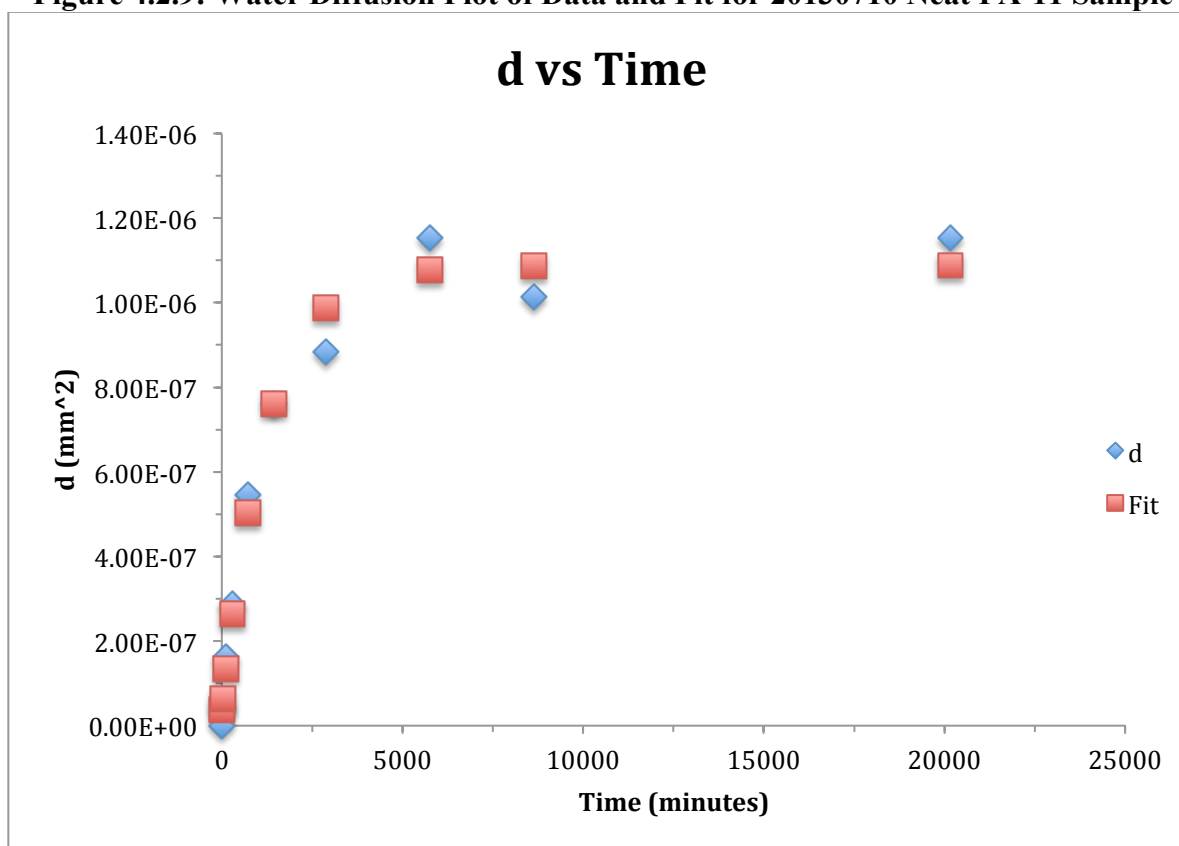


**Table 4.2.10: Water Diffusion Data and Fit for 20130710 1.0% GO/PA-11 Sample\***

Time (minutes)	d (mm <sup>2</sup> )	f(t)=Ae <sup>-bt</sup>	A	b
0	0.00E+00	0.00E+00	-6.13E-07	7.61E-04
30	2.02E-08	1.38E-08		
120	4.54E-08	5.35E-08		
300	1.26E-07	1.25E-07		
720	3.23E-07	2.58E-07		
1,440	4.08E-07	4.08E-07		
2,880	5.04E-07	5.44E-07		
5,760	6.10E-07	6.05E-07		
8,640	6.10E-07	6.12E-07		
20,160	6.10E-07	6.13E-07		

\*SSE is 2.58E-16 and R<sup>2</sup> is 0.9957

**Figure 4.2.10: Water Diffusion Plot of Data and Fit for 20130710 1.0% GO/PA-11 Sample**

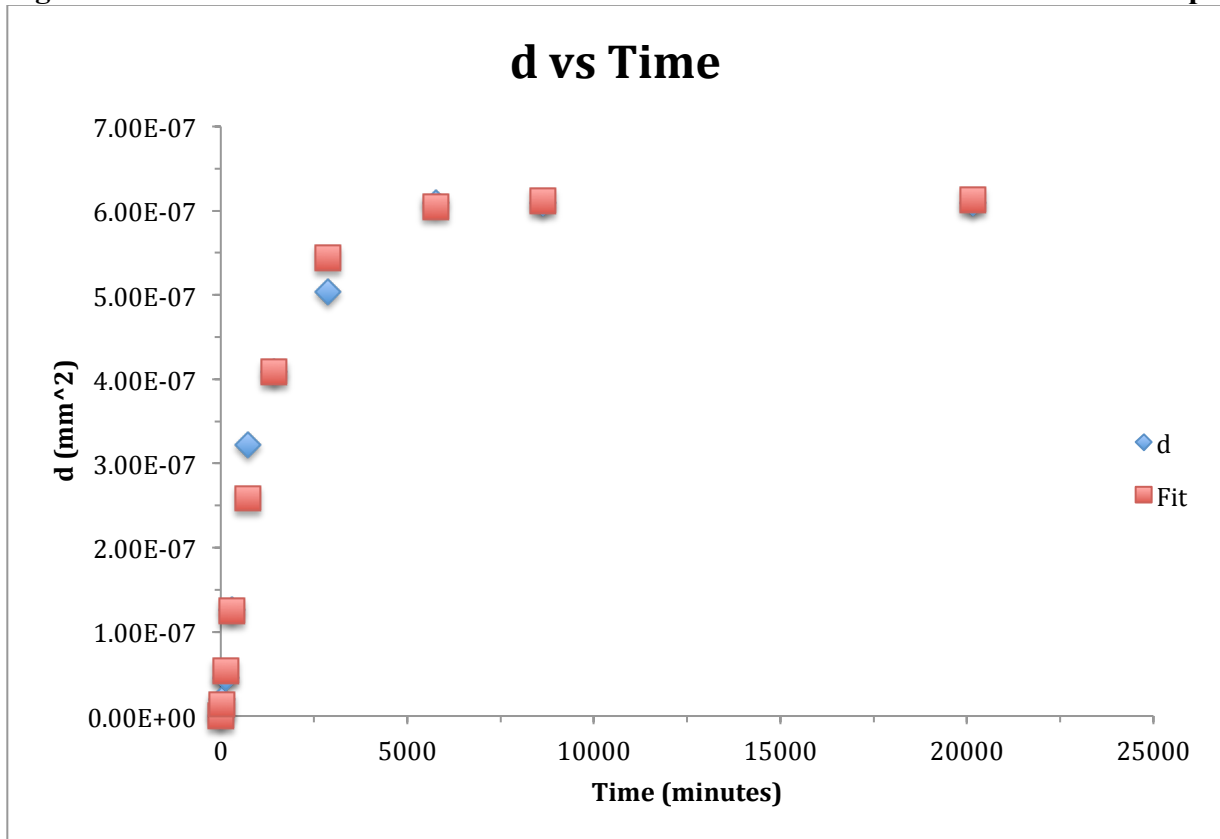


**Table 4.2.11: Water Diffusion Data and Fit for 20130919 Neat Sample\***

Time (minutes)	d (mm <sup>2</sup> )	f(t)=Ae <sup>-bt</sup>	A	b
0	0.00E+00	-2.80E-08	-2.07E-06	5.80E-04
30	0.00E+00	7.71E-09		
120	5.67E-08	1.11E-07		
300	2.27E-07	3.03E-07		
739	6.95E-07	6.94E-07		
1,440	1.15E-06	1.14E-06		
2,880	1.42E-06	1.65E-06		
8,640	2.04E-06	2.03E-06		
20,160	2.04E-06	2.04E-06		

\*SSE is 1.96E-14 and R<sup>2</sup> is 0.9969

**Figure 4.2.11: Water Diffusion Plot of Data and Fit for 20130919 Neat Sample**

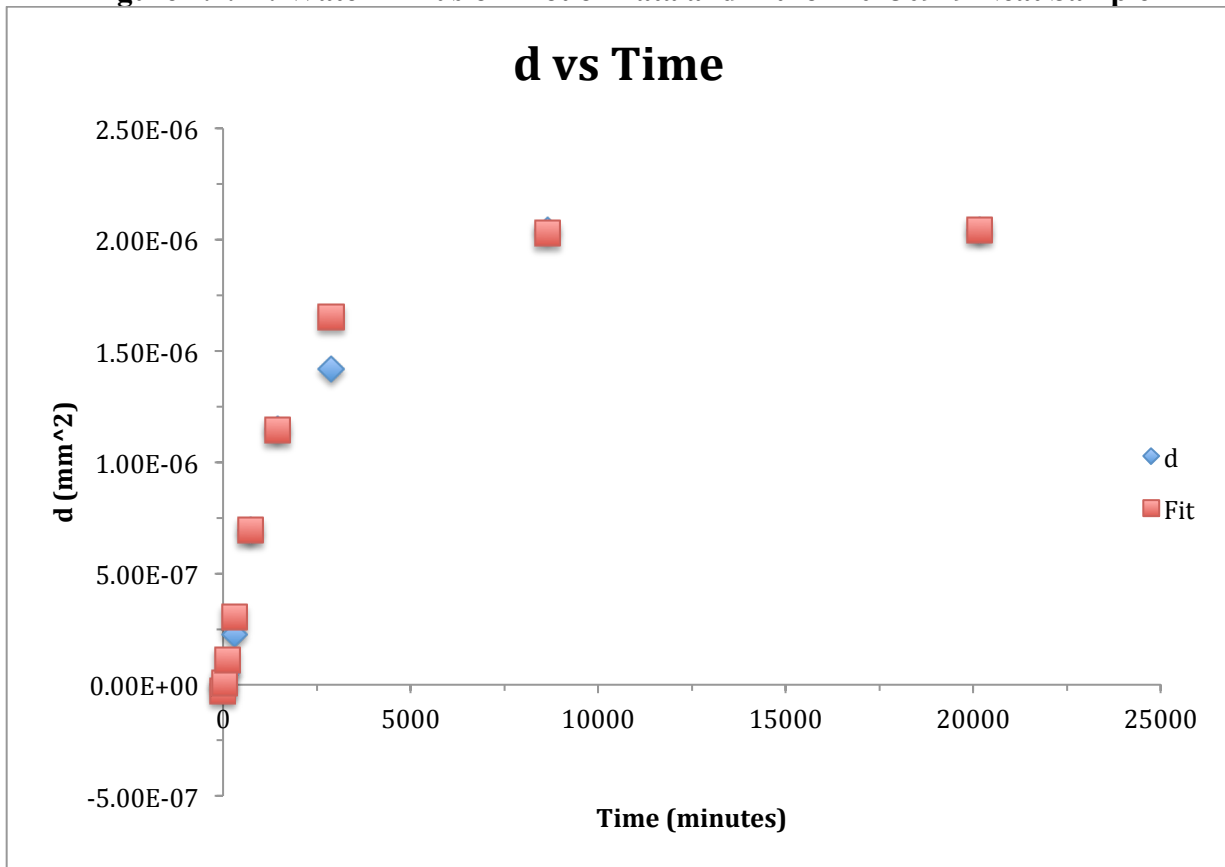
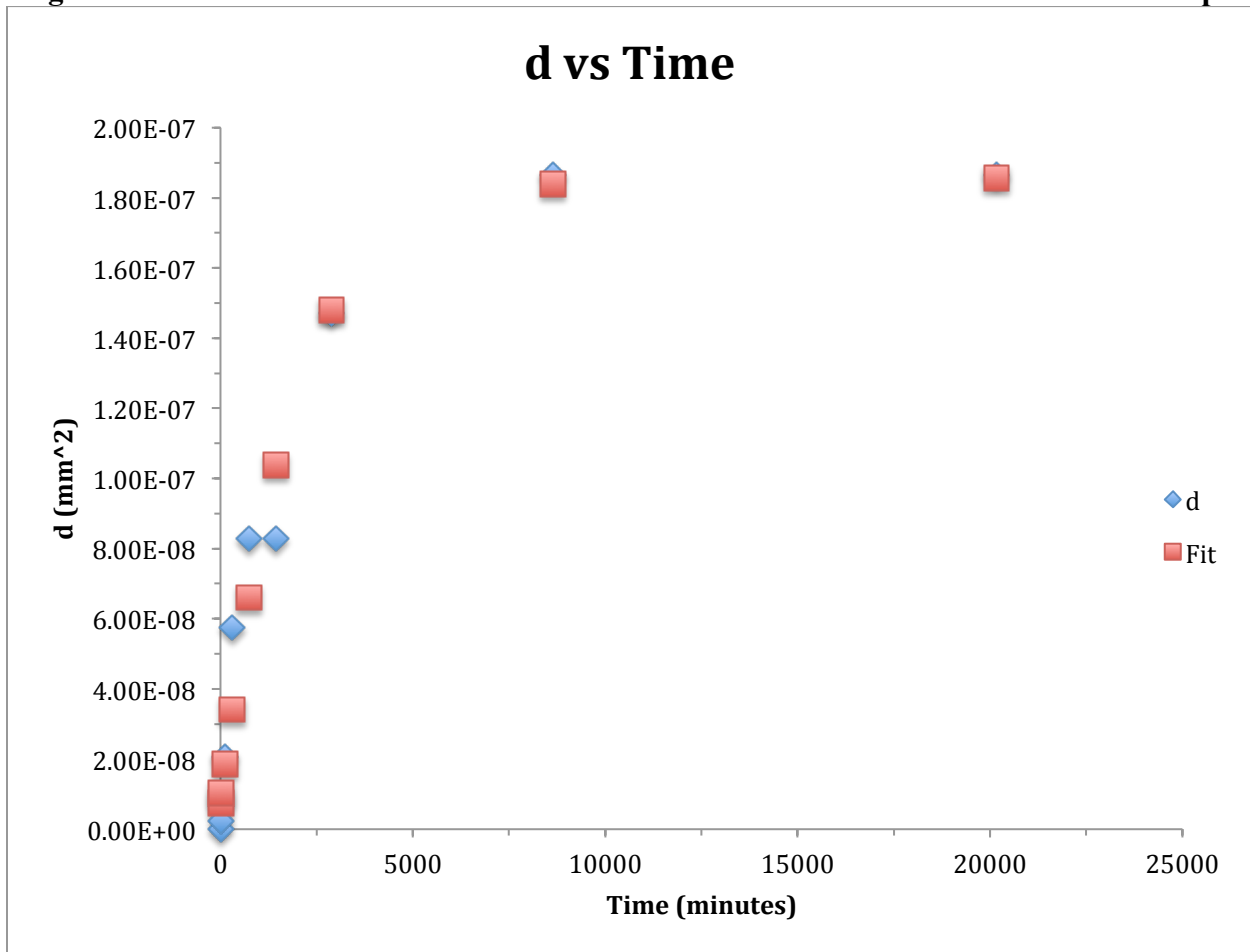


**Table 4.2.12: Water Diffusion Data and Fit for 20130919 1.5% GO/PA-11 Sample\***

Time (minutes)	d (mm <sup>2</sup> )	f(t)=Ae <sup>-bt</sup>	A	b
0	0.00E+00	7.50E-09	-1.78E-07	5.40E-04
30	2.30E-09	1.04E-08		
120	2.07E-08	1.87E-08		
300	5.75E-08	3.42E-08		
739	8.29E-08	6.61E-08		
1,440	8.29E-08	1.04E-07		
2,880	1.47E-07	1.48E-07		
8,640	1.86E-07	1.84E-07		
20,160	1.86E-07	1.86E-07		

\*SSE is 1.45E-15 and R<sup>2</sup> is 0.9709

**Figure 4.2.12: Water Diffusion Plot of Data and Fit for 20130919 1.5% GO/PA-11 Sample**



### 4.3 GO/PA-11 Aging Study Data

Only the November GO/PA-11 samples were used for the 100 C° aging study as mentioned previously. Because we measure  $M_w$  using two different instruments, two different sets of data are shown below. First, the Size Exclusion Chromatography values for  $M_w$  are listed in Table 4.3.1. These values are plotted in Figure 4.3.1. The Multi-Angle Light Scattering values for  $M_w$  are listed in Table 4.3.2 and then plotted in Figure 4.3.2. For comparison, the SEC and MALLS values for the summer samples are shown individually in Table 4.3.3 and then with the neat samples averaged in Table 4.3.4.

**Table 4.3.1: Size Exclusion Chromatography  $M_w$  ( $\frac{g}{mol}$ ) For November GO/PA-11 Samples**

<b>Loading (% GO by weight)</b>	<b>0.0% GO by weight</b>	<b>0.1% GO by weight</b>	<b>0.5% GO by weight</b>	<b>1.0% GO by weight</b>	<b>1.5% GO by weight</b>
<b>Day 0<sup>a</sup></b>	142,000±5,000	102,000±4,000	90,000±20,000	70,000±10,000	50,000±10,000
<b>Day 1</b>	73,300	74,500	62,500	40,200	41,700
<b>Day 3</b>	72,300	70,700	56,000	55,000±6,000*	37,000
<b>Day 10</b>	39,000	69,000±7,000*	66,000±5,000*	51,400	34,000
<b>Day 19</b>	30,300	51,800	60,000	35,500	29,800
<b>Day 28</b>	37,000±3000*	45,900±400*	50,000±2,000*	37,000±3,000*	24,000±2,000*
<b>Day 55</b>	22,200	33,600	39,500	26,700	26,700
<b>Day 83</b>	25,000	36,300	36,000±5,000*	27,000	24,000±4,000*

<sup>a</sup>The “Day 0”  $M_w$  was measured three times to test accuracy of instrument

\*Values are averages of multiple values because the first value measured did not fit the trend

**Table 4.3.2: Multi-Angle Light Scattering  $M_w$  ( $\frac{g}{mol}$ ) For November GO/PA-11 Samples**

Loading (% GO by weight)	0.0% GO by weight	0.1% GO by weight	0.5% GO by weight	1.0% GO by weight	1.5% GO by weight
Day 0 <sup>a</sup>	150,000±30,000	119,000±6,000	110,000±20,000	70,000±20,000	53,000±4,000
Day 1	95,000	73,900	74,500	40,800	40,400
Day 3	98,700	67,600	54,000	55,100±400*	44,800
Day 10	40,500	69,000±7,000*	70,000±10,000*	60,000	41,000
Day 19	45,300	57,600	69,400	41,800	34,500
Day 28	37,000±1000*	46,000±9000*	53,700±800*	41,000±3000*	30,700±100*
Day 55	22,600	34,000	40,600	29,400	27,700
Day 83	30,800	40,900	44,000±6,000*	37,100	29,400±200*

<sup>a</sup>The “Day 0”  $M_w$  was measured three times to test accuracy of instrument

\*Values are averages of multiple values because the first value measured did not fit the trend

**Table 4.3.3: SEC and MALLS  $\bar{M}_w$  values for Neat summer samples**

Loading (% GO by weight)	Cut Date	SEC-EF $\bar{M}_w$ ( $\frac{g}{mol}$ )	MALLS $\bar{M}_w$ ( $\frac{g}{mol}$ )
0.0	20130709	93,900	119,900
0.0	20130715	36,900	39,900
0.0*	20130724	50,000±10,000	70,000±10,000
0.0	20130710	73,500	86,300
0.0	20130919	133,700	170,800

\* Three values taken for an instrument accuracy check; values are averaged

**Table 4.3.4: SEC and MALLS  $\bar{M}_w$  of loaded summer samples With Neat Values Averaged**

Loading (% GO by weight)	Cut Date	SEC-EF $\bar{M}_w$ ( $\frac{g}{mol}$ )	MALLS $\bar{M}_w$ ( $\frac{g}{mol}$ )
0.0	-----	80,000±40,000	100,000±50,000
0.1	20130709	39,000	46,400
0.1	20130715	63,200	70,600
0.5	20130724	46,800	36,600
1.0	20130710	43,800	45,200
1.5	20130919	36,700	41,400



Figure 4.3.1: Size Exclusion Chromatography  $M_w$  For November GO/PA-11 Samples

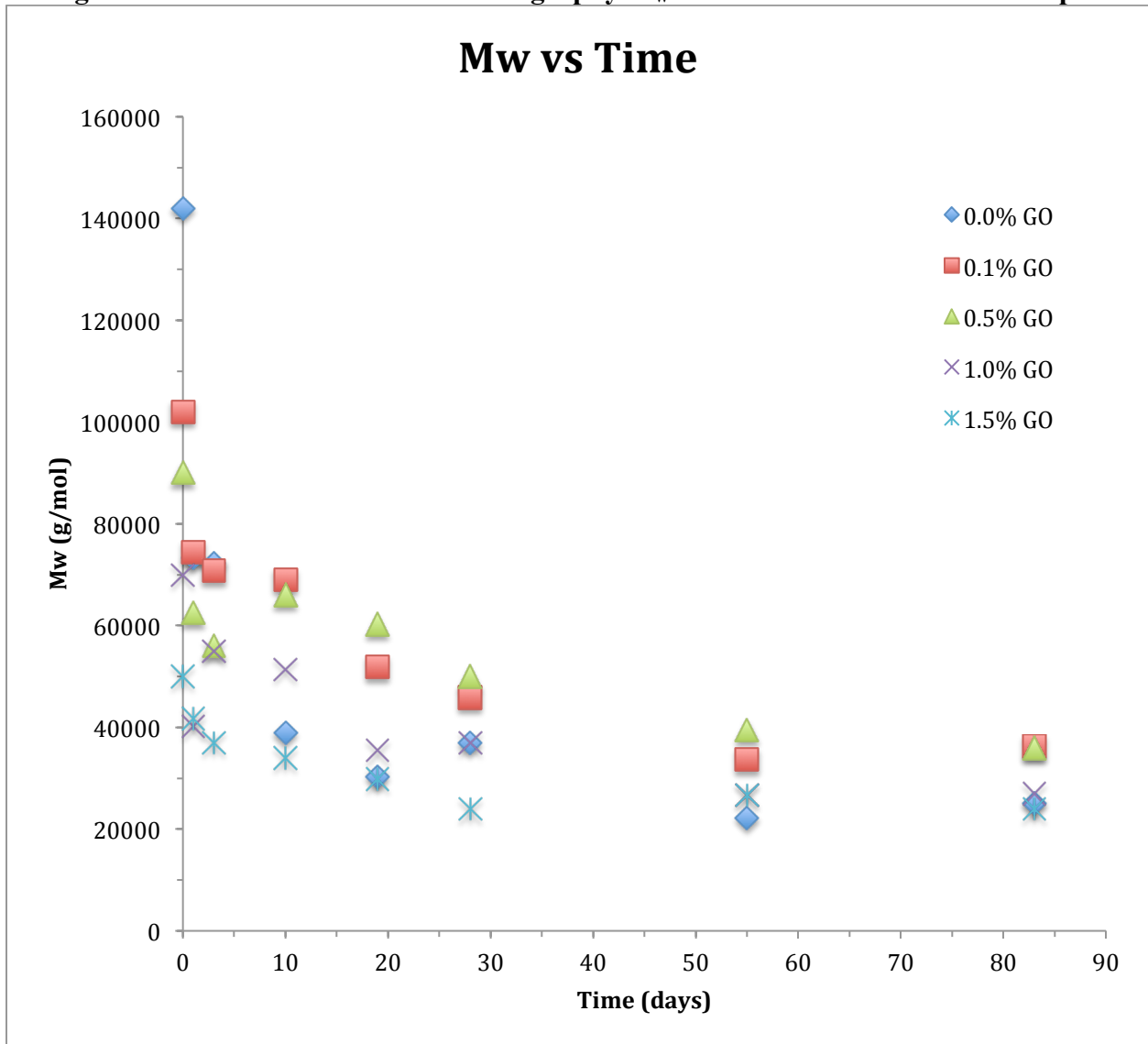
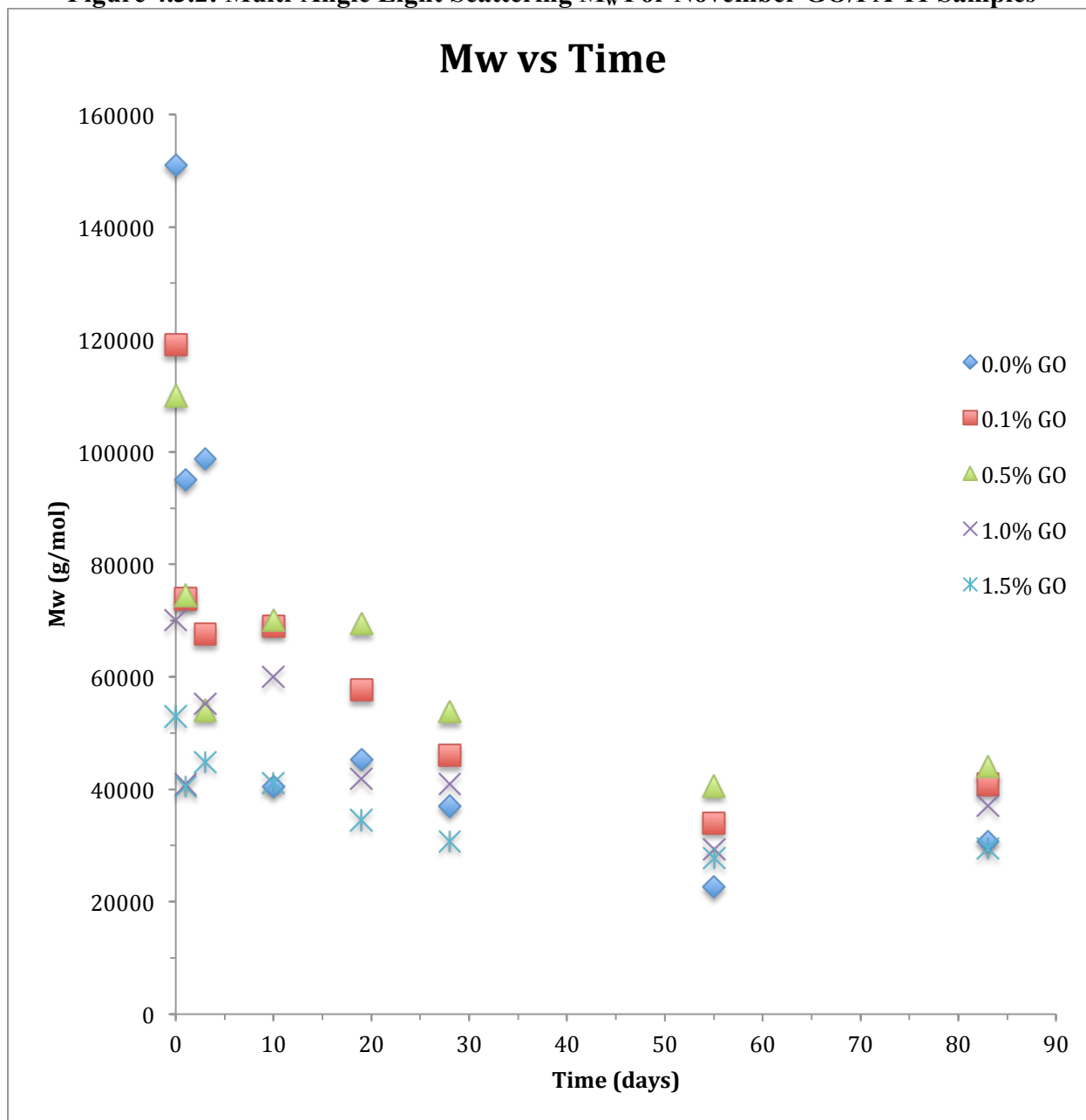


Figure 4.3.2: Multi-Angle Light Scattering  $M_w$  For November GO/PA-11 Samples



#### 4.4 GO/PA-11 Differential Scanning Calorimetry Data

DSC results for both the summer and November samples are presented below. As mentioned in the instrumentation section, a ramp up to 250 C° was followed by cooling 3C°/minute to 50 C° before a second ramp back up to 250 C° at 3C°/minute. Values were obtained using constant integration limits between 140 C° – 200 C°. Table 4.4.1 lists the individual T<sub>m</sub> and crystallinity values for each neat summer sample in both ramp cycles. Table 4.4.2 lists the T<sub>m</sub> and crystallinity values for the neat summer samples averaged together along with the individual DSC values for the loaded samples in both ramp cycles. Table 4.4.3 lists the T<sub>m</sub> and crystallinity values for the November samples in both ramp cycles. Figure 4.4.1 plots the T<sub>m</sub> and crystallinity versus the GO loading for the summer and November samples during the first ramp—the neat values are averaged. Figure 4.4.2 plots the T<sub>m</sub> and the crystallinity versus the GO loading for the summer and November samples during the second ramp.

**Table 4.4.1: Individual Neat DSC Values for Summer GO/PA-11 Samples**

Loading (% GO by weight)	1st Ramp			2nd Ramp	
	Date Cut	Melting Temperature (C°)	Crystallinity (%)	Melting Temperature (C°)	Crystallinity (%)
0.0	20130709	188.89	26.57	188.11	28.59
0.0	20130724	188.87	26.88	187.97	29.53
0.0	20130710	188.82	26.00	187.90	28.17
0.0	20130919	186.30	24.75	186.87	26.28
0.0	20130715	189.42	27.45	188.64	29.78

**Table 4.4.2: Averaged Neat and Individual Loaded GO/PA-11 DSC Values for Summer Samples**

	1 <sup>st</sup> Ramp		2 <sup>nd</sup> Ramp	
Loading (% GO by Weight)	Melting Temperature (C°)	Crystallinity (%)	Melting Temperature (C°)	Crystallinity (%)
0.0*	188±1	26±1	187.9±0.6	28±1
0.1 <sup>a</sup>	190.7±0.2	33±2	190.08±0.08	30±1
0.1 <sup>b</sup>	190.65	27.06	189.07	29.32
0.5	190.06	27.43	189.55	30.41
1.0	190.00	27.77	189.36	30.72
1.5	189.42	29.84	189.10	32.36

\* Each loaded sample was polymerized together with one neat sample; the neat samples were averaged together

<sup>a</sup>20130709 values are an average among 3 measurements on the same sample because of abnormally high crystallinity; this sample was used in the Water Absorption Tests but not the tensile tests because the film was full of defects

<sup>b</sup>20130715 sample used in the Tensile Tests but not in the Water Absorption Tests

**Table 4.4.3: Individual DSC Values For November GO/PA-11 Samples**

	1 <sup>st</sup> Ramp		2 <sup>nd</sup> Ramp	
Loading (% GO by Weight)	Melting Temperature (C°)	Crystallinity (%)	Melting Temperature (C°)	Crystallinity (%)
0.0 <sup>a</sup>	186±1	25.4±0.8	186±2	27±2
0.1	190.08	26.51	187.91	28.04
0.5	189.80	27.81	189.03	29.79
1.0	190.09	28.01	189.09	30.57
1.5 <sup>b</sup>	190.0±0.2	30±2	189.6±0.3	31.9±0.8

<sup>a</sup>Values are averaged between two samples

<sup>b</sup>Values are averaged between three samples

Figure 4.4.1: GO/PA-11 Sample 1st Ramp with Neat Values Averaged

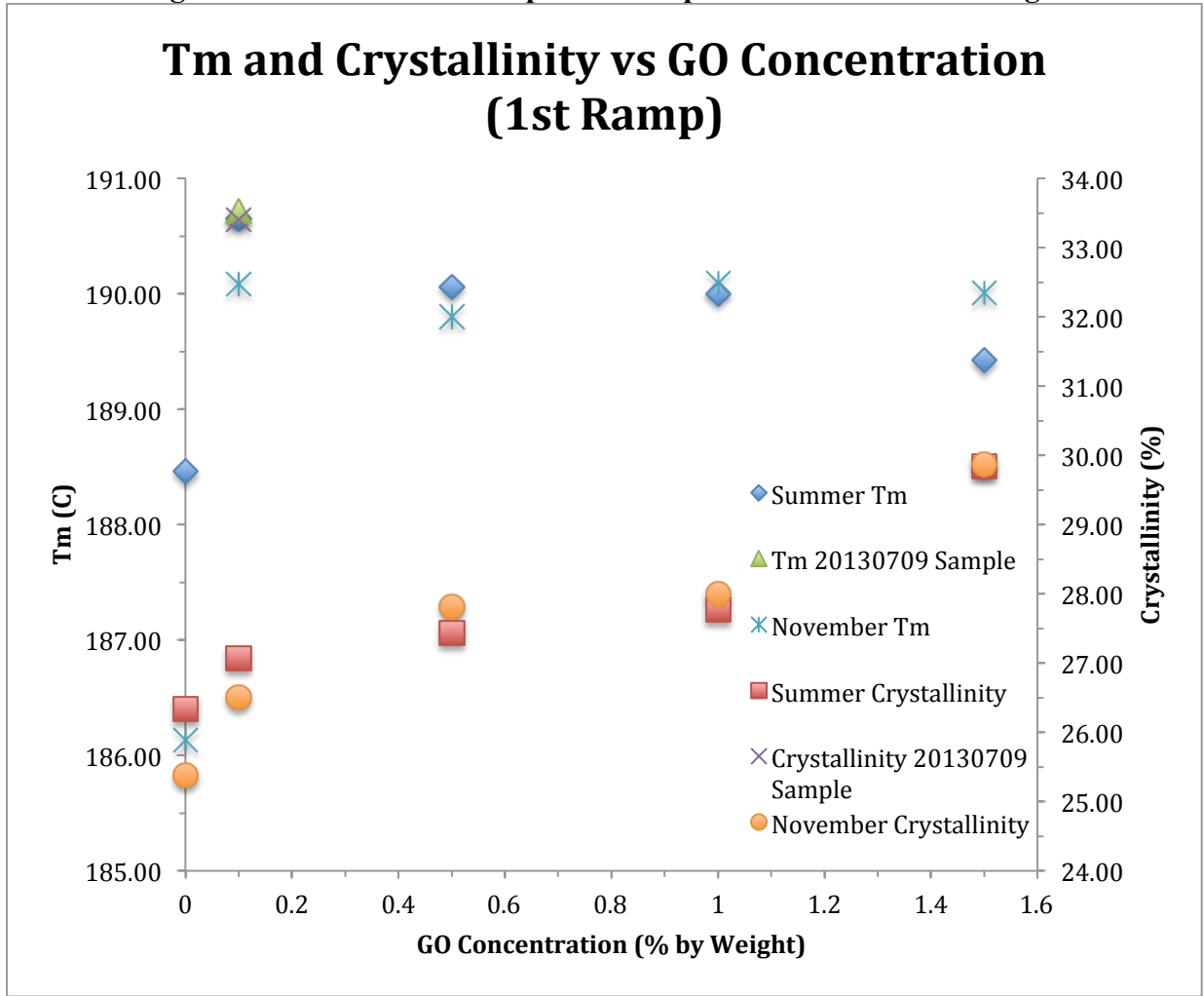
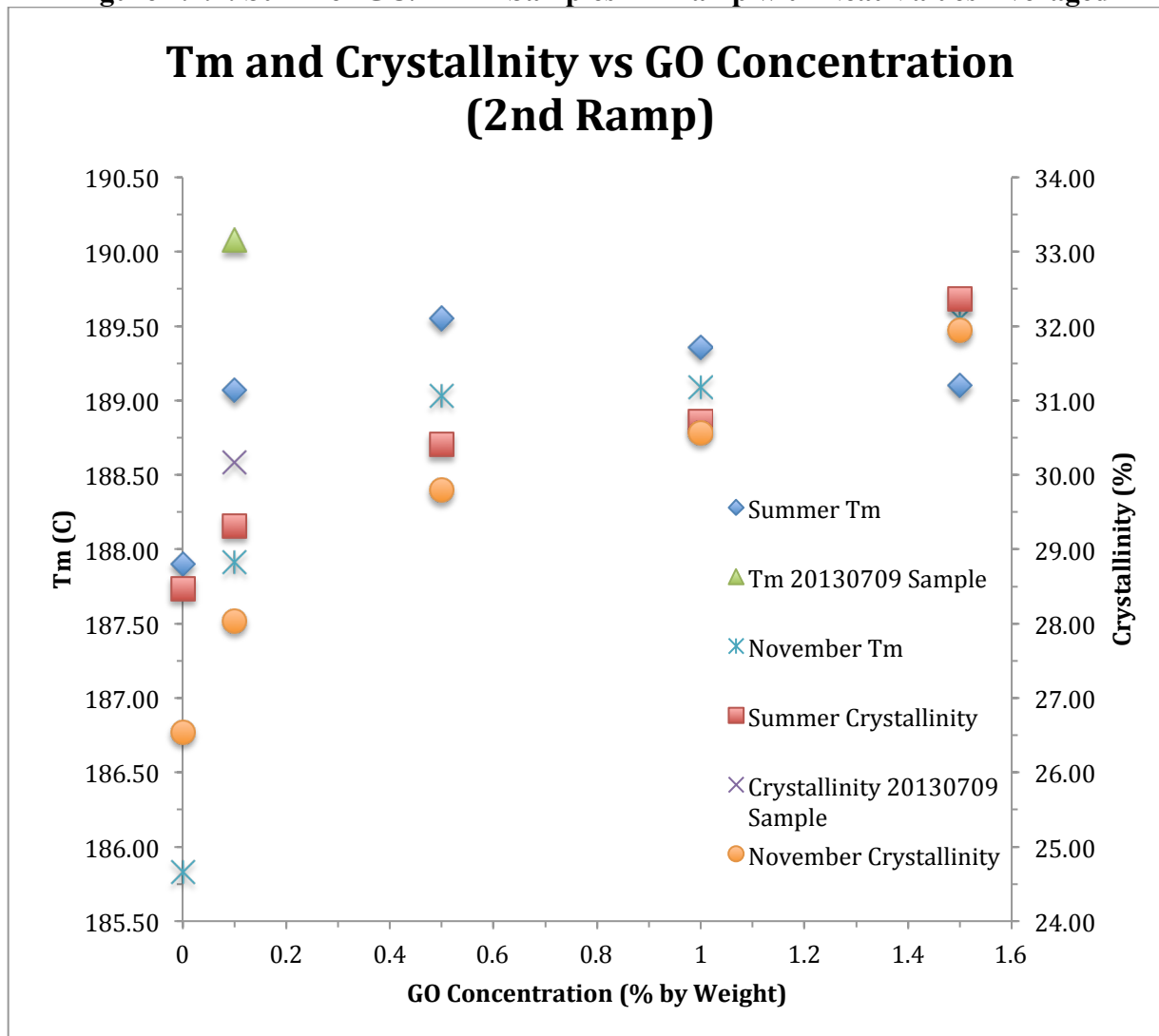


Figure 4.4.2: Summer GO/PA-11 Samples 2<sup>nd</sup> Ramp with Neat Values Averaged



## Chapter 5: Discussion

### 5.1 Differential Scanning Calorimetry

The crystallinity of our samples have important implications on the tensile, water diffusion, and aging studies. For this reason, it is important that I address the crystallinity data first.

Table 4.4.2 and Figures 4.4.1 and 4.4.2 show the crystallinity data for the summer samples. First, there appears to be a continuous increase in crystallinity with GO concentration for the first ramp cycle of the summer samples illustrated in Figure 4.4.1. All loaded samples seem to have a  $T_m$  around  $\sim 190\text{ C}^\circ$  compared to the neat samples' average  $T_m$  at  $188\text{ C}^\circ$ . There is a significant outlier for the 0.1% GO summer sample cut on 20130709 shown in Table 4.4.2. Its crystallinity is roughly 4-6% higher than the rest of the loaded summer samples. However, the 0.1% GO sample cut on 20130715 shows a  $T_m$  that is very similar to the 20130709 outlier even though it is a separate system—polymerized and cut on a different date. But, the 20130715 0.1% GO sample has a crystallinity that falls more in line with the other samples on the first ramp.

On the second ramp for the summer samples, the crystallinity increases somewhat more linearly with GO concentration shown in Figure 4.4.2. Additionally, the crystallinity is generally higher than the values for the 1<sup>st</sup> ramp cycle. The  $T_m$  for the second ramp on the summer samples shows more of a trend by increasing gradually to a maximum value of  $189.55\text{ C}^\circ$  at 0.5% GO and then decreases at higher GO concentration. The 0.1% 20130709 outlier still shows higher crystallinity and  $T_m$  than the rest. The second ramp should show the effects of GO concentration on  $T_m$  and crystallinity more accurately since the thermal history of all of the samples is controlled and identical.

Table 4.4.3 and Figures 4.4.1 and 4.4.2 show the crystallinity data for the November samples. The first ramp cycle shown in Figure 4.4.1 indicates a linear increase in crystallinity very similar to that of the summer samples. Additionally the  $T_m$  is higher for all GO concentrations relative to the neat system and approach the same value of 190 C° as was shown for the loaded summer samples.

The second ramp cycle for the November samples shows another linear increase in crystallinity with GO concentration; however, these values are higher than the values listed during the first ramp cycle as seen for the summer samples. Lastly the  $T_m$  values follow what looks to be an inverse exponential increase with increasing GO concentration. Given that more variables are controlled for in these November samples, the second ramp is most likely to give the best correlation of GO concentration with crystallinity in PA-11.

As noted above, both the summer and November samples show an approximately linear increase in crystallinity with GO concentration. The cause of this increase in crystallinity is most likely due to the hydrogen bonding, dipole-dipole, and London dispersion forces between the GO sheets and the PA-11 chains. Hydrogen bonding was shown to be present in GO/PA-11 by Jin, et al.<sup>22</sup> These hydrogen bonds could also act to bind the polymer chains in place on the surface of the GO sheets. This ordering of PA-11 chains on the surface of the GO sheets would create an ordered substrate on which other PA-11 chains could interact given the right orientation. Thus, the linear increase in crystallinity with GO concentration is most likely the result of hydrogen bonding between the GO sheets and the PA-11 chains.

As a result of these non-covalent interactions, it is possible that the DSC is not only measuring the enthalpy required to melt the crystalline regions but also the enthalpy required to break the dipole-dipole and hydrogen bonds between the GO particles and the PA-11 chains.



Theoretically, the dipole-dipole and hydrogen bonds would only break when the PA-11 chains enter the mobile phase and disrupt these interactions. Since these interactions would hinder mobility, additional enthalpy would be required for the PA-11 chains to enter the mobile phase. This concept would explain why the  $T_m$  is also higher for the loaded samples than for the neat ones in both the summer and November batches. A higher average kinetic energy of the polymer chains and GO particles would be necessary to break these additional dipole-dipole and hydrogen bonds.

Therefore, it is unclear whether this increase in measured enthalpy necessary correlates to increased crystallinity of the polymer systems or to the increase in hydrogen bonds between the GO sheets and PA-11 chains. I suggest that a future study be done on these GO/PA-11 interactions using computational chemistry software as well as atomic force microscopy (AFM) measurements on the GO/PA-11 films. For now, the crystallinity measurements will be referred to as “measured crystallinity” until this ambiguity is elaborated on later in this section.

## 5.2 Tensile Properties

As shown by tables 4.1.2 and 4.1.3, two different and conflicting sets of data were obtained between the summer samples and the November samples. The summer samples show an improvement in tensile properties for the 0.1% system and then a decay with increasing GO concentration. However, the Modulus increases continuously. The November samples show no improvement in tensile properties at 0.1% and a trend of decaying properties vs GO concentration except for the Modulus readings. After examining both sets of data individually, the differences in the methods used to make them must be elaborated.

Despite less control over the polymerization and press processes, the summer samples show the most interesting trends in Figures 4.1.1 and 4.1.2. The 0.1% GO by weight sample shows improvements in all properties. Not only does this sample show the highest strain, it also displays the highest tensile strength. The strain and the tensile strength decay as more GO is added to the polymer matrix above 0.1% GO by weight. However, the Young's modulus steadily increases as more GO was added to the polymer matrix and levels off at 1.0 -1.5% GO by weight. All of these trends were predicted by my original hypothesis stating that the tensile properties would increase at low GO concentrations and decay at higher concentrations.

Lahiri, et al.<sup>10</sup> described an initial increase in the ultimate strain, Young's modulus, and tensile strength in graphene/polyethylene composites at low concentrations of graphene particles. It is important to note that this group used non-oxidized graphene nanoplatelets that they ultrasonicated in acetone unlike our samples which are oxidized.<sup>10</sup> It is doubtful that the Lahiri group was able to achieve complete exfoliation of these graphene particles since all of the literature indicate that graphite must be oxidized and then sonicated in order to be properly exfoliated on a mass scale.<sup>8</sup> Lahiri attributed this increase in tensile properties at 0.1% by weight

graphene concentration to individual graphene sheets being more homogeneously dispersed throughout the polymer matrix.<sup>10</sup> Thus, the polymer chains are able to more effectively wrap each individual graphene particle since there would be favorable London dispersion interactions between the polyethylene chains and the graphene sheets.<sup>10</sup> If a stress is applied to the system, each one of these points of contact transfers stress from a polymer chain to the strong C—C bonds of a graphene sheet.<sup>10</sup> Additionally, this group attributed a decay in the elongation and tensile stress at 1.0% by weight graphene concentration to agglomeration of the graphene particles and less wrapping of these agglomerates by the polymer chains.<sup>10</sup> Lahiri, et al.<sup>10</sup> claim to have identified agglomerated graphene sheets within fracture surfaces on their graphene/polyethylene systems at 1.0% graphene concentration using scanning electron microscopy (SEM) images. Their images of both graphene concentrations seem clear and their interpretation of the images seems logical given the difference in observed textures between graphene sheets and the surrounding polymer matrix. They attributed the continuous increase in the modulus with graphene concentration to an increase in the probability that the basal planes will be oriented along the tensile axis; the force would thus be applied in-plane with the graphene sheets where it would be distributed amongst the strong C—C bonds.<sup>10</sup> Additionally, they attribute the increase of the modulus from 0.1% to 1.0% graphene as not being ten times as great because of the agglomeration of graphene which reduces entanglement and stress transfer.<sup>10</sup> Although the composite system used in this paper is significantly different than ours, the favorable interactions between unoxidized graphene and polyethylene should mirror that of our GO/PA-11 systems but the strengthening effects in our composites should be stronger.

Bhattacharyya, et al.<sup>27</sup> wrote a paper where they dispersed GO in ultra high molecular weight polyethylene (UHMWPE) using two techniques. The first technique involved pre-

reducing the GO before dispersing it in UHMWPE dissolved in DMF while the second technique dissolved the unreduced GO particles and UHMWPE in DMF before chemically reducing the dispersion in-situ.<sup>27</sup> They indicate that there is significantly more agglomeration in the pre-reduced GO/UHMWPE samples than the in-situ reduced GO/UHMWPE samples via D band analysis of Raman spectroscopy.<sup>27</sup> Their Raman peaks look very significant and their analysis using the increase in the D band correlating with greater exfoliation seems valid. Thus, Bhattacharyya stated that the large increase in the Young's modulus with a decrease in percent elongation is correlated with agglomeration of GO particles.<sup>27</sup> These results and conclusions agree with that of Lahiri, et al.<sup>10</sup> Moreover, they explain the increase in modulus as due to crystallinity since more exfoliated GO particles would hinder the chain mobility and thereby nucleation.<sup>27</sup> This most likely results from unfavorable interactions between the polar GO sheets and the non-polar polyethylene chains. However since they are using a non-polar polymer with relatively more polar, reduced GO sheets, this system differs from ours even more so than Lahiri et al.'s due to less favorable interactions between polymer and reduced GO sheets.

Jin, et al.<sup>22</sup> synthesized GO/PA-11 composites using commercial PA-11 in a "melt-compounding" and "compression molding" technique with an extrusion device. Their GO was synthesized via the Hummers' method similar to ours.<sup>22</sup> Their tensile data shows a direct correlation between increasing Young's modulus with increased GO concentration. Moreover, their ultimate strain shows a maximum around 0.1% and 0.3% GO by weight and then decreases with increasing GO concentration.<sup>22</sup> This group used SEM and transmission electron microscopy (TEM) to claim that they had well-dispersed GO/PA-11 composites at 0.6% GO by weight but they do not show any SEM or TEM images of any other GO/PA-11 concentrations.<sup>22</sup> Moreover, these images that they do show do not appear to definitively isolate any individual GO sheets.<sup>22</sup>

Therefore, it is unclear how they differentiated between agglomerations and individual GO sheets.<sup>22</sup> Regardless, they attribute the decay in the tensile properties—other than the modulus—at higher GO concentrations due to agglomeration and a less uniform dispersion.<sup>22</sup> Lastly, they indicate using Fourier transform-infrared spectroscopy (FT-IR) that hydrogen bonding exists between the amide groups in the PA-11 and the carboxylic acid groups in the GO sheets.<sup>22</sup> Their FT-IR spectra show significant peaks with little noise and their reasoning that hydrogen bonding between these groups would shift the FT-IR peaks seems reasonable. This paper by Jin, et al.<sup>22</sup> should be the most comparable to our GO/PA-11 systems and results.

The increase in ultimate strain for the 0.1% GO by weight summer sample can be explained as a matter of hydrogen bonding and stress transfer to the GO sheets similar to what Lahiri, et al.<sup>10</sup> described. The points of contact that result from this wrapping effect arise in the form of hydrogen bond attractions between segments of the polymer chain and the surface of the GO sheets.<sup>10</sup> These hydrogen bond interactions are much stronger than the London dispersion forces in Lahiri, et al.'s graphene/polyethylene systems.<sup>10</sup> Therefore, the more points of contact present in a GO/polymer system, the more non-covalent interactions will result. Because the 2-dimensional surface area of the GO sheets is much greater than the 1-dimensional surface area of the other polymer chains, more points of contact are established when GO particles are well dispersed in the polymer matrix. Thus, the polymer system can elongate further before fracturing because there is more interactions between each individual polymer chain and a corresponding GO particle—which is presumably wrapped by other polymer chains.

Additionally, the trend in tensile strength mirrors that of the ultimate strain for the summer samples shown in Figures 4.1.1 and 4.1.2. It follows that more points of contact between polymer chains and GO particles requires more total stress to break all of the non-covalent

interactions.<sup>10</sup> Therefore, the peak in tensile strength at 0.1% GO by weight is observed along with the peak in ultimate strain most likely due to a better dispersed GO/PA-11 system.

The decay of mechanical properties in the summer samples above a concentration of 0.1% GO can also be explained in terms of entanglement and stress transfer. At higher GO concentrations—such as 0.5%, 1.0%, and 1.5% GO by weight—, the GO particles most likely agglomerate back into stacks during polymerization since the melt phase of PA-11 initially has a relatively low viscosity until it reaches a high molecular weight.<sup>10</sup> These stacks result in a decrease in the surface area available for the polymer chains to wrap.<sup>10</sup> Less effective wrapping results in less non-covalent interactions per GO particle which results in less stress transfer per particle.<sup>10</sup> It is important to note that the total number of non-covalent interactions between polymer chains and GO particles increases at higher GO concentrations but the points of contact between polymer chains decreases. If these stacks exist, they create fracture points within the polymer matrix since the interface between agglomerated GO sheets is weak—due to the repulsive oxygen functionalities on each face.<sup>10</sup> Any significant amount of stress applied to the system will cause the points of contact between polymer and GO agglomerates to break the stacked GO sheets apart due to the shear stress applied by the PA-11 chains wrapped around them.<sup>10</sup> In theory, the noncovalent interactions between polymer and GO sheet should be stronger than the non-covalent interactions between multiple unreduced GO sheets. Thus, material with lots of agglomerates in it will fail before any appreciable load is applied.<sup>10</sup> Therefore, the macroscopic result of agglomeration in GO/PA-11 would be a shorter ultimate strain and lower tensile strength. A further investigation by our lab should consist of using AFM to see if agglomerates can be identified in the fracture regions of our summer samples to confirm this hypothesis.

The trend in the Young's modulus requires a different kind of analysis. Lahiri, et al.'s explanation cannot be the case.<sup>10</sup> We can see SEM images from Compton, et al.<sup>11</sup> and Bhattacharyya, et al.<sup>27</sup> that show GO sheets are crumpled in the polymer matrix and do not have a defined basal plane. Even Lahiri's own SEM images show that his unoxidized graphene particles take a wrinkled morphology in the polymer matrix.<sup>10</sup> Additionally, the stress transfer via non-covalent bond interactions between GO sheets and polymer chains would occur in any orientation of the GO sheets due to random entanglement.

Thus, a more viable explanation originates from changes in crystallinity. Tables 4.4.2 and 4.4.3 show that the measured crystallinity increases with GO concentration even in the first ramp cycle in both the summer and November samples. This increase in crystallinity is in direct correlation with the Young's modulus shown in Tables 4.1.2 and 4.1.3. Increases in crystallinity of different polymers have been well documented as causing a stiffening of the polymer chains and increasing the Young's modulus.<sup>17</sup> As described previously, there appears to be an increase in the entanglement between GO particles and the PA-11 chains due to the addition of dipole-dipole and hydrogen bonding forces. These forces likely allow the GO sheets to serve as nucleating sites for the PA-11 chains. However as the particles agglomerate at higher GO concentrations, there is less surface area available for the PA-11 chains to form favorable hydrogen bonding interactions. Although there are certainly more total hydrogen bonding interactions at higher GO concentration, they are not able to form as efficiently since the PA-11 chains cannot wrap the large agglomerates as effectively as they can individual GO sheets.<sup>10</sup> This hypothesis would explain why there is a larger increase in measured crystallinity (~1%) between 0.0% GO and 0.1% GO than the 0.5% and 1.0% GO summer samples shown in Table 4.4.2. The GO sheets in the 0.1% GO sample are theoretically more exfoliated and have more points of

contact with the PA-11 chains per GO particle. This same increase between 0.0% and 0.1% GO relative to the 0.5% and 1% GO samples is also shown for the November samples in Table 4.4.3. This causal explanation between crystallinity and Young's modulus concurs with Bhattacharyya, et al.<sup>27</sup> and their analysis on GO/polyethylene composites; except our GO particles increase crystallinity rather than quench it as seen in their system.

However, there is another explanation that could account for the increase the Young's modulus with increasing GO concentration. It is possible that the London dispersion, dipole-dipole, and hydrogen bonding attractions between the polymer and the GO particle itself increase the Young's modulus. Just as the increased non-covalent interactions helped improve the tensile strength, it is possible that these additional hydrogen bonding and dipole-dipole interactions also contribute to bind the polymer chains in place making them stiffer especially when the GO particles are well dispersed. As the GO particles agglomerate, the number of hydrogen bonding interactions per particle decreases significantly. It is likely that if the agglomeration becomes significant enough, the decrease in elongation due to enlarged fracture sites overtakes the stiffening effect of more GO interactions with PA-11 chains. When this occurs, the material fails before any significant stress is applied even though it is stiffer. This results in the leveling off of the Young's modulus as shown in Table 4.1.2 and Figure 4.1.1.

One additional factor that could increase the Young's modulus of these samples is a free volume effect. As Compton notes in his gas permeation work, GO particles occupy more free volume within the polymer matrix as their concentration increases regardless of whether or not they agglomerate.<sup>11</sup> As larger and more GO particles occupy the free volume and interstitial cavities within a polymer matrix, the amount of conformations that a single polymer chain can take decreases.<sup>11</sup> This reduction in free volume hinders the movement of the polymer chains and



effectively “locks” them into fewer and fewer conformations. Thus, the increase in GO concentration would result in a stiffening of the individual polymer chains. The macroscopic result is that the material becomes stiffer meaning that the Young’s modulus increases continuously with GO concentration. Both optical microscopy and AFM should be used to confirm the existence of agglomerates in these concentrations for a future study.

Initially, we believed that the November samples—being more controlled during the polymerization and press processes—would produce more consistent and accurate results. But instead, the results are puzzling. The ultimate strain for the November neat system is relatively close to that of the summer samples given their standard deviations as shown in Tables 4.1.2 and 4.1.3. Additionally, the strain decays linearly with increasing GO concentration in the November samples. This result is in stark contrast to the improvement in ultimate strain for the 0.1% summer sample. Moreover, the tensile strength for the November neat system is even more similar to that of the neat system of the summer samples in Table 4.1.2. Yet, the tensile strength also decays with increasing GO concentration in the November samples. The only trend that shows any consistency with the summer samples is the Young’s modulus which increases linearly with GO concentration as shown in figure 4.1.1. However, these moduli are about 200 – 400 MPa higher than the moduli in the summer samples except for the 0.5% GO concentration.

This difference in the moduli between the summer and November samples is most likely the result of more agglomeration in the November samples than in the summer samples. Unlike Bhattacharyya, et al.<sup>27</sup>, our system has favorable interactions between the polar GO particles and relatively polar PA-11 chains. Although Bhattacharyya’s analysis—based on crystallinity—possibly explains the correlation between the Young’s modulus and GO concentration, it cannot explain the difference in mechanical properties between the summer and November samples.<sup>27</sup>

A more viable explanation for the reduction in tensile properties in the November samples corresponds to the exfoliation quality. The 0.1% GO summer sample in Table 4.4.2 actually appears more crystalline than the 0.1% November sample in Table 4.4.3. The 0.1% GO summer sample has a longer ultimate strain and a lower modulus than the November 0.1% GO system as shown in Tables 4.1.2 and 4.1.3. Thus, the crystallinity alone cannot explain the different behavior of the Young's modulus between the summer and November samples. The only viable explanation for an increase in measured crystallinity but a lower modulus for the summer 0.1% GO sample relative to the November sample at the same GO concentration is a reduction in the total number of hydrogen bonding interactions between PA-11 chains and individual GO particles due to agglomeration in the November samples. Once the GO concentration reaches 0.5% - 1.5% GO concentration, the November samples have a higher measured crystallinity than the summer samples as shown in Tables 4.4.2 and 4.4.3. Given this higher measured crystallinity above 0.1% GO concentration for the November samples, it is important to note that the Young's modulus continues to increase rather than level off as it does in the summer samples. In fact, the Young's modulus at 1.5% GO concentration for the November sample is 300 MPa higher than the corresponding summer sample. This continuous increase in the Young's modulus for the November samples in Table 4.1.3 is likely the result of the stiffening of the GO sheets themselves when they agglomerate. The hydrogen bonds that form between GO sheets as they reduce and agglomerate could restrict bond rotations of the sheets making them less flexible. If the sheets agglomerate significantly, it is possible that the sheets become locked into the planar conformation exclusively with little or no crumpling. Once embedded into the polymer matrix, these very stiff particles would form some favorable hydrogen bonds with adjacent polymer chains and would significantly reduce their mobility. It is

important to note that although well exfoliated GO sheets restrict mobility to an extent, they mostly serve to dissipate stress. Therefore, the difference in tensile properties between the November and the summer samples may be the result of the GO particles agglomerating to form more fracture sites as well.

The cause of the differences in exfoliation between the summer and November GO/PA-11 samples is most likely due to the heating rate of the oven and the masses of the monomer used. Not only were all five beakers with monomer, water, and GO in the oven during the November polymerization, but there were 3 g of monomer per dispersion. Thus, there was more matter for the oven to heat than the two beakers polymerized at a time for the summer samples with only 2 g of monomer per dispersion. Therefore, more heat input and more time is required to heat the samples to the same temperature. A sufficient difference in heating rates would theoretically result in different exfoliation properties for the GO. Preliminary tests show that GO sheets can be reduced at as low a temperature as 125 C°. <sup>2</sup> Whenever GO is reduced, it has a tendency to agglomerate due to the increased, hydrophobic  $\pi$ -stacking interactions. <sup>8</sup> Our polymer (and monomer) samples have a melting temperature around 190 C° as shown by Tables 4.4.2 and 4.4.3; however, we noticed that the monomer does not start to polymerize appreciably until the temperature reaches at least ~220 C°. Thus, the slower heating rate would allow the monomer dispersions to remain between 190 - 220 C° for a longer period of time. Therefore, the GO sheets will have more time to reduce in a relatively low viscosity melt phase of the reacting monomers. The faster heating rate will shorten this time between 190 – 220 C° and allow the monomers to react quickly enough to reach a higher viscosity melt phase preventing the GO sheets from agglomerating. In other words, the polymer chains become long enough to disrupt the agglomeration of GO particles as they reduce.

The average rate of heating for the summer samples was about 1.27 C° per minute while heating rate of the November samples was about 1.11 C° per minute. This difference may seem insignificant at first but it is important to keep in mind that this correlates to a difference of ~5 minutes between 190 – 220 C°. This difference also assumes that the samples are the same temperature as the oven at any given time. The samples most likely lag behind the oven in temperature as its measured temperature increases. It is possible that the reduction that GO undergoes in this temperature range could be sufficient to cause significantly more agglomeration in just five more minutes if not longer. I suggest that an experiment be conducted where the oven is preheated to temperature and all five dispersions are immediately placed in the oven for polymerization. Another possible solution would be to use an extruder to polymerize the samples since it would be able to stir the melted polymer and theoretically keep the GO particles exfoliated. All pressing techniques for the November samples should remain the same. Then the films should be evaluated for tensile testing and crystallinity to see if the dispersion and tensile properties are improved.

The ultimate strain of the summer samples and the Young's modulus of the November samples most closely resembles that of Jin, et al.<sup>22</sup> and is thus worth some comparison. First of all, the Jin group used some industrial samples with  $\bar{M}_n = 3,000$  g/mol.<sup>22</sup> This value is significantly below the ductile-brittle transition  $\bar{M}_w$  of ~25,000 g/mol ( $\bar{M}_n = \sim 12,500$  g/mol).<sup>3,4</sup> Unless they have a very low crystalline content allowing their material to be more ductile, one would expect their tensile results to be dismal.<sup>28</sup> Indeed, their crystallinities were 15.7 – 19.8% which is significantly lower than the crystallinity of any of our samples listed in Tables 4.4.2 and 4.4.3.<sup>22</sup> Their data for Ultimate Strain has the same trend as the data we took for ultimate strain for the summer samples.<sup>22</sup> However, their strain is about 200% lower than ours for the 0.1% and

neat summer samples.<sup>22</sup> Yet, their 0.1% GO sample shows one of the highest elongations just like our summer 0.1% sample does.<sup>22</sup> Their 1.0% GO sample shows an ultimate strain comparable with our 1.0% summer sample.<sup>22</sup> However, their 3% GO sample has an Ultimate Strain significantly longer than our 1.5% sample.<sup>22</sup> Moreover, Jin's Young's modulus is significantly higher than our summer samples for all concentrations of GO by 200-400 MPa and more similar to our November samples.<sup>22</sup>

This discrepancy between our measured strain and that of Jin, et al.'s fits the trend of increased agglomeration from the previous discussion. Jin's group states that they used a "melt compounding" technique with an extruder at 210 C°; then the sample was compression molded at 210 C° at a pressure of 20 MPa.<sup>22</sup> Although the use of an extruder in the first step of "melt compounding" would theoretically keep the GO sheets exfoliated for the most part, there is very little polymerization at this temperature especially for the 10 minute duration stated.<sup>22</sup> Therefore, the melted mixture would have a very low viscosity due to its starting molecular weight causing the polymer chains to have very low entanglement.<sup>3</sup> Once put into a mold under pressure at 210 C°, the system is no longer agitated by the extruder allowing the GO undergoing reduction to agglomerate in the relatively low viscosity medium.<sup>22</sup> The agglomeration may not be as prevalent in their systems as our November samples because the first part of their composite synthesis used an extruder but it will still be significant as a result of the stagnant compression molding technique in the second step. Agglomeration would account for why their lower GO concentration samples do not have the same elongation as our summer samples. Out of two other papers done on this topic, Jin et al.'s data set is the only one that is close to ours.

Another paper was published by Yuan, et al.<sup>29</sup> describing the tensile properties of in-house polymerized GO/PA-11 composites. However, their tensile data differs significantly from

any of ours or that of Jin, et al. at all concentrations of GO including their neat system.<sup>22,29</sup> It is possible that this difference is due to their use of a different dog bone geometry and nearly double the strain rate for their tensile tests.<sup>29</sup> Therefore, their tensile data is not worth further comparison.

### 5.3 GO/PA-11 Water Diffusion/Absorption

As Table 4.2.2 and Figure 4.2.2 show, there is a reduction in the average diffusion coefficient for all of the loaded samples. What is very interesting is that there is a 70% reduction in the diffusion coefficient with just 0.1% GO by weight. Then the diffusion coefficient increases at 0.5% GO—yet is still lower than the average neat diffusion coefficient—and decreases linearly as more GO is added to the system.

First, it is worth comparing our measured diffusion coefficient for the neat samples with that of the literature. Wessel, et al.<sup>21</sup> used FT-IR to measure a diffusion coefficient for D<sub>2</sub>O in commercial PA-11 with the value of  $6.54 \times 10^{-10}$  cm<sup>2</sup>/sec. This value corresponds to a value of  $3.92 \times 10^{-6}$  mm<sup>2</sup>/minute. As seen in table 4.2.2, our averaged neat diffusion constant is lower by a factor of ~3,000. It is important to note that the crystallinity of Wessel's system is listed as 23% whereas the average crystallinity of our neat systems used in this study was 26% as seen in Table 4.4.2.<sup>21</sup>

Klepac, et al.<sup>30</sup> reported that an increase of 2% crystallinity reduced the diffusion coefficient of oxygen through polyethylene as much as 42% since diffusion does not occur in the crystalline regions. These values correspond to a 21% reduction of the diffusion coefficient per percent increase in crystallinity. Our samples being approximately 3% higher in crystallinity would theoretically give a 63% reduction in D. It is possible that an equal increase in crystallinity of PA-11 would reduce the diffusion coefficient more than that of polyethylene because PA-11 crystallinity results from stronger hydrogen bonding and dipole-dipole bonds instead of the weak London dispersion forces in polyethylene. Therefore, it is possible that these stronger interactions stiffen the polymer chains more in PA-11 than they do in polyethylene leading to a further reduction in the observed diffusion coefficient. Thus, it is unclear whether

this factor accounts for the 100% reduction that we see in our neat sample compared to Wessel's.<sup>21</sup>

There is conflict in the literature as to whether the intermolecular hydrogen bond is stronger than a corresponding intermolecular deuterium bond or vice versa. Tylli, et al.<sup>31</sup> wrote a paper on the intramolecular hydrogen and deuterium bonding of catechol where they showed that the deuterium bond is twice as strong in solid phase catechol. If this is the case in Wessel's solid phase PA-11 using D<sub>2</sub>O as the diffusion agent, their diffusion coefficient would theoretically be lower due to more favorable interaction with the solid PA-11 chains.<sup>21</sup> However, Tylli et al.<sup>31</sup> also state that the intermolecular deuterium bond can be stronger or weaker than the corresponding hydrogen bond depending on the shape of the potential function and the geometry of the interaction. Indeed, Tylli states that some previous experiments indicated that the deuterium bond is weaker.<sup>31</sup> The fact remains that Wessel's experiment differed significantly from ours in both material and technique and would logically yield very different results.<sup>21</sup> I suggest a future diffusion test be done on a neat PA-11 film using D<sub>2</sub>O and H<sub>2</sub>O so that we can acquire a valid comparison of our results to the literature.

Regardless of the correlation—or lack thereof—between our neat system and that of Wessel's, this diffusion test still provides a valid, relative comparison of the diffusion coefficients between our neat and loaded samples. One possible hypothesis for the reduction in diffusion coefficient as the GO concentration increases is the increase in crystallinity with GO concentration. As seen in Table 4.2.1 and Table 4.4.1, there seems to be a direct correlation between measured crystallinity and diffusion coefficient for the neat samples used in this water diffusion/absorption study. The only outlier is the 20130709 neat PA-11 sample. However given the precision of the data shown in Table 4.2.2, it's not possible to completely isolate crystallinity



as a variable in the neat samples. Given that the 0.1% GO sample—cut on 20130709—used in this study has 7% higher measured crystallinity than the neat samples and 4% higher than the 1.5% GO sample in Table 4.4.3, it is safe to assume that the drastic increase in measured crystallinity accounts for at least part of the enormous decrease in its diffusion coefficient shown in Table 4.2.2. To determine how much its crystallinity affects its diffusion coefficient, I suggest that another water diffusion/absorption test be conducted on the 0.1% GO 20130715 system given its lower measured crystallinity at the same GO concentration with the tensile and neck regions cut off. Given this data, there is evidence to suggest that an increase in crystallinity decreases the diffusion coefficient but we cannot tell by how much from this data.

It is unlikely that crystallinity alone results in the decrease in the diffusion coefficient seen in Table 4.2.2 and Figure 4.2.2. I hypothesize that the reduction in the diffusion coefficients for the loaded samples can be partly attributed to increased hydrogen bonding interactions, kinetic obstruction, and free volume reduction caused by the GO sheets. As noted previously, the polar GO sheets exhibit hydrogen bonding interactions with the PA-11 chains including dipole-dipole and hydrogen bonding.<sup>22</sup> At low concentrations, the good dispersion of GO particles maximizes the number of these interactions per GO particle. These intermolecular forces help to bind the polymer chains in place suppressing local perturbations that could allow small molecules to diffuse through the polymer matrix faster. We know this to be the case from the effects of GO on the Young's modulus discussed earlier. Additionally, GO particles themselves are completely impermeable to most gases.<sup>32</sup> Because of this characteristic, GO particles—when well dispersed—are able to create multiple overlapping layers forcing small molecules to travel around them in a “tortuous path” in order to diffuse through the polymer matrix.<sup>22</sup> In essence, the GO particles' physical presence creates a kinetic barrier to diffusion through the material. Also,

Compton et al.<sup>11</sup> discovered that the GO particles tend to crumple when fully dispersed at low concentrations. Thus, the GO sheets fill voids between polymer chains—also known as the free volume—and block any favorable routes through which small molecules can diffuse.<sup>11</sup> Moreover, it is likely that these two effects vary at different concentrations of GO.

At low concentrations of GO, the free volume effects would theoretically be minimal. Thus, the predominant effect at low concentrations would be stiffening of the PA-11 chains due to the hydrogen bond entanglement with the GO sheets and efficient kinetic obstruction due to the well-dispersed GO sheets. As the GO concentration increases, the GO sheets aggregate and are less efficiently entangled with the polymer matrix but the free volume effects increase in magnitude. At 0.5% GO concentration, it is likely that the increase in free volume effects are not enough to offset the decrease in kinetic obstruction due to the aggregate particles not being able to provide sufficient overlap in the polymer matrix. This would theoretically result in a higher diffusion coefficient for the 0.5% GO sample compared to the 0.1% GO sample in Table 4.2.2. At higher GO concentrations, free volume effects and hydrogen bond stiffening of PA-11 chains predominate and act to decrease the diffusion coefficient linearly. Therefore, free volume effects and hydrogen bonding interactions occur in all concentrations of GO but become more pronounced at higher concentrations while kinetic obstruction predominates at lower concentrations.

As noted earlier, it is important to differentiate between gas permeability and gas diffusion. Gas permeability is defined by equation 3.1.7.<sup>11</sup> Compton, et al.<sup>11</sup> reports that the measured diffusion, although significant, has a relatively low effect on gas permeability at low GO concentrations in their GO/polystyrene systems. Additionally, they report that it is the decrease in solubility of a gas in a GO/polymer composite that predominates at low

concentrations. Jin, et al.<sup>22</sup> also state that the solubility effect predominates at low concentrations with their GO/PA-11 composites. Additionally, they state that the water permeability was reduced in their 0.1% GO/PA-11 sample by ~49%.<sup>22</sup> Given these literature results, I suggest that we collaborate with another lab to conduct a gas permeation study of our own so that we can calculate the solubility from the diffusion and permeation coefficients.

As seen in Table 4.2.4 and Figure 4.2.4, the water uptake results are rather imprecise given the standard deviation of the neat samples. However, the result that is significant is the increased water uptake by the 0.5% and 1.5% GO/PA-11 samples. The result for the 1.5% GO/PA-11 sample would seem to contradict the diffusion coefficient results since the 1.5% GO/PA-11 sample had the lowest value. However, it is important to keep in mind that gas permeation consists of both diffusion and solubility effects as previously stated.<sup>11</sup> These higher values for these two loadings indicate that the samples are absorbing more water due to the hydrophilic nature of the GO sheets.<sup>16</sup> This increase in water absorption will be discussed further in the next subsection.

This water diffusion/absorption test gave some interesting data but its precision can be improved in the future. Sample masses for this study were on the order of 0.07 – 0.1 grams and fluctuations in mass changes were in fractions of a percent. Therefore, I suggest conducting future water diffusion/absorption studies with sample masses of at least 0.5 grams.

## 5.4 Aging Study

The GO/PA-11 aging study gave very interesting results shown in Tables 4.3.1 and 4.3.2. First, the molecular weights of the unaged GO/PA-11 decrease with increasing GO concentration. Secondly, the equilibrium molecular weights at Day 83 peak at 0.1% GO by weight and then decrease linearly at higher GO concentrations. In fact, the 1.5% GO sample has an equilibrium molecular weight below that of the neat system. Although the values between the SEC and MALLS instruments differ slightly, both instruments show the same trends as seen in Figures 4.3.1 and 4.3.2.

The reduction in initial molecular weight as GO concentration increases can only be explained by the GO particles serving as kinetic barriers to polymerization. All other variables during the polymerization process were controlled for and any minor variations in pressing technique are not likely to make much difference. It follows that if GO particles are impermeable to most small-molecule gases that they are also impermeable to monomers, oligomers, and larger polymer chains.<sup>32</sup> Therefore, the GO particles inhibit the polymerization of PA-11 via mobility reduction. This reduction in mobility results in a kinetic obstruction effect.

Our equilibrium molecular weight at 100 C° for our neat system correlates well with that of Jacques, et al.<sup>5</sup> whose equilibrium molecular weight for neat, in-house polymerized PA-11 was 26,500  $\frac{g}{mol}$  at 80 C° and Meyer et al.<sup>4</sup> whose equilibrium molecular weight for neat, in-house polymerized PA-11 was 25,000  $\frac{g}{mol}$  at 90, 105, 120, and 135 C°. The variation between Jacques, et al.'s result and ours is negligible given their standard deviation.<sup>5</sup>

The significant increase in equilibrium molecular weight of the 0.1% GO/PA-11 sample cannot be the result of higher crystallinity. As shown in Table 4.4.3, the measured crystallinity increases with GO concentration and the 0.1% GO/PA-11 sample does not have the highest

measured crystallinity. In fact, the 1.5% GO/PA-11 sample has the highest measured crystallinity yet it has the lowest equilibrium molecular weight. As mentioned previously, crystalline regions are generally impermeable to small molecules such as water.<sup>22</sup> Therefore one would normally expect the higher crystalline sample to have a higher equilibrium molecular weight because the water molecules would be inhibited from permeating the matrix and performing hydrolysis of the amide bonds. Therefore, this result supports my hypothesis that the increase in measured crystallinity in our DSC runs is due to the added non-covalent interactions between the GO particles and the PA-11 chains rather than an increase in the crystallinity of the PA-11 matrix itself.

I hypothesize that the aging of these samples is significantly reduced at low concentrations of GO due to reduced solubility of water molecules onto the PA-11 chains. We have previously established in literature studies and through observations of our own samples suggesting that our 0.1% GO/PA-11 sample has the best dispersion quality of the loaded samples. Given this assumption, the polymer chains would wrap around the GO sheets very efficiently. This wrapping would maximize the hydrogen bonding interactions between the polar sites near the amide bonds of the PA-11 chains and the oxygenated groups of the GO sheets. In other words, the GO sheets would be solvating the polar amide bonds via dipole-dipole and hydrogen bonding interactions. Therefore, the adjacent lattice sites to the PA-11 chain segments—from Flory theory on polymer dissolution—will be preoccupied by segments of the GO sheets.<sup>17</sup> Thus, the GO sheets would provide a kinetic and thermodynamic obstruction for water molecules solvating and hydrolyzing the PA-11 chains since an input of enthalpy would be necessary to break the dipole-dipole and hydrogen bonds.<sup>17</sup> However at higher GO concentrations, the PA-11 chains wrap the GO particles less efficiently. As GO particles

aggregate, they can create hydrophilic cavities in between GO sheets that attract more water molecules into the PA-11 matrix. Dreyer et al.<sup>13</sup> reported that graphite oxide agglomerates swell in humid environments due to water intercalation. These voids in between agglomerated GO sheets would expose the amide bonds of PA-11 chains wrapped around them to hydrolysis. Moreover, a higher water concentration in the PA-11 matrix would drive the equilibrium between hydrolysis and condensation to the left.<sup>4</sup> Although water diffuses more slowly into the matrix given the data in Table 4.2.2, the water absorption and aging study results suggest that more total water is absorbed at saturation. Therefore, the equilibrium molecular weight is highest at low GO concentrations but decreases at higher concentrations due to agglomeration.

We know from Jin, et al. that the 0.1% concentration of GO provides the lowest permeability coefficient for water into the PA-11 matrix.<sup>22</sup> Even though our diffusion coefficient is somewhat in question, it is clear that it is somewhat reduced by the addition of GO particles via kinetic obstruction or chain stiffening. Therefore, the primary reduction in permeability must be the very large reduction in the solubility coefficient for low GO concentrations as reported by both Jin, et al.<sup>22</sup> and Compton, et al.<sup>11</sup> In complete agreement with my hypothesis about the creation of hydrophilic cavities, Jin et al.<sup>22</sup> reports that the water permeation of GO/PA-11 increases as the GO concentration increases. Therefore my hypothesis describing the aging behavior in our GO/PA-11 samples is supported both by experiment and literature.

Perhaps the most rewarding aspect of this study is the fact that the equilibrium molecular weights of the 0.1% and the 0.5% GO/PA-11 samples are above the ductile-brittle transition molecular weight of  $25,000 \frac{g}{mol}$  in both instrument readings.<sup>3</sup> This indicates that PA-11 with 0.1% or 0.5% GO by weight could inhibit the aging of PA-11 in risers indefinitely given certain conditions. At the very least, the rate of aging in the 0.1% and 0.5% GO/PA-11 samples is much

more gradual than any of the other systems as shown in Figures 4.3.1 and 4.3.2. This more gradual rate of hydrolysis indicates that pipes made from these composites could have longer service lives even in non-ideal environments.

## Chapter 6: Conclusion

The tensile, water diffusion, and aging studies conducted in this paper provide evidence that GO particles increase the tensile properties and reduce the water hydrolysis in PA-11 at low concentrations when GO is properly exfoliated.

The tensile results for the summer samples show an increase in tensile properties at 0.1% GO by weight while they decay at higher concentrations. However, the November GO/PA-11 samples show no improvement in tensile properties except the Young's modulus which increases continuously with increasing GO concentration. The different behavior in the November samples is most likely due to increased agglomeration as a result of a lower heating rate. Increased agglomeration would result in less hydrogen bond interactions between the PA-11 chains and the GO sheets at the same concentration. Moreover, this agglomeration would create fracture sites within the PA-11 matrix since the interface between agglomerated GO sheets is very weak resulting in lower elongation at break and tensile strength. The increase in Young's modulus for both the November and the summer samples is most likely due to hydrogen bonding interactions between the surface of the GO sheets and the polymer. Clearly, these interactions increase with concentration but decrease if there is agglomeration. The ultimate strain and tensile strength of PA-11 increase at 0.1% GO by weight in the summer sample is probably due to good exfoliation within the PA-11 matrix.

Greater exfoliation results in increased hydrogen bonding between GO particles and polymer. This effect allows for stress transfer from the PA-11 chains to the GO sheets. The decay in these properties at higher GO concentrations is probably due to agglomeration resulting in less hydrogen bonding and the creation of fracture sites between agglomerated GO sheets.



The DSC results indicate an increase in crystallinity with an increase in GO concentration. It is unclear whether the DSC readings are measuring crystallinity because the enthalpy to break the hydrogen bonds between GO sheets and the PA-11 chains would be of similar magnitude to the enthalpy required to break hydrogen bonds between PA-11 chains.

The water diffusion coefficient shows a decrease with increasing GO concentration. The 70% reduction in the diffusion coefficient for the 0.1% GO by weight sample could be caused by an increase in crystallinity rather than a direct effect of the GO sheets themselves. If the measured increase in enthalpy of melting correlates to hydrogen bond interactions between GO and PA-11 chains, then it is possible that the GO sheets decrease the diffusion coefficient by stiffening the PA-11 chains, acting as kinetic obstructions to diffusion, and occupying the free volume.

The aging study shows significantly reduced hydrolysis in 0.1% and 0.5% GO by weight PA-11 samples. These results could be due to the reduced solubility of water on the PA-11 chains. It is more likely that the GO particles could serve as kinetic and thermodynamic barriers to hydrolytic attack of the amide bonds by water molecules since they would occupy adjacent lattice sites. Evidence for the GO particles hindering chain mobility and thereby reaction rates is shown by the decreasing initial molecular weights with GO concentration when polymerized over the same time interval at the same temperature. However at higher concentrations, the GO particles appear to agglomerate and the hydrolysis is similar to the neat PA-11 polymer. The equilibrium molecular weights increase at 0.1% and 0.5% GO by weight and then decrease at 1.0% and 1.5% GO concentrations.

## References

- [1] Odian, George. *Principles of Polymerization*, 4<sup>th</sup> Edition; John Wiley & Sons, Inc.: Hoboken, New Jersey, 2004; 1-9, 50-51, 98-99.
- [2] Glover, Arthur Jaeton Mitman. Characterization of PA-11 Flexible Pipe Liner Aging in the Laboratory and in Field Environments Throughout the World. Ph.D. Dissertation, The College of William and Mary, Williamsburg, Virginia, January 2011.
- [3] Hocker, John-Andrew Samuel. The Role of Small Carboxylic Acids During Poly(amide) 11 Hydrolysis. M.S. Thesis, The College of William and Mary, Williamsburg, VA, April 2012.
- [4] Meyer, Andrew; Jones, Nick; Lin, Yao; Kranbuehl, David. Characterizing and Modelling the Hydrolysis of Polyamide-11 in a PH 7 Water Environment. *Macromolecules* **2002**, 35, 2784-2798.
- [5] Jacques, B.; Werth, M.; Merdas, I.; ThomINETTE, T.; Verdu, J. Hydrolytic ageing of polyamide 11. 1. Hydrolysis kinetics in water. *Polymer* **2002**, 43, 6439-6447.
- [6] Romão, Wanderson; Castro, Eustáquio V.R.; Filho, Elói A.S.; Guimarães, Regina C.L.; Silva, Ana L.N.; Teixeira, Sylvia C.S.; Paoli, de Marco-A.; de Sena, Geovane L. Ageing of Polyamide 11 Used in the Manufacture of Flexible Piping. *J. Appl. Polym. Sci.* **2009**, 114, 1777-1783.
- [7] Cai, Minzhen; Thorpe, Daniel; Adamson, Douglas H.; Schniepp, Hannes C. Methods of graphite exfoliation. *Mater. Chem.* **2012**, 22, 24992-25002.
- [8] Sun, Yiqing; Shi, Gaoquan. Graphene/Polymer Composites for Energy Applications. *Polym. Phys.* **2012**, 51, 231-253.
- [9] McCallister, M.J.; Li, J.L.; Adamson, D.H.; Schniepp, H.C.; Abdala, A.A.; Liu, J.; Herrera-Alonso, M.; Milius, D.L.; Car, R.; Prud'homme, R.K.; Aksay, I.A. Single sheet functionalized graphene by oxidation and thermal expansion of graphite. *Chem. Mater.* **2007**, 19, 4396-4404.
- [10] Lahiri, Debrupa; Dua, Rupak; Zhang, Cheng; Socarraz-Novoa, Ignacio de; Bhat, Ashwin; Ramaswamy, Sharan; Agarwal, Arvind. Graphene Nanoplatelet-Induced Strengthening of UltraHigh Molecular Weight Polyethylene and Biocompatibility in Vitro. *Appl. Mater. Interfaces* **2012**, 4, 2234 -2241.
- [11] Compton, Owen C.; Kim, Soyung; Pierre, Cynthia; Torkelson, John M.; and Nguyen, Soninh T. Crumpled Graphene Nanosheets as Highly Effective Barrier Property Enhancers. *Adv. Mater.* **2010**, 22, 4759-4763.
- [12] Nano Enhanced Wholesale Technologies. <http://www.nano-enhanced-wholesale-technologies.com/faq/carbon-forms.htm> (accessed 02/11/2014).

- [13] Dreyer, Daniel R.; Park, Sungjin; Bielawski, Christopher W.; Ruoff, Rodney S. The Chemistry of Graphene Oxide. *Chem. Soc. Rev.* **2010**, *39*, 228-240.
- [14] Gómez-Navarro, Christina; Burghard, Marko; Kern, Klaus. Elastic Properties of Chemically Derived Single Graphene Sheets. *Nano Lett.* **2008**, *8*, 2045-2049.
- [15] Connexions. <http://cnx.org/content/m29187/latest/> (accessed 02/11/2014).
- [16] Stankovich, Sasha; Dikin, Dmitriy A.; Dommett, Geoffrey H.B.; Kohlhaas, Kevin M.; Zimney, Eric J.; Stach, Eric A.; Piner, Richard D.; Nguyen, SonBinh T.; Ruoff, Rodney S. Graphene-based composite materials. *Nature (London, U.K.)* **2006**, *442*, 282-286.
- [17] Allcock, Harry R.; Lampe, Frederick W.; Mark, James E. *Contemporary Polymer Chemistry*, 3<sup>rd</sup> Edition; Pearson Education, Inc.: Upper Saddle River, New Jersey, 2003; 13-14, 414-432, 451-468, 478-487, 492-503, 523, 542-556, 665-666.
- [18] Hocker, John-Andrew Samuel. Poly(amide)-11 and Poly(amide)-12, Mechanical Property Prediction and Rentention Enhancement. Masters of Science, the College of William and Mary, Williamsburg, Virginia, April 2012.
- [19] Laun, Sandra; Pasch, Harald; Longiéras, Nicolas; Degoulet, Christophe. Molar mass analysis of polyamides-11 and -12 by size exclusion chromatography in HFiP. *Polymer* **2008**, *49*, 4502-4509.
- [20] Cowie, J.M.G. *Polymers: Chemistry And Physics of Modern Materials*, 3<sup>rd</sup> Edition; Taylor and Francis Group, LLLC: Boca Raton, Florida, 2008; 234-240, 264, 279-288.
- [21] Wessel, Elke; Vogel, Christian; Siesler, Heinz W. Fourier Transform Infared Imaging Spectroscopy of the Diffusion Process of D<sub>2</sub>O into Polyamide 11. *Soc. Appl. Spec.* **2009**, *63*, 1-5.
- [22] Jin, J.; Rafiq, R.; Gill, Y.Q.; Song, M. Preparation and Characterization of High Performance of Graphene/Nylon Nanocomposites. *Eur. Polym. J.* **2013**, *49*, 2617-2626.
- [23] Flaconnèche, B.; Martin, J.; Kloppfer, M.H. Permeability, Diffusion, and Solubility of Gases in Polyethylene, Polyamide 11, and Poly(vinylidene fluoride). *Oil Gas Sci. Technol.* **2001**, *56*, 261-278.
- [24] Wijmans, J.G.; Baker, R.W. The solution-diffusion model: a review. *J. Membr. Sci.* **1995**, *107*, 1-21.
- [25] Brigham Young University: Department of Electrical and Computer Engineering. <http://bio.groups.et.byu.net/EquilibriumSS.phtml> (accessed April 7, 2014), Equilibrium Relative Humidity of Some Saturated Salt Solutions 25°C.

- [26] Zahn, Dirk. On the Role of Water in Amide Hydrolysis. *Eur. J. Org. Chem.* **2004**, 4020-4023.
- [27] Bhattacharyya, A.; Chen, S.; Zhu, M. Graphene reinforced ultra high molecular weight polyethylene with improved tensile strength and creep resistance properties. *Express Polym. Lett.* **2013**, 8, 74-84.
- [28] Hochstetter, Gilles; Dang, Patrick. Correlation between hydrolysis and the ultimate mechanical properties of polyamides in offshore conditions. , Proceedings of the ASME 2009 28<sup>th</sup> International Conference on Ocean, Offshore and Arctic Engineering, Honolulu, Hawaii, May 31 – June 5, 2009; American Society of Mechanics: New York, N.Y., 2009; 79976, 797-803.
- [29] Yuan, Ding; Wang, Biaobing; Wang, Liuyang; Wang, Yupeng; Zhou, Zuowan. Unusual toughening effect of graphene oxide on the graphene oxide/nylon 11 composites prepared by in situ melt polycondensation. *Composites Part B* **2013**, 55, 215-220.
- [30] Klepac, Damir; Ščetar, Mario; Kurek, Mia; Mallon, Peter E.; Luyt, Adriaan S.; Galić, Kata; Valić, Srećko. Oxygen permeability, electron spin resonance, differential scanning calorimetry and positron annihilation lifetime spectroscopy studies of uniaxially deformed linear low-density polyethylene film. *Polym. Int.* **2013**, 62, 474-481.
- [31] Tylli, Henrik; Konschin, Henrik. A RAMAN SPECTROSCOPIC STUDY OF THE OH AND OD TORSION IN 1,2-DIHYDROXYBENZENE, *J. Mol. Struct.* **1979**, 57, 13-19.
- [32] Yang, You-Hao; Bolling, Laura; Priolo, Morgan A.; Grunlan, Jaime C. Super Gas Barrier and Selectivity of Graphene Oxide-Polymer Multilayer Thin Films. *Adv. Mater.* **2013**, 25, 503-508.